The low-pressure micro-resistojet

Modelling and optimization for future nano- and pico-satellites

Cordeiro Guerrieri, D.

DOI
10.4233/uuid:cfcf1f65-4190-46cb-8688-54389a682c57

Publication date
2018

Document Version
Final published version

Citation (APA)
Cordeiro Guerrieri, D. (2018). *The low-pressure micro-resistojet: Modelling and optimization for future nano- and pico-satellites*. [Dissertation (TU Delft), Delft University of Technology].
https://doi.org/10.4233/uuid:cfcf1f65-4190-46cb-8688-54389a682c57

Important note
To cite this publication, please use the final published version (if applicable).
Please check the document version above.

THE LOW-PRESSURE MICRO-RESISTOJET

MODELLING AND OPTIMIZATION FOR FUTURE NANO- AND PICO-SATELLITES

THE LOW-PRESSURE MICRO-RESISTOJET

MODELLING AND OPTIMIZATION FOR FUTURE NANO- AND PICO-SATELLITES

Dissertation

for the purpose of obtaining the degree of doctor
at Delft University of Technology
by the authority of the Rector Magnificus Prof.dr.ir. T.H.J.J. van der Hagen
chair of the Board for Doctorates
to be defended publicly on
Monday 10 September 2018 at 12:30 o'clock

by

Daduí CORDEIRO GUERRIERI

Master of Science in Mechanical Engineering
Universidade Federal do Rio de Janeiro, RJ, Brazil
born in Rio de Janeiro, RJ, Brazil.

This dissertation has been approved by the promotors:

promotor: Prof.dr. E.K.A. Gill
copromotor: Dr. A. Cervone

Composition of the doctoral committee:

Rector Magnificus,	chairperson
Prof.dr. E.K.A. Gill,	Delft University of Technology, promotor
Dr. A. Cervone,	Delft University of Technology, copromotor
Independent members:	
Prof.dr. M.M. Micci,	Pennsylvania State University, USA
Prof.dr. L. D'Agostino,	University of Pisa, Italy
Prof.dr. ir. C.R. Kleijn,	Delft University of Technology
Dr. C. Bramanti,	ESTEC-ESA
Prof.dr. S. Hickel,	Delft University of Technology, reserve member
Other member:	
Dr.ing. H.W. van Zeijl,	Delft University of Technology

This research was funded by the CNPq (Conselho Nacional de Desenvolvimento Científico e Tecnológico - Brasil), and also supported by the Delft University of Technology and CEFET-RJ (Centro Federal de Educação Tecnológica Celso Suckow da Fonseca do Rio de Janeiro).

Keywords: LPM, Micro-Resistojet, Micro-Thruster, Micro-Propulsion System, "Green" Propellant, Water propellant

Printed by: Ipskamp Printing

Cover by: Daduí C. Guerrieri

ISBN 978-94-028-1157-5

An electronic version of this dissertation is available at
http://repository.tudelft.nl/.

To my lovely Fernanda and Zoé.

CONTENTS

SUMMARY

The aerospace industry is recently experiencing growing interest in very small spacecraft like nano- and pico-satellites. However, these very small satellites are still being developed in most cases without a dedicated propulsion system limiting their capabilities. The micro-resistojet has been recognized as a suitable propulsion system for these classes of satellites due to its scalability and performance. Additionally, it can be classified as a "green" propulsion system since it can use naturally any kind of propellant, including "green" propellants. The Low-Pressure Micro-Resistojet (LPM) is a type of micro-resistojet concept that works under very low pressure. This PhD thesis is focussed on the development of this propulsion system concept with the goal to enable very small satellites to perform manoeuvres. This improvement allows, for instance, to increase the spacecraft lifetime by active orbit keeping. Furthermore it can enable orbit change manoeuvres and formation flight.

A key starting point to address in the development of such devices is the propellant selection, since it directly influences the performance of the thruster. A novel methodology has been developed and applied to select and to characterize fluids that are suitable for use as propellants in micro-resistojet specially for the LPM. The developed methodology is divided into four steps: Data Collection; Feasibility Assessment; Qualitative Selection; and Conclusive Analysis. The first step is to collect data on a large number of fluids that could be used as propellants in micro-resistojet systems. The second step is to select, among the identified fluids, only the ones which meet the criteria of being in solid or liquid phase under a specific thermodynamic condition. The third step is to use the Analytical Hierarchy Process (AHP) combined with a Pugh Matrix tool to compare the remaining fluids with respect to the three main criteria: performance, system density, and safety. Finally, the fourth step is to analyze in detail the substances that score the highest in the previous step and conclude on highly promising candidates for propellants. Even though water shows the highest power consumption among the analyzed propellants, it presents the best velocity increment per volume of propellant. Furthermore, water is the safest propellant and the easiest one to handle and acquire.

The thruster for this particular micro-resistojet concept is designed to work at a relatively high Knudsen number ($10 > Kn > 0.1$) in the transitional flow regime. The propellant velocity is increased in the microchannels not by geometrical expansion as in conventional thermal propulsion concepts, but by the thermal energy of the walls, transferred to the particles through collisions. Heat transfer and fluid flow through different microchannel geometries are analyzed by means of Direct Simulation Monte Carlo (DSMC) simulations. Four types of three-dimensional microchannels, intended to be used as expansion slots in micro-resistojet concepts, are investigated using nitrogen as working fluid. The main purpose is to understand the impact of the microchannel geometry on the exit velocity and the transmission coefficient, parameters which are well known to affect directly the thruster performance. Although this analysis can be applied

in principle to several possible microfluidics scenarios, particular focus is given to its application in the field of space propulsion for very small satellites, for which the requirements ask for low thrust levels from some micro-Newtons to a few milli-Newtons and moderate specific impulse, as well as a low power consumption in the order of a few Watts. Additionally, a sensitivity analysis was performed aiming to define the best microchannel geometry to be applied as thruster. A microchannel divided into two parts with a first-part divergent and a second-part straight causes a small reduction of the specific impulse with a significant increase of thrust and, additionally, a considerable reduction in power consumption.

To simplify the engineering design of this propulsion system, an analytical model of the thruster performance has been developed using fundamental physical models. This analytical model is based on the Kinetic Theory of gases and the Maxwell-Boltzmann distribution of molecular velocities to describe the macroscopic flow parameters such as mass flow rate, velocity and pressure. Based on these paramenters the thruster performance can then be described and analyzed. Although equations are well known, they are applied in this case using a particular approach in order to describe the physics of this micro-propulsion system. This is considered a significant improvement with respect to the former analytical model which neglects the pressure thrust. A maximum difference of 3% between numerical result and semi-analytical result, which uses the transmission coefficient from the numerical result, is found.

Three different LPM devices with integrated heater and temperature measurement were designed, manufactured and characterized at the Department of Space Engineering in cooperation with the Else Kooi Laboratory at Delft University of Technology. Each device has a different microchannel geometry. One has a grid of circular microchannels and the other two have a grid of rectangular slots with different dimensions each. The devices were manufactured using Silicon-Based Micro Electro Mechanical Systems (MEMS) technology including a heater made of Molybdenum (Mo) for better operations at high temperature. The resistance of the heaters is used to determine the chip temperature giving them a double function both as heater and sensor simultaneously. The manufacturing steps are described in detail. A special interface is manufactured to hold the MEMS device considering both the mechanical and electrical aspects. The MEMS devices are characterized for three different aspects: mechanical, electrical and propulsion performance. The three designed devices are tested mechanically and electrically, and one design is tested in terms of propulsion performance under near-operational conditions. Promising results are presented as well as further solutions for the next device version.

Finally, the optimum design of the LPM applied to two different mission scenarios is discussed, one for a CubeSat mission with two satellites flying in formation, the other for a PocketQube mission in which the propulsion system will be used as a technology demonstrator. The LPM is discussed and analyzed in terms of two main aspects, scalability and performance. The focus is placed on heater chip sizing and innovative tank design. It is shown that increasing the heater chip size by increasing the number of microchannels does not results in increasing the thruster performance, limited mainly by the available power.

This PhD thesis brings the Low-Pressure Micro-Resistojet to a higher level of devel-

opment, which in terms of Technology Readiness Level (TRL) means from TRL-2 to TRL-5 for the thruster part, and to TRL-3 for the storage part. However, there is still further required development in terms of research and engineering. The analytical model can be improved by mapping the transmission coefficient for a number of geometries of a particular interest. The heater chip design device can be improved by implementing an isolation layer on the side faced to the plenum, integrating a pressure sensor, and integrating a electric circuit to improve the temperature sensor. The interface used to hold the devices can be improved to enable the heater chip achieving higher temperatures. The propellant tank is the part of the Low-Pressure Micro-Resistojet that needs further research and development. The storage is expected to have a multiphasic state, and be controllable for phase change in order to deliver the desired mass flow rate. Furthermore, a flight demonstration of this propulsion system is expected and currently scheduled in 2019.

SAMENVATTING

In de ruimtevaartindustrie is er vandaag de dag een groeiende interesse in zeer kleine ruimteevaartuigen, zoals nano- en pico satellieten. De meeste van deze systemen worden echter ontwikkeld zonder specifiek voorstuwingssysteem, wat de hun mogelijkheden beperkt. De micro-resistojet wordt gezien als een geschikt voortstuwingssysteem voor deze klasse van satellieten vanwege haar schaalbaarheid en prestaties. Daarnaast kan het gezien worden als een een "groen" voortstuwingssysteem, omdat het syseem van nature elke soort drijfgas kan gebruiken, waaronder "groene" drijfgassen. De Lage-Druk Micro-Resistojet (LPM) is een type micro-resistojet dat werkt met een hele lage druk. Deze PhD thesis is gericht op de ontwikkeling van een concept voor een voorstuwingssysteem met het doel maneuvres voor zeer kleine satellieten mogelijk te maken. Dit maakt het bijvoorbeeld mogeelijk om de levensduur van een ruimtevaartuig te verlengen door middel van actief baanonderhoud. Het is daarnaast mogelijk om de baan te veranderen of te formatievliegen.

Een belangrijke eerste stap in de ontwikkeling van zo een apparaat is de selectie van het stuwgas, aangezien dit dirct de prestaties van het voortstuwingssysteem beinvloed. Een nieuwe methodologie is ontwikkeld en toegepast voor het selecteren en karakteriseren van vloeistoffen die geschikt zijn voor gebruik als drijfgassen in een micro-resistojet, volledig gericht op de LPM. De ontwikkelde methodologie is onderverdeeld in vier stappen: gegevensverzameling, haalbaarheidsonderzoek, kwalitatieve selectie, en Conclusive Analysis. De eerste stap is om gegevens te verzamelen over een groot aantal vloeistoffen die kunnen worden gebruikt als drijfgassen in micro-resistojetsystemen. De tweede stap is om uit de geïdentificeerde vloeistoffen alleen de vloeistoffen te selecteren die voldoen aan de criteria om in vaste of vloeibare fase te verkeren onder een specifieke thermodynamische toestand. De derde stap is het gebruik van het Analytisch Hierarchisch Proces (AHP) in combinatie met een Pugh Matrix-tool om de resterende vloeistoffen te vergelijken met betrekking tot de drie belangrijkste criteria: prestaties, systeemdichtheid en veiligheid. Tot slot, de vierde stap is om in detail de stoffen te analyseren die de hoogste score behaalden in de vorige stap en conclusies te trekken over veelbelovende kandidaten voor drijfgassen. Hoewel water het hoogste stroomverbruik van de geanalyseerde drijfgassen vertoont, heeft het de beste snelheidstoename per volume drijfgas. Bovendien is water het veiligste drijfgas en het gemakkelijkst te hanteren en te verkrijgen.

Het voortstuwingssysteem voor dit specifieke micro-resistojetconcept is ontworpen om te werken met een relatief hoog Knudsen-getal ($10 > Kn > 0.1$) in het overgangsregime. De drijfsnelheid wordt verhoogd in de microkanalen, niet door geometrische expansie zoals bij conventionele thermische voortstuwingsconcepten, maar door de thermische energie van de wanden, overgedragen aan de deeltjes door botsingen. Warmteoverdracht en vloeistofstroming door verschillende microkanaalgeometrieën worden geanalyseerd door middel van Directe Simulatie Monte Carlo (DSMC) simulaties. Vier

soorten driedimensionale microkanalen, bedoeld om te worden gebruikt als expansieslots in micro-resistojetconcepten, worden onderzocht met stikstof als werkvloeistof. Het belangrijkste doel is om de impact van de microkanaalgeometrie op de uitgangssnelheid en de transmissiecoëfficiënt te begrijpen, parameters waarvan algemeen bekend is dat zij direct de voortstuwingsprestaties beïnvloeden. Hoewel deze analyse in principe kan worden toegepast op verschillende mogelijke micro-fluïdica-scenario's, wordt bijzondere aandacht besteed aan de toepassing ervan op het gebied van ruimtevoortstuwing voor zeer kleine satellieten, waarvoor de vereisten vragen om lage stuwkrachtniveaus van enkele micro-Newtons tot enkele milli-Newtons en een matige specifieke impuls, evenals een laag stroomverbruik in de orde van enkele Watts. Bovendien werd een gevoeligheidsanalyse uitgevoerd om de beste microkanaalgeometrie te definiëren die in het voortstuwingssysteem moet worden toegepast. Een microkanaal verdeeld in twee delen, waarbij het eerste deel divergent en het tweede deel recht is, veroorzaakt een kleine reductie van de specifieke impuls met een aanzienlijke toename van de stuwkracht en bovendien een aanzienlijke vermindering van het stroomverbruik.

Om het technische ontwerp van dit voortstuwingssysteem te vereenvoudigen, is een analytisch model van de voortstuwingsprestaties ontwikkeld met behulp van fundamentele natuurkundige modellen. Dit analytische model is gebaseerd op de kinetische theorie van gassen en de Maxwell-Boltzmann-verdeling van moleculaire snelheden om de macroscopische stromingsparameters zoals massastroomsnelheid, snelheid en druk te beschrijven. Op basis van deze paramenters kunnen de voortstuwingsprestaties vervolgens worden beschreven en geanalyseerd. Hoewel vergelijkingen algemeen bekend zijn, worden ze in dit geval toegepast met een bepaalde benadering om de fysica van dit micro-voortstuwingssysteem te beschrijven. Dit wordt als een significante verbetering beschouwd ten opzichte van het voormalige analytische model dat de drukstoot verwaarloost. Er wordt een maximaal verschil van 3% gevonden tussen het numerieke resultaat en het semi-analytische resultaat, dat de transmissiecoëfficiënt uit het numerieke resultaat gebruikt.

Drie verschillende LPM-apparaten met geïntegreerde verwarming en temperatuurmeting werden ontworpen, vervaardigd en gekarakteriseerd door de Ruimtevaarttechniekafdeling in samenwerking met het Else Kooi Laboratorium van de Technische Universiteit Delft. Elk apparaat heeft een andere microkanaalgeometrie. De ene heeft een raster van ronde microkanalen en de andere twee hebben een raster van rechthoekige sleuven met elk verschillende afmetingen. De apparaten zijn vervaardigd met behulp van op silicium gebaseerde micro-elektromechanische systemen (MEMS) -technologie, waaronder een verwarmer gemaakt van molybdeen (Mo) voor een betere werking bij hoge temperaturen. De weerstand van de verwarmers wordt gebruikt om de spaandertemperatuur te bepalen waardoor ze een dubbele functie hebben, ze dienen tegelijkertijd als verwarming en als sensor. De productiestappen worden in detail beschreven. Er is een speciaal interface vervaardigd om het MEMS-apparaat vast te houden, waarbij zowel de mechanische als de elektrische aspecten in aanmerking worden genomen. De MEMS-apparaten worden gekenmerkt door drie verschillende aspecten: mechanische, elektrische en voortstuwingsprestaties. De drie ontworpen apparaten worden mechanisch en elektrisch getest en één ontwerp wordt getest in termen van voortstuwingsprestaties onder vrijwel operationele omstandigheden. Veelbelovende resultaten wor-

den gepresenteerd, evenals verdere oplossingen voor de volgende apparaatversie.

Ten slotte wordt het optimale ontwerp van de LPM voor twee verschillende missiescenario's beschreven, namelijk voor een CubeSat-missie met twee satellieten die in formatie vliegen en voor een PocketQube-missie waarbij het voortstuwingssysteem zal worden gebruikt als een technologiedemonstratie. De LPM wordt beschrven en geanalyseerd op basis van twee hoofdaspecten, te weten de schaalbaarheid en prestaties. De focus ligt op de dimensionering van de verwarmingsplaat en het innovatieve ontwerp van de tank. Er wordt aangetoond dat het vergroten van de grootte van de verwarmingschip door het aantal microkanalen te vergroten niet resulteert in een verhoging van de stuwkrachtprestaties, die hoofdzakelijk beperkt wordt door het beschikbare vermogen.

Dit proefschrift brengt de lagedruk-micro-resistojet naar een hoger ontwikkelingsniveau, wat betekent dat het technologiebereidheidsniveau (TRL) van TRL-2 naar TRL-5 is gebracht voor het voortstuwingsdeel en naar TRL-3 voor het opslagdeel. Echter, er is nog verdere ontwikkeling vereist op het gebied van onderzoek en ontwikkeling. Het analytische model kan worden verbeterd door de transmissiecoëfficiënt in kaart te brengen voor een aantal interssante geometrieën. De inrichting voor het ontwerpen van de verwarmingchip kan worden verbeterd door een isolatielaag aan te brengen op de zijde die is gericht naar het plenum, een druksensor te integreren en een elektrisch circuit te integreren om de temperatuursensor te verbeteren. De interface dat wordt gebruikt voor het vasthouden van de apparaten kan worden verbeterd om de verhittingschip hogere temperaturen te laten bereiken. De drijfgastank is het onderdeel van de lagedruk-microresistojet dat verder onderzoek en ontwikkeling vereist. Er wordt verwacht dat de opslag een meer-fasentoestand heeft en dat faseverandering controleerbaar zijn om zo de gewenste massastroomsnelheid te leveren. Bovendien wordt een vluchtdemonstratie van dit voortstuwingssysteem verwacht en gepland voor 2019.

1

INTRODUCTION

True wisdom comes to each of us when
we realize how little we understand about
life, ourselves, and the world around us.

Socrates

There is a clear need for the development of micro-propulsion systems to enhance the capabilities of nano- and pico-satellites. A promising propulsion option to meet the strict requirements of these small satellites is the Low-Pressure Micro-Resistojet (LPM) which works in the rarefied gas dynamic regime. In this chapter, an overview is presented of the propulsion systems applied for very small satellites, the state-of-the-art of the LPM, and how the dissertation is structured.

1

1.1. NANO- AND PICO-SATELLITES

During the past decade, the market of very small satellites [1] has been rapidly growing, see Figure 1.1. Several factors have led to this trend, such as the low-cost access to space since they are usually launched as a secondary payload and the standardization of these very small satellites. This makes these spacecraft an interesting platform for the purpose of technology demonstration, science proof-of-concept and validation, communication and education. Additionally, this class of satellites evolves from an educational and research tool to a business for emerged and consolidated companies (Selva and Krejci, 2012; Boshuizen et al., 2014; Nervold et al., 2016), as can be seen in Figure 1.2.

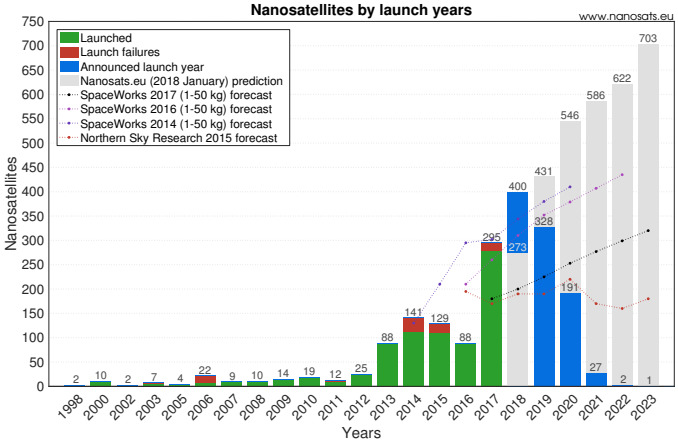

Figure 1.1: Trend of the number of nanosatellites per years. From (Kulu, 2018).

One well known standardization for nanosatellites is the CubeSat which is characterized by 1U (1-unit) cube shape of 10×10×10 cm^3. Another standardization that is becoming popular is the PocketQube, classified however as pico-satellite, which is characterized by 1p (1-unit) cube shape of 5×5×5 cm^3. The spacecraft can be designed with more than 1-unit such as CubeSats of 1.5U, 2U, 3U, 6U, usually depending on the desired mission (Poghosyan and Golkar, 2017). For instance, Cubsats are often designed as 3U, see Figure 1.3.

The satellite standardization decreases the development time and cost because of the increase of available Commercial-Off-The-Shelf (COTS) components. However there is still a lack of sufficient choices of micro-propulsion systems for these very small satellites. The development of micro-propulsion systems for this class of satellites is essential to improve their mission lifetime and performance. Additionally, some specific classes of missions as those involving distributed space systems are requiring a capable propulsion system to enable, for instance, formation flying, orbit change or station keeping. These propulsion systems need to be extremely miniaturized and highly integrated due

[1] Small satellites are broadly defined as satellites weighting less than about 180 kg. They are subdivided into Minisatellites (mass range of 100 - 180 kg), Microsatellites (mass range of 10 - 100 kg), Nanosatellites (mass range of 1 - 10 kg), Picosatellites (mass range of 0.01 - 1 kg) and Femtosatellites (mass range of 0.001 - 0.01 kg) (NASA, 2018). In this thesis, "very small satellites" term is used to refer to nano- and pico-satellites.

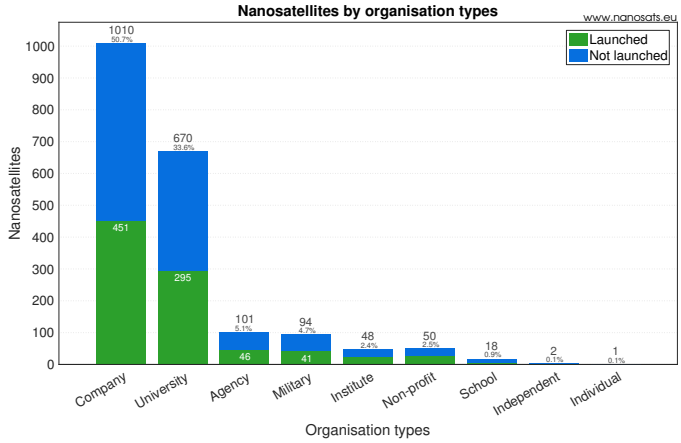

Figure 1.2: Number of nanosatellites by organisation types. From (Kulu, 2018).

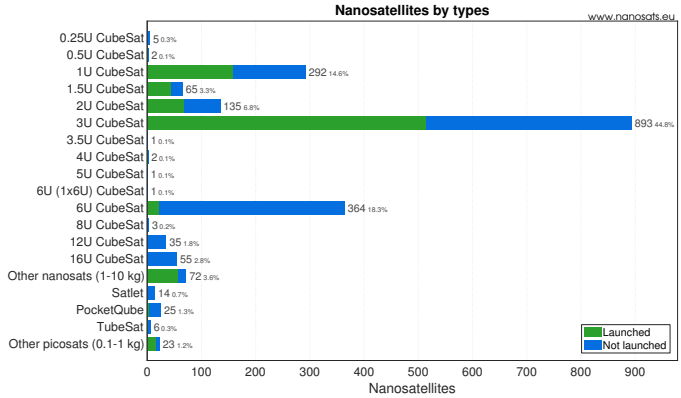

Figure 1.3: Nanosatellites by types. From (Kulu, 2018).

to the strict requirements imposed by this class of satellites.

Two mission scenarios are used in this PhD thesis as reference. One consists of two identical 3U CubeSats intended to perform a formation flight in a low altitude Earth orbit. The satellites are designed to keep in along-track formation at nominal 1000 km separation, and to maintain a predetermined distance by counteracting atmospheric drag and other possible causes of drifting. Table 1.1 presents the requirements posed by the formation flight mission. The maximum thrust level is defined to avoid too large induced disturbance torques in case of misalignment of the thrust direction with respect to the center of mass of the spacecraft. The minimum thrust level is derived to overcome the atmospheric drag. Both spacecraft need to be able to delivery a velocity increment (Delta-v) of 15 $\mathrm{m\,s^{-1}}$, of which 1 $\mathrm{m\,s^{-1}}$ for formation acquisition and 14 $\mathrm{m\,s^{-1}}$ for formation keeping. This allows for a formation duration of 18, 30 or 47 days at altitudes of 300, 350 and 400 km, respectively. The total mass, volume and power consumption

are dictated by the global budgets for the whole satellite. Moreover, those satellites are usually put into orbit by piggy-back launches and, due to that, launch providers impose a number of constraints related to the safety of the main payload of the rocket, i.e., low internal pressure, no pyrotechnic devices, and no hazardous propellants (Gill et al., 2013; Cervone et al., 2015a).

Another mission scenario consists is based on 3p PocketQube intended to perform a flight demonstration of the propulsion system. Table 1.2 presents the requirements in order to fulfill the flight propulsion system demonstration mission. Similar to the previous mission, the maximum thrust level is defined to avoid too large induced disturbance torques in case of misalignment of the thrust direction with respect to the center of mass of the spacecraft. The minimum thrust level is derived to overcome the atmospheric drag. Since it is a flight demonstration, there is no specific Delta-V requirement. The total mass, volume and power consumption are dictated by the global budgets for the whole satellite (Speretta et al., 2016). Those satellites are also put into orbit by piggy-back launches by meaning they present the same constrains related to low internal pressure, no pyrotechnic devices, and no hazardous propellants (Pallichadath et al., 2017, 2018).

Table 1.1: Main requirements for the CubeSat formation flying mission, (Cervone et al., 2015a)

Parameter	Value
Thrust [mN]	0.5 - 9.5
Delta-V [m s^{-1}]	>15
Total wet mass [g]	<459
Total size [mm]	$< 90 \times 90 \times 80$
Peak power consumption [W]	<10.0
Internal pressure [bar]	<10
Pyrotechnic devices	No
Hazardous propellants	No

Table 1.2: Main requirements for the PocketQube propulsion demonstration mission, (Pallichadath et al., 2018)

Parameter	Value
Thrust [mN]	0.2 - 3.0
Delta-V [m s^{-1}]	N/A
Total wet mass [g]	<75
Total size [mm]	$< 42 \times 42 \times 30$
Peak power consumption [W]	<4.0
Internal pressure [bar]	<10
Pyrotechnic devices	No
Hazardous propellants	No

1.2. MICRO-PROPULSION SYSTEMS

Differently to macro propulsion systems which have already reached a high level of development, micro-propulsion systems are still, for a large part, at a low Technology Readiness Level (TRL). It is not simply a matter to scale down the existing macro-propulsion systems. There are several miniaturization effects in terms of power, mass, volume, temperature, and pressure which have to be taken into account when scaling down. Figure 1.4 shows the types of micro-propulsion systems which have been proposed, discussed or under development (Silva et al., 2018; Krejci and Lozano, 2018; Tummala and Dutta, 2017). As it is possible to see there are different propulsion concepts for different ranges of specific impulse and thrust. However, not all of them are applicable for all types of mission mainly because some missions pose strict requirements in terms of power, mass, and volume.

Propulsion systems such as Pulsed Plasma Thruster, Electrospray Thruster and Ion Thruster have a high specific impulse, but low power efficiency, for instance, to achieve a thrust level of 1 mN it is necessary to provide a power of more than 30 W. Chemical propulsion systems using liquid propellants or solid propellants usually need very low power consumption and provide higher thrust level, but their high temperature is a limitation for miniaturized spacecraft. Water electrolysis thrusters may be interesting for some very small satellite missions, but the thrust level is relatively high for requirements such as the ones showed in Tables 1.1 and 1.2. To accomplish these requirements Cold Gas and Micro-Resistojets are the most promising ones.

The main advantage of Cold Gas is that relatively low power is needed, but the disadvantage is that it usually requires high pressure to store the propellant. Additionally, the specific impulse is limited to about 70 s. Nevertheless some missions such as the Orbcomm, Inspector, Rapideye, and UK-DMC satellites have already used the Cold Gas thruster in an orbit demonstration using Xenon or Nitrogen as propellant (Amri and Gibbon, 2012). Cold gas thrusters have also been flown on board of very small satellites such as the CanX-2 (Rankin et al., 2005) and Delfi-N3xt (Guo et al., 2016) satellites.

On one hand, Micro-resistojets need more power than Cold Gas thrusters. On the other hand, the propellant can be easily stored as liquid or solid decreasing dramatically the storage pressure, and the specific impulse is higher than that of Cold Gas thrusters. Resistojet propulsion systems for mini- and micro-satellites have also been used in missions such as UK-DMC, UoSAT-12, and Alsat-1 satellites using Butane and Nitrous Oxide as propellant (Amri and Gibbon, 2012). However, micro-resistojets for very small satellites are still under development and have not flown yet. Additionally, the micro-resistojet has interesting characteristics such as high integration capability, small volume, low mass, fast response, high reliability, and easy integrability in a thruster array (Amri and Gibbon, 2012).

Besides thruster performance needs, all the roadmaps of space agencies urge the need of moving towards “green” space systems (Meyer and Johnson, 2015; ESA, 2015). Many propellants are known for their high potential hazards in a propulsion system. One well known example is hydrazine, which is both toxic and carcinogenic. Space agencies are actively working to find an alternative to these propellants, as an important step towards low hazard and reduced cost and a way to provide viable and safer alternatives to the space industry. Current nano- and pico-satellite regulations demand for propellants

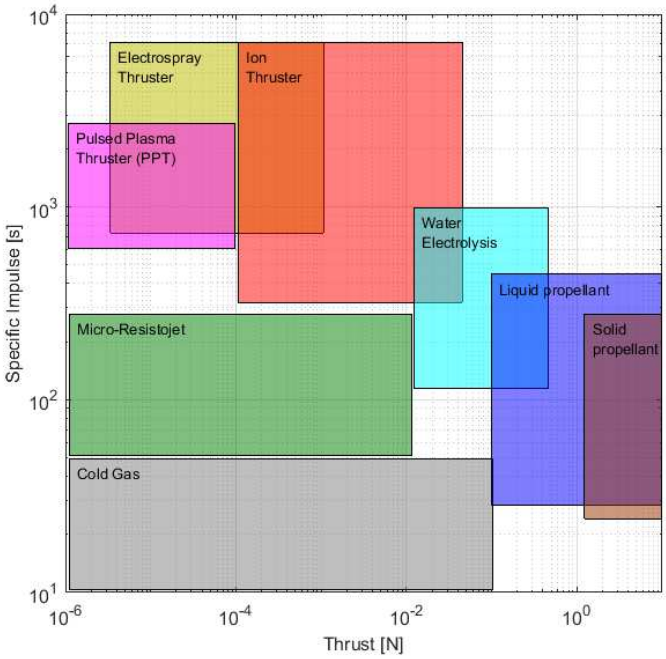

Figure 1.4: Estimated performance of different micro-propulsion systems based on (Silva et al., 2018; Krejci and Lozano, 2018; Tummala and Dutta, 2017).

that shall be non-corrosive, non-flammable and non-toxic (Gohardani et al., 2014).

Based on this analysis, the Space System Engineering (SSE) chair at Delft University of Technology (TU Delft) is currently developing two green micro-resistojet concepts in order to provide future nano- and pico-satellites with the capability of performing maneuvers. They are known as Vaporizing Liquid Micro-Resistojet (VLM) and Low-Pressure Micro-Resistojet (LPM) (Cervone et al., 2017). The main difference between them is the working pressure level, the VLM works under a pressure in the order of 10^5 Pa while the LPM works under a pressure in the order of 10^2 Pa. Cervone et al. (2017) have made a comparison between the two concepts where they showed a similar performance under similar temperature conditions and with the same amount of propellant. The LPM has the advantage of working under a much lower pressure which results in a lighter and more reliable system. Another advantage is that the LPM can move at any power level, including cold gas conditions. This PhD thesis is focused on the LPM.

1.2.1. FUNDAMENTAL THEORY

From space propulsion theory, thrust $\Im$ and specific Impulse I_{sp} are the two parameters used to estimate the thruster performance. The theoretical thrust is well known to be the sum of momentum thrust $\Im_m$ and pressure thrust $\Im_p$ as

$$\Im = \Im_m + \Im_p = \dot{m} u_e + (P_e - P_a) A_e \tag{1.1}$$

where $\dot{m}$ is the mass flow rate, u_e is the exhaust velocity, P_e is the exhaust pressure, P_a the external ambient pressure. The specific impulse is the total impulse delivered per unit weight of consumed propellant expressed as

$$I_{sp} = \frac{\Im}{\dot{m} g_0} \tag{1.2}$$

where g_o is the Earth gravitational acceleration at sea level. Another well known parameter used when designing a mission is the velocity increment (ΔV) or just Delta-V. For cases when the propellant mass used is significantly small compared to the total spacecraft mass ($\frac{M_p}{M} \ll 1$), the Delta-V can be calculated by using the linear approximation of the rocket equation:

$$\Delta V = g_0 I_{sp} \frac{M_p}{M} \tag{1.3}$$

where M is the initial spacecraft mass and M_p is the propellant mass. Different methods are applied to define the mass flow rate, the exit velocity, and the exit pressure, due to the different fluid dynamics involved. For instance, the VLM works in the continuum flow regime which uses the classical Ideal Rocket Theory equations. The equations 1.4, 1.5, 1.6, and 1.7 are derived based on the three conservation laws mass, momentum and energy using a few assumptions such as perfect gas, calorically ideal gas, homogeneous and constant chemical composition, steady state, isentropic, purely axial, no external forces, and negligible velocity at the chamber. The mass flow rate can be calculated as

$$\dot{m} = \frac{p_c \cdot A^*}{\sqrt{\frac{R_A}{M_w} \cdot T_c}} \cdot \Gamma \tag{1.4}$$

where p_c is the chamber pressure, A^* is the nozzle throat area, R_A the universal gas constant, M_w the molecular mass, T_c the chamber temperature, and Γ the Vandenkerckhove function of the specific heat ratio γ, defined as

$$\Gamma = \sqrt{\gamma \cdot \left(\frac{1+\gamma}{2}\right)^{\frac{1+\gamma}{1-\gamma}}}. \tag{1.5}$$

In addition, the nozzle expansion ratio (ratio of the exit area to the throat area) is a function of the pressure ratio (ratio of exit pressure to chamber pressure), according to the following equation

$$\frac{A_e}{A^*} = \frac{\Gamma}{\sqrt{\frac{2\gamma}{\gamma-1} \cdot \left(\frac{p_e}{p_c}\right)^{\frac{2}{\gamma}} \cdot \left[1 - \left(\frac{p_e}{p_c}\right)^{\frac{\gamma-1}{\gamma}}\right]}}. \tag{1.6}$$

Finally, the nozzle exit velocity (jet velocity) can be calculated as

1

$$u_e = \sqrt{\frac{2\gamma}{\gamma-1}\cdot\frac{R_A}{M_W}\cdot T_c\cdot\left[1-\left(\frac{p_e}{p_c}\right)^{\frac{\gamma-1}{\gamma}}\right]}. \tag{1.7}$$

1.3. LOW-PRESSURE MICRO-RESISTOJET STATE-OF-THE-ART

The Low Pressure Micro-Resistojet (LPM) is an extension of a similar design previously developed and tested by Ketsdever et al. (2005), called Free Molecule Micro-Resistojet (FMMR). This propulsion system concept is divided into three main parts: tank, feed system, and thruster, see Figure 1.5. The tank stores the propellant in solid or liquid state, and a heater is used to sublime/evaporate the propellant. The feed system is basically composed of a valve which receives the opening or closing command allowing the passage of the propellant vapour. The thruster is composed of a plenum and a heater chip where the propellant gas is expelled to outer space. The heater chip is usually made of silica wafer and presents a grid of straight microchannels which heat up the propellant increasing its velocity. On the right hand side of Figure 1.5, an example of microchannel is shown where L is the length of the microchannel, a represents the small cross-sectional dimension in case of a cuboid microchannel and d represents the diameter in case of a circular microchannel. This propulsion system has the main characteristic to work in the rarefied flow regime.

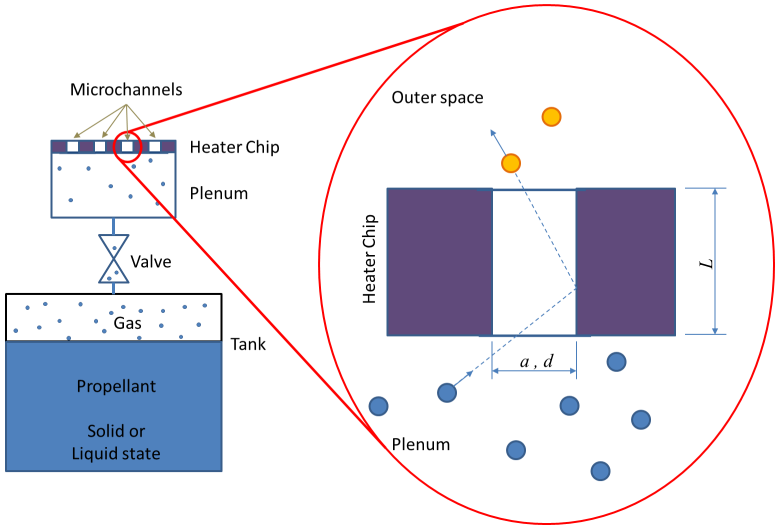

Figure 1.5: Schematic of the LPM. Left: the complete system composed by tank, feed system and thruster. Right: The detailed microchannel and the particles behavior.

The first design of the thruster part was proposed in the late 90's (Ketsdever et al., 1998), see Figure 1.6. The heater is uncoupled with the expansion slots chip meaning that the molecules are heated before reaching the slots where they are expelled generating thrust. In 2005 (Ketsdever et al., 2005), a new design was proposed where the heater is now coupled with the expansion slots chip and then called heater chip as showed in

Figure 1.7. In this version, the molecules are heated up inside the slots and then expelled giving thrust. The heater chip was manufactured using micro-electro-mechanical system (MEMS) technology. The Silica wafer was used as main structural part with a deposition of a gold layer for the heaters. The heater chip presents 44 expansion slots with 100 μm width, 5.375 mm length and 500 μm thickness, which is the thickness of the Silica wafer. In 2013, Palmer et al. (2013) fabricated and tested a different design with thick silicon dioxide insulation and suspension to reduce the heat losses improving the thruster efficiency. They showed that it is possible to keep the temperature at about 270 °C in the heated walls, while the surrounding silicon is about 50 °C.

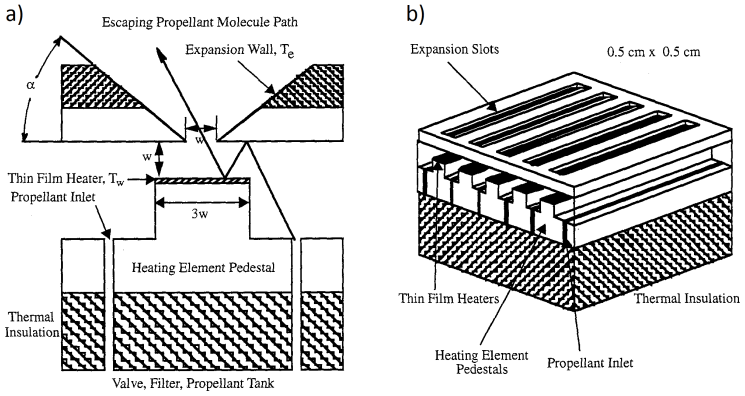

Figure 1.6: First FMMR conceptual design schematic: a) 2D - Cross section and b) 3D - Multislot configuration. From Ref. (Ketsdever et al., 1998).

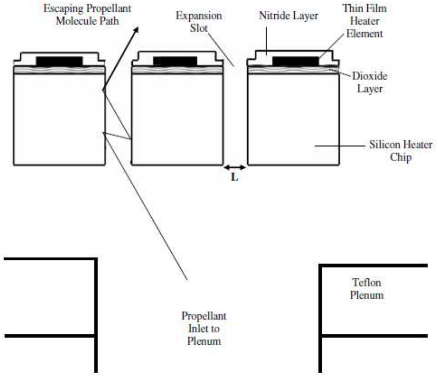

Figure 1.7: Second FMMR conceptual design schematic. From Ref. (Ketsdever et al., 2005).

Cervone et al. (2015b) present a complete conceptual design of the Low-Pressure Micro-Resistojet (LPM) system based on a subliming solid propellant, see Figure 1.8. The tank works under sublimation conditions at low pressure of about 600 Pa. The propellant vapour goes through a plenum and is expelled through heater chip slots to outer

space, producing thrust. They also proposed an optimized expansion slot of 200 × 500 μm with 15° divergence angle for the last half of the expansion slot length.

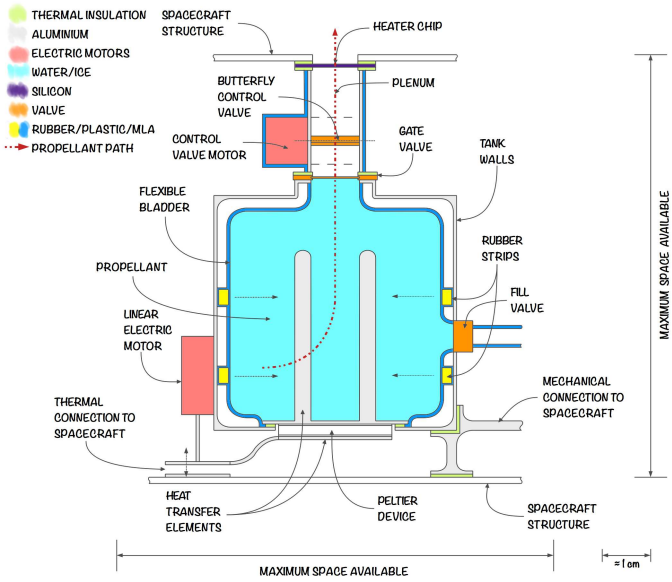

Figure 1.8: The design concept proposed by Cervone et al. (2017).

This particular propulsion concept based on rarefied gas dynamics was indicated as an alternative to meet the specific requirements and constraints imposed by nano- and pico-satellites. It presents several advantages when compared to more traditional micro-thrusters, such as reduced tank pressure, lower power consumption, avoidance of nozzle plugging, ease and flexibility of construction and reduced valve actuation (Ketsdever et al., 1998; Cervone et al., 2017).

1.3.1. THEORETICAL BACKGROUND

The LPM cannot be modeled based on the continuum flow regime as the example presented in Subsection 1.2.1, instead, the rarefied gas dynamics must be applied. Rarefied gas dynamics is important in different applications such as vacuum technology and space dynamics, but it is becoming even more popular in the microfluidics field (Lafferty, 1998; Muntz, 1989). The Knudsen number (Kn) is the dimensionless number which defines the degree of gas rarefaction. It depends on the average distance travelled by the molecules between collisions, known as the mean-free path (λ), and a characteristic dimension of the flow (L_0), and is expressed as $Kn = \lambda / L_0$. Different rarefied gas dynamics regimes are defined, depending on the value of Kn: continuum flow regime with slip flow ($0.1 > Kn > 0.01$); transitional flow regime ($10 > Kn > 0.1$); and free-molecular flow regime ($Kn > 10$) Karniadakis et al. (2005).

The flow behaviour inside the microchannel (nozzle part of the LPM) can be studied using the transitional flow regime equations. In this regime the Boltzmann equation is often used to describe the fluid dynamics, and it is define as follows

$$\frac{\partial(f)}{\partial t} + \frac{\mathbf{p}}{m_a} \cdot \frac{\partial(f)}{\partial \boldsymbol{r}} + \mathbf{F} \cdot \frac{\partial(f)}{\partial \boldsymbol{p}} = \left(\frac{\partial f}{\partial t}\right)_{coll} \tag{1.8}$$

where f is the Maxwell–Boltzmann probability distribution function defined as

$$f(\mathbf{c}) = \left(\frac{m_a}{2\pi kT}\right)^{3/2} e^{-\frac{m_a(\mathbf{c}^2)}{2kT}} \tag{1.9}$$

where m_a is the mass of the particles, $\mathbf{p}$ the momentum vector, $\mathbf{r}$ the position vector, $\mathbf{F}(\mathbf{r}, t)$ the external force vector, k is the Boltzmann's constant, T is the thermodynamic temperature and $\mathbf{c}$ is the particle velocity vector Bird (1994). The right term of Equation 1.8 describes the effect of collisions between particles. In the transitional flow regime the effect of collisions plays an important role with the fluid dynamics, mainly because the flow is a non-isothermal condition. It makes the Boltzmann equation a non-linear equation which is usually solved by numerical simulations such as Direct Simulation Monte Carlo (DSMC) and Discretization method as Lattice gas cellular automata methods.

Ketsdever et al. (2005) have proposed an analytical model to approximately estimate the thruster performance based on the transitional regime theory. One of their main assumptions was to neglect the pressure thrust $\Im_p$ simplifying the Thrust Equation (Equation 1.1) to $\Im = \dot{m}u_e$. Then, they proposed the thrust equation as

$$\Im = \dot{m}u_e = \frac{\alpha P_0 A_e}{2}\sqrt{\frac{T_w}{T_0}} \tag{1.10}$$

and the specific impulse equation as

$$I_{sp} = \frac{\Im}{\dot{m}g_0} = \sqrt{\frac{\pi kT_w}{2mg_0^2}} \tag{1.11}$$

where P_0 is the plenum pressure, m is the mass of propellant molecules, k the Boltzmann constant, T_0 the plenum temperature, T_w the heater chip temperature, A_e the exit area, and α the transmission coefficient. The transmission coefficient, which is also known as conductance (Lafferty, 1998) or dimensionless mass flow rate (Sazhin, 2008; Varoutis et al., 2008), is a parameter that represents the actual mass flow rate ($\dot{m}$) to the mass flow rate in free molecular limit ($\dot{m}_{fm}$), thus $\alpha = \dot{m}/\dot{m}_{fm}$. The transmission coefficient is usually lower than 1 because the actual mass flow rate under the rarefied condition depends on the aspect ratio of the expansion channel, defined as thickness to diameter ratio. Basically, the mass flow rate decreases with increasing aspect ratio, meaning that for an infinitely thin channel the transmission coefficient is equal to 1. For instance, a cylindrical channel with an aspect ratio of 5 implies a transmission coefficient equal to 0.19 (Lafferty, 1998; Varoutis et al., 2008).

1.4. RESEARCH MOTIVATION AND THESIS ROADMAP

As described previously the LPM has the potential to be one of the main choices as propulsion system for nano- and pico-satellites. However, it is still in a maturation technology phase, in terms of Technology Readiness Level (TRL) means TRL-2. Some LPM features still need to be explored and explained in a scientific and engineering context.

This PhD thesis aims to fulfill some current scientific and engineering lacks of the LPM development.

Even though there are some known propellants able to deliver a high thrust performance, they usually do not meet the typical requirements for nano- and pico-satellites. Either they are classified as hazardous or need to be stored under very high pressure to achieve the desired Delta-V. Based on that, the first research question (**RQ1**) is: **Which is the most promising "green" propellant for the proposed propulsion concept?**. In order to answer this research question, Chapter 2 presents a methodology for selection and characterization of propellants to be applied to the LPM or the VLM. 95 different fluids are investigated including conventional and unconventional propellants. A feasibility assessment step is carried out following a trade-off using a combination of the Analytical Hierarchy Process (AHP) and the Pugh matrix. A final list of nine best-scoring candidates is analyzed in depth with respect to the thermal characteristics involved in the process, performance parameters and safety issues.

As already discussed this propulsion system works under very low pressure, and the fluid dynamics of the system cannot be studied by means of the usual continuum Navier-Stokes equations. Rarefied gas dynamics has to be applied. Based on that, the second research question (**RQ2**) is: **How can we describe the fluid dynamics and the thermal properties of the fluid used in propulsive applications at high values of Knudsen number?**. To this end, a Direct Simulation Monte Carlo simulation (DSMC) numerical solver is used in order to describe the fluid and thermal behaviour through the microchannels (nozzles). Additionally, a sensitivity analysis is performed aiming to define the best microchannel geometry to be applied as thruster. This is presented in Chapter 3.

As highlighted in the previous section the actual thruster performance is therefore significantly different to the one estimated with the classical Ideal Rocket Theory. Additionally, an analytical model has been proposed by Ketsdever et al. (2005), but it is used just as an approximated estimation. Based on that, the third research question (**RQ3**) is: **How accurately can an analytical model characterize the performance of the proposed propulsion concept?**. In order to answer this research question, an analytical model is proposed in Chapter 4 as an improvement of the model proposed by Ketsdever et al. (2005). They neglect the pressure thrust which in fact should not be neglected according to what is presented in Chapter 3. The analytical model is based on the Kinetic theory of gases and the Maxwell-Boltzmann distribution of molecular velocities to describe the macroscopic flow parameters such as mass flow rate, velocity and pressure, and then to estimate the thruster performance. The equations are well known, but they are applied in this case using a particular approach in order to describe the physics behind this micro-propulsion system. Comparisons between numerical simulations using the DSMC method and the results of the analytical model, as well as experimental results, are carried out.

This propulsion system is proposed to be applied to very small satellites where mass, volume and power are important factors to be taken into account. A natural last question is related to the optimization of this system to be suitable to very small satellites. Therefore, the fourth research question (**RQ4**) is: **Which optimization technique can be used for the proposed propulsion concept, and what is the result of this optimization?**. In order to answer this research question, it is necessary not just to look at the research

perspective, but also at the engineering perspective. One of the main challenges is how to have a miniaturized and integrated propulsion system, therefore Chapter 5 is exclusively dedicated to design, fabricate and characterize the heater chip of the proposed propulsion system. Based on the knowledge acquired from the performed experiments and the answers of RQ1, RQ2, and RQ3, Chapter 6 is used to optimize the LPM for very small satellites using two different mission cases. One is a CubeSat with two satellites flying in formation (Table 1.1), and the other a PocketQube mission which will be used as a flight demonstration platform (Table 1.2).

2

Selection And Characterization Of Green Propellants

How could they see anything but the shadows
if they were never allowed to move their heads?

Plato, The Republic

One of the key points to address in the development of micro-propulsion systems is the propellants selection since it directly influences their performance. This chapter presents a methodology for the selection and characterization of fluids that is suitable for use as propellants in two micro-resistojet concepts: Vaporizing Liquid Micro-Resistojet (VLM) and Low-Pressure Micro-Resistojet (LPM). In these concepts, the propellant is heated by a non-chemical energy source, in this case an electrical resistance. In total 95 fluids have been investigated including conventional and unconventional propellants. A feasibility assessment is carried out following a trade-off using a combination of the Analytical Hierarchy Process (AHP) and the Pugh matrix. A final list of nine best-scoring candidates has been analyzed in depth with respect to the thermal characteristics, performance parameters and safety issues.

The content of this chapter has been published in ASME Journal of Heat Transfer **139**, 10 (2017).

2.1. INTRODUCTION AND REQUIREMENTS

Due to the significant high number of potential choices, propellant selection is a difficult trade-off between performance, safety, and any other desired features such as density, heat capacity, storability, and availability (Sutton and Biblarz, 2010). A selection methodology is proposed in this chapter to provide a fair comparison of propellants in the specific case of micro-resistojets. This methodology is divided into four steps: 1) data collection of the 95 fluids that have been selected, 2) feasibility assessment to discard unfeasible fluids in terms of storage, 3) Analytical Hierarchy Process (AHP) tool (Zahedi, 1986) with Pugh Matrix (Pugh, 1991) comparison to classify the selected feasible fluids in terms of safety and design, and 4) final analysis regarding thermal characteristics, propulsive performance and safety.

The miniaturization of satellites creates constraints mainly in size, mass, and power, that have to be taken into account when designing propulsion subsystems. Moreover, those satellites are usually put into orbit by piggy-back launchers and, due to that, launch providers impose a number of constraints related to the safety of the main payload of the rocket. Other constraints come from the standardization of these satellite classes as well as the specific mission.

As an example, the requirements proposed in Cervone et al. (2015a) for a formation flying mission are considered here, see Table 1.1. Each mission has its own specific requirements, but the ones listed in the table represent a good example of a typical formation flying mission in low altitude Earth orbits, which is expected to become a more and more common type of mission for small satellites. These requirements will be used as a reference along the chapter.

From these suggested requirements, guidelines for the propellant selection are derived. The main points of interest, later on used as selection criteria, are performance (associated mainly to thrust and specific impulse), system density (associated to mass and size), and safety. Other characteristics such as power consumption can be more relaxed as they also depend on other factors, such as structural design, solar panel design, mission design and operation management (for example, the operation of the engines can be restricted to when the batteries are full or during eclipse).

The safety level can be divided in turn into flammability, instability and health hazard. It is discussed here based on the possible consequences of these different aspects. The flammability and instability of the propellant have two main consequences: one is the reduction of the satellites' reliability and the other is associated to the risks for the main payload (in case of a piggy-back launch). The health hazard concerns the propellant handling before launch. This can be seen from two different perspectives, depending on whether the satellite is assembled by integrator companies, that normally have the proper facilities to handle hazardous propellants, or by Academic groups, that usually have more limitation on these facilities and prioritize the safety of their students and researchers.

2.2. SELECTION METHODOLOGY

The methodology to select the most suitable propellant is based on four sequential steps:

1. Data Collection

2. Feasibility Assessment

3. AHP and Pugh Matrix

4. Analysis

The first step is to collect data on a large number of fluids that could be used as propellants in micro-resistojet systems. The second step is to select, among the identified fluids, only the ones which might be feasible to work on. The third step is to use the Analytical Hierarchy Process (AHP) combined with a Pugh Matrix tool to compare the remaining fluids with respect to the three main criteria: performance, system density, and safety. Finally, the fourth step is to analyze in a more detailed manner the substances that score the highest in the previous step.

In the data collection step, a total of ninety-five fluids used in engineering applications were considered, including single and compound chemical substances. These include fluids typically used as refrigerants, fuels, propellants, oxidizers, but also fluids used in everyday life. The list of all fluids can be seen in Appendix-A.

In the feasibility assessment, the main criteria considered were: the required pressure to correctly store the propellant in the tank, and the required propellant mass. Looking at the requirements listed in Table 1.1, the only option is to store the propellant as a liquid or a solid, due to the low density achieved if stored as a gas at the required maximum pressure. The fluids that cannot be liquid or solid at a temperature of 293.15 K and pressure of 10 bar (1 MPa) or lower were discarded. In this stage, the most common fluids used by cold gas thrusters, such as Nitrogen and Carbon Dioxide, were excluded.

The criteria selected for the Pugh Matrix are classified into a first (FL) and second (SL) level. The first level includes the safety branch and design branch. The second level better specifies the safety criterion into flammability, instability and health hazard, and the design one into performance and system density. The weighting factor (WF) for each criterion was defined by using the AHP tool. Figure 2.1 shows the decision hierarchy from how the WR (Weight Ratio) was considered. Five academic staff members from the Space System Engineering chair at TU Delft performed a pairwise comparison of the criteria in order to define the values of WF.

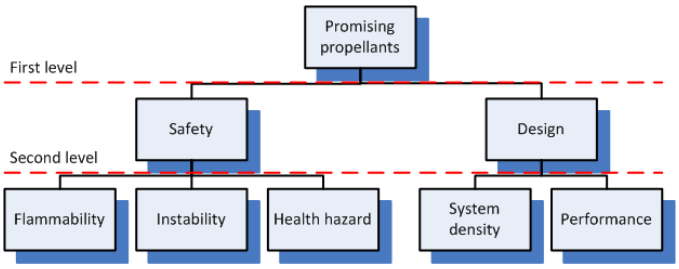

Figure 2.1: The hierarchy used in the AHP in order to get the weight ratio for each criterion.

The WF considered in this work is ranged from 1 to 6, where 1 means least important and 6 means most important. For each criterion, based on the pairwise comparison, a different WF was defined in accordance to the resulted WR. It was done as follows:

$$WF_i = \frac{WR_i^{FL}}{WR_{\max}^{FL}} \cdot \frac{WR_i^{SL}}{WR_{\max}^{SL}} \cdot WF_{\max} \tag{2.1}$$

where i is the criteria, FL is the first level, SL is the second level, and the WF_{max} is equal to 6 in this case. Table 2.1 presents the WF for each one of the evaluators that performed the pairwise comparison. Each of these WF is used in different Pugh Matrices resulting in different outcomes that are dependent on the specific values given by each evaluator.

Table 2.1: Weight Factor (WF) result of each evaluator from the pairwise comparison, compared to the average $\overline{WF}$ and standard deviation σ among all evaluators.

WF	1	2	3	4	5	$\overline{WF}$	σ
Flammability	1.9	5.6	0.9	1.3	1.5	2.2	1.7
Health hazard	3.3	2.4	4.0	6.0	2.0	3.5	1.4
Instability	6.0	6.0	1.5	3.6	3.2	4.1	1.7
Performance	6.0	6.0	6.0	4.0	6.0	5.6	0.8
System density	4.0	4.0	4.0	2.7	6.0	4.1	1.1

The other element of the Pugh Matrix are the scores given in each criterion to each fluid. The fluids were scored by + (positive), − (negative), or 0 (neutral) in all criteria.

From the safety perspective, Ref. (NFPA, 2010), was used to derive the scores. All criteria indicated in this document were considered in the analysis except, for the sake of simplicity, the special hazards. If special hazards are present for a selected fluid, a specific additional analysis is expected to be done. The 0-4 range used in (NFPA, 2010) to quantify the degree of hazard in each category was translated into a trade-off score by considering 2 as neutral (0), 0 and 1 as positive (+), and 3 and 4 as negative (−).

From an engineering perspective, a simplified first-order approximation was used to derive the scores. It is known that the specific impulse is inversely proportional to the square root of the molecular mass. Using this approximation, a value lower than 30.5 $\mathrm{g\,mol^{-1}}$ is considered as positive (+), higher than 69.5 $\mathrm{g\,mol^{-1}}$ as negative (−), and between them as neutral (0). Looking at the system density, since the remaining fluids were in a range of density from 500.56 $\mathrm{kg\,m^{-3}}$ to 1636.80 $\mathrm{kg\,m^{-3}}$ at 283.15 K and 1 MPa, a density lower than 879.31 $\mathrm{kg\,m^{-3}}$ was scored as positive (+), higher than 1258.05 $\mathrm{kg\,m^{-3}}$ as negative (−), and between them as neutral (0). Those values were considered into the range between the lowest and the highest molecular mass or density divided by three.

With all settings defined, the Pugh Matrix was completed for each evaluator with their different defined WF. Following this step, the Pugh Matrix result for each fluid, specific of each evaluator, was used to calculate an average score and a standard deviation. After that the result was used to select a final group of the most promising fluids.

This detailed analysis (final step of the selection method) has been carried out for the two different resistojet concepts, the VLM and the LPM. The performance factors considered in this analysis were the thrust, the specific impulse and the power needed to heat up the propellant. Equations 1.1 and 1.2 are used to calculate the thruster performance of the VLM and LPM using the parametric equations presented in Chapter 1.

In the LPM case, the exit pressure was estimated from the results obtained in (Guerrieri et al., 2016), where it was shown that the pressure thrust (second term on the right-hand side of Equation 1.1) represents about 42% of the total thrust for a heater chip based on microchannels.

2.3. APPLICATION OF THE METHODOLOGY AND RESULTS

From the feasibility assessment step, 63 fluids were selected (see the complete table provided in Appendix-A for more details). All those fluids were evaluated by means of a Pugh Matrix, with different criteria and different weights based on the evaluators perspectives, as explained in the previous section. The result of the Pugh Matrix evaluation is shown by the boxplot in Figure 2.2 in terms of average score and standard deviation of evaluations based on each expert's weights. The scores can go up to 30 which is the score for an ideal substance where all criteria score the maximum possible points (6). Similarly, a score of −30 represents the worst possible substance.

Based on the Pugh Matrix results, the nine best-scored fluids were selected for further performance analysis, namely: Acetone, Ammonia, Butane, Cyclopropane, Ethanol, Isobutane, Methanol, Propene, and Water. All other fluids, even in their best-case score, would receive less points than the worst-case score of any of these nine selected fluids.

Figure 2.3 shows the saturation curve of each selected fluid in terms of pressure and temperature. Even though the saturation curve allows us to understand the thermodynamic state of the fluid independently on the resistojet concept considered, it is also necessary to analyze the two concepts separately, since they work at operational pressures on different orders of magnitude.

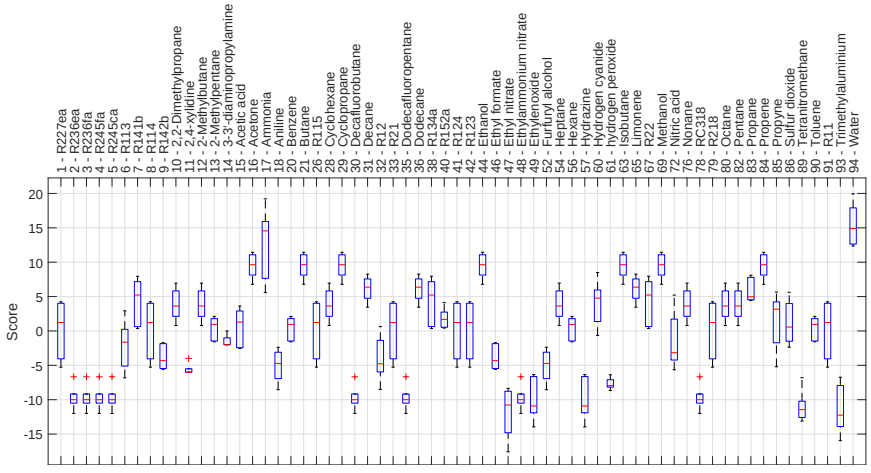

Figure 2.2: Results of the Pugh Matrix presented as a boxplot where the red line is the median, the upper and lower borders of the box represent the upper and lower quartiles respectively, the black line is the maximum and minimum value, and the red crosses represent the outliers.

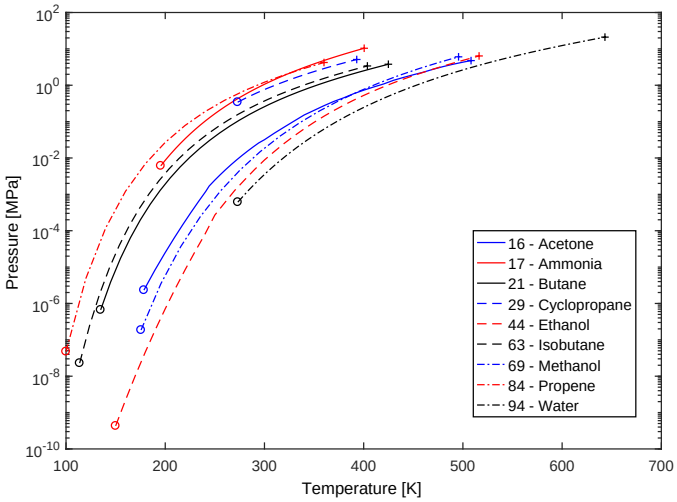

Figure 2.3: Saturation curve. ^{o} denotes the triple point and $^{+}$ denotes the critical point. The fluid is liquid on the left side of the curve, and gaseous on its right side.

2.3.1. VLM PERFORMANCE

To analyse the VLM performance some assumptions are needed. The VLM design characteristics have been taken according to the current design of TU Delft's VLM (Cervone et al., 2017), where the nozzle expansion ratio ($\frac{A_e}{A^*}$) is 11, the chamber pressure (P_c) varies from 200 kPa to 500 kPa , and the chamber temperature varies within different ranges depending on the fluid, as shown by Table 2.2 and Table 2.3. These chamber temperature ranges are the average maximum and minimum commonly found in literature for VLMs (Cheah and Low, 2015; Kundu et al., 2012; Cen and Xu, 2010; Chen et al., 2010; Karthikeyan et al., 2012). In addition, it is assumed that at the inlet of the micro-resistojet chamber, before heating, the propellant temperature is 283.16 K.

Table 2.2: Chamber temperature, mass flow rate and thrust obtained with different propellants, for chamber pressures of 200 kPa (VLM case).

Propellant	T [K]	$\dot{m}$ [mg s^{-1}]	$\Im$ [mN]
16 - Acetone	360 - 550	2.79 - 2.25	1.82
17 - Ammonia	300 - 550	1.75 - 1.29	1.69
21 - Butane	300 - 550	3.03 - 2.24	1.83
29 - Cyclopropane	300 - 550	2.65 - 1.96	1.76
44 - Ethanol	370 - 550	2.46 - 2.01	1.80
63 - Isobutane	300 - 550	3.07 - 2.27	1.79
69 - Methanol	360 - 550	2.13 - 1.73	1.74
84 - Propene	300 - 550	2.62 - 1.94	1.79
94 - Water	400 - 550	1.56 - 1.33	1.69

Table 2.3: Chamber temperature, mass flow rate and thrust obtained with different propellants, for chamber pressures of 500 kPa (VLM case).

Propellant	T [K]	$\dot{m}$ [mg s^{-1}]	$\Im$ [mN]
16 - Acetone	400 - 550	6.59 - 5.62	4.54
17 - Ammonia	300 - 550	4.37 - 3.23	4.23
21 - Butane	330 - 550	7.22 - 5.59	4.58
29 - Cyclopropane	300 - 550	6.63 - 4.90	4.41
44 - Ethanol	400 - 500	5.90 - 5.04	4.51
63 - Isobutane	320 - 550	7.44 - 5.67	4.49
69 - Methanol	390 - 550	5.13 - 4.32	4.35
84 - Propene	300 - 550	6.56 - 4.84	4.47
94 - Water	430 - 550	3.76 - 3.33	4.22

Figure 2.4 presents the needed enthalpy to increase the propellant temperature under the given conditions. Some fluids, in the initial conditions considered here (283.16 K and 200 kPa), are still liquid and need a phase change to become gaseous. This leads to a significantly higher required enthalpy to achieve their final temperature.

Under the above explained assumptions, Figure 2.5 shows the ranges of heating power and specific impulse for each propellant. Ammonia shows the best performance or, in other words, a higher specific impulse with a lower power consumption.

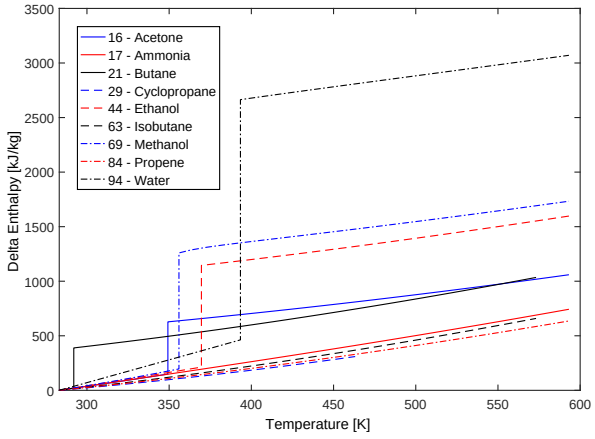

Figure 2.4: Delta Enthalpy for each propellant, at a chamber pressure of 200 kPa, as a function of the desired final chamber temperature.

2.3.2. LPM PERFORMANCE

To analyse the LPM performance some assumptions are also needed. The LPM characteristics have been taken according to one of the current design of TU Delft's LPM, with

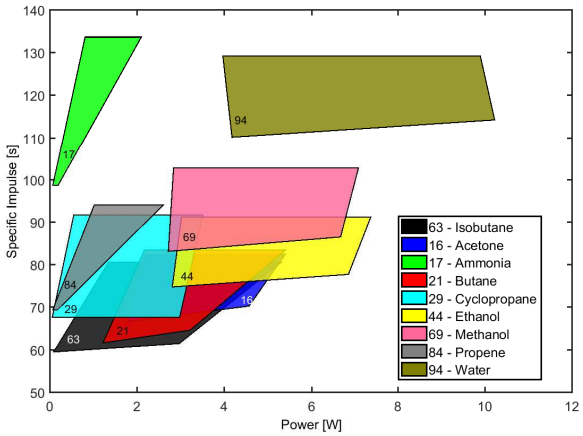

Figure 2.5: Specific Impulse vs. Heating Power for various propellants (VLM case) according to the variations of temperature and pressure considered in Table 2.2, and Table 2.3.

a grid of 67×67 circular microchannels with an aspect ratio of 5 in a 10×10 mm heater chip area (Guerrieri et al., 2015). The total cross-sectional exit area (A_e) of the channels is equal to 10,000 μm^2, and the transmission coefficient for this kind of holes is equal to 0.19 (Lafferty, 1998). The temperature varies from 300 to 700 K, and the plenum pressure from 50 to 300 Pa. These values are the average maximum and minimum commonly found in the literature regarding LPMs (Ketsdever et al., 2005; Ahmed et al., 2005; Lee et al., 2007; Palmer et al., 2013). In addition, it is assumed again that at the inlet of the plenum the temperature is 283.16 K.

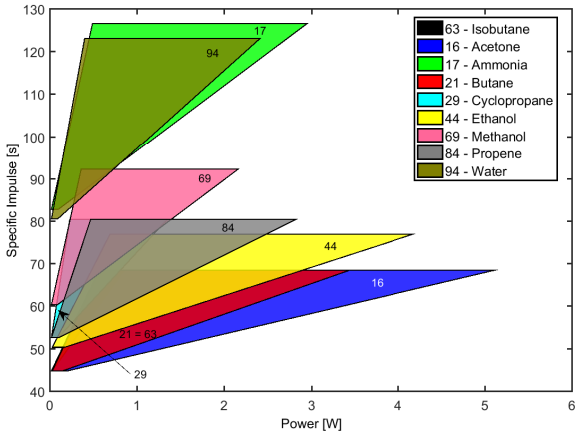

Figure 2.6: Specific Impulse vs. Heating Power for various propellants (LPM case) according to the variations of temperature and pressure considered in Table 2.4.

Under those assumptions, Figure 2.6 shows the relation between heating power and specific impulse for each propellant. Ammonia and water show the best performance in this case, as they provide a high specific impulse with a similar level of required power as the others.

Table 2.4 presents the mass flow rate for the plenum pressure of 50 and 300 Pa, and for a range of wall temperatures from 300 to 700 K. It is important to emphasize that according to the theory presented in Subsection 1.3.1 the temperature does not affect the mass flow rate. Additionally, the thrust range varies from 0.39 to 3.59 mN independently of the kind of fluid, depending only on the setting of temperature and pressure.

Table 2.4: Mass flow rate obtained with different propellants for a temperature range from 300 to 700 K and two different pressures (LPM case).

Propellant	$\dot{m}$ [mg s^{-1}] for 50 Pa	$\dot{m}$ [mg s^{-1}] for 300 Pa
16 - Acetone	0.89	5.34
17 - Ammonia	0.48	2.89
21 - Butane	0.89	5.34
29 - Cyclopropane	0.76	4.55
44 - Ethanol	0.79	4.76
63 - Isobutane	0.89	5.34
69 - Methanol	0.66	3.97
84 - Propene	0.76	4.55
94 - Water	0.50	2.98

2.4. DISCUSSION

Performance, although very important in the design of propulsion systems, is not always the main criterion in the selection of a design option. Safety is also very important and has to be taken into account when designing micro-propulsion systems, recalling that they are usually designed for small missions that have limitations in the budget or are for educational purposes. The former results in a need to reduce costs related to the use of dedicated facilities or special equipment for handling the propellant, and the latter is to assure the safety of students and researchers.

2.4.1. PERFORMANCE

In terms of performance, as anticipated in the previous sections, it is possible to rank the propellants according to different parameters. In terms of thrust for the VLM, although the values are quite similar among the different analysed propellants, it can be seen in Table 2.2 and Table 2.3 that Acetone and Butane present the best values, and Ammonia and Water present the worst values. For the LPM the values are the same independently on the kind of propellant. However, more important performance parameters for a propellant are the specific impulse and the power consumption. Figure 2.5 and Figure 2.6 show that Ammonia, Water, and Methanol present the highest specific impulse values in both propulsion systems. The power consumptions are quite similar when looking at the

LPM, while in the VLM we can see a higher power consumption for water and Methanol than Ammonia. This is easily explained by the fact that a phase change is not needed for Ammonia, since it is already gaseous into the thruster. A complementary analysis is done in subsection 2.4.4, where the Delta-V will also be taken into account.

2.4.2. SAFETY

Table 2.5 shows the selected propellants level in terms of flammability, health hazard and instability. They do not present instability issues, with the exception of Propene that can become unstable at elevated temperatures and pressures. As a conclusion, instability is not expected to be a major aspect to be taken into account in the selection process.

Table 2.5: Safety characteristics of the selected propellants.

Propellant	Flammability	Health hazard	Instability
16 - Acetone	High	Low	N/A
17 - Ammonia	Low	High	N/A
21 - Butane	Extreme	Low	N/A
29 - Cyclopropane	Extreme	Low	N/A
44 - Ethanol	High	Low	N/A
63 - Isobutane	Extreme	N/A	N/A
69 - Methanol	High	Low	N/A
84 - Propene	Extreme	Low	Low
94 - Water	N/A	N/A	N/A

Most of the selected propellants present a low level of health hazard, meaning that exposure to them may cause irritation with only minor residual injury, and Water and Isobutane do not present any health hazard. On the other hand, Ammonia has the highest level of health hazard, with short exposure causing serious, temporary or moderate residual injury. In summary, the choice of ammonia as a propellant should be done only if the facilities and operators are well equipped to safely handle it.

All the organic fluids considered have high or even extreme level of flammability, meaning that they can be easily ignited under ambient temperature conditions. Water does not present any flammability, and Ammonia presents a low level of flammability, since it requires considerable preheating before ignition. As it is well known, having fire means meeting the fire triangle (oxygen, fuel, and heat), so this criterion should be analyzed from different perspectives when applied to micro-resistojets. When the satellite is in orbit, it is very unlikely to have ignition since there is no oxygen, thus there are no threats for the system. Even though during launch the tank is well sealed with very low possibility to leak, it could be an issue due to the restriction posed by the main payload. However, flammability may become an important issue while handling the propellant. The fluids with an extreme level of flammability have to be very carefully handled by well-trained operators, into well-equipped facilities since those substances will rapidly vaporize at normal atmospheric pressure and temperature, or are rapidly dispersed in

air where they could burn readily.

2.4.3. SYSTEM DENSITY

Table 2.6 presents the density of the considered propellants in their liquid state, at a pressure of 1 MPa and temperature lower than 293.15 K, the assumed best-case conditions into the tank. The lowest density is obtained for propene and the highest is for Water. Roughly speaking, Water fills the same volume with double the mass than Propene. Basically, from the miniaturization point of view, highest density is obviously the best case, because it allows for a higher propellant mass in the same volume.

Table 2.6: Density of the considered fluids, in their liquid state at a pressure of 1 MPa.

Propellant	Density [kg m^{-3}]
16 - Acetone	791
17 - Ammonia	610.33
21 - Butane	579.88
29 - Cyclopropane	627.53
44 - Ethanol	789
63 - Isobutane	558.24
69 - Methanol	791.88
84 - Propene	514.31
94 - Water	998.62

2.4.4. FINAL CONSIDERATIONS

The last comparison that needs to be done is related to velocity increments (ΔV)achieved with different fluids. This is an important parameter to estimate the performance of the propulsion system, when installed in a specific spacecraft. Equation 1.3 is used considering a nanosatellite of 3.6 kg that will perform a formation flying mission with the requirements indicated in Section 2.1. Figure 2.7 and Figure 2.8 present the Delta-V per volume of propellant, as a function of the heating power, for the two micro-resistojet concepts. In both cases, Water provides the best Delta-V per volume. For the VLM, water has also the highest power consumption, but this does not apply to the LPM, which presents similar power consumption for almost all propellants as we can see in Figure 2.8. This difference is due to the relatively high energy of vaporization of water which is needed in the process of the VLM while in the LPM, due to the low-pressure in the plenum, the water is already in a gaseous state in that part of the propulsion system. It is important to highlight these calculations do not take into account the needed power to be applied to the tank and feed system.

All the selected propellants have a potential to be selected for the specific mission requirements considered in this chapter. However, Water shows to be the most promising one, especially for the LPM. It scores very high in all the criteria considered, even though the power consumption is higher in the VLM case. It presents the highest Delta-V per unit volume, and no safety issues. Ammonia is, in fact, the superior one in terms

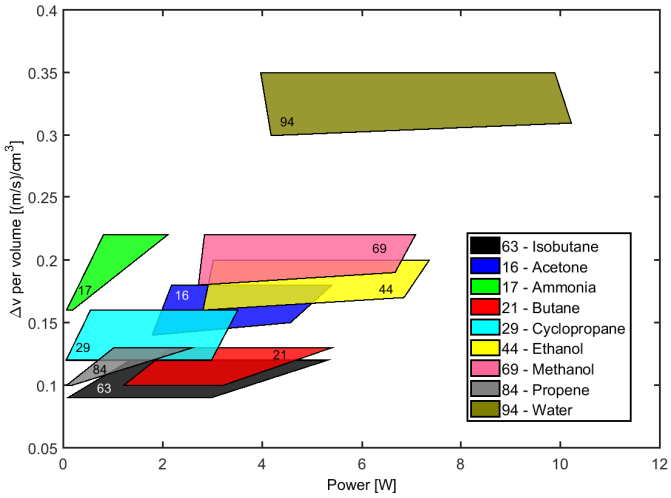

Figure 2.7: ΔV per volume of fluid vs. Heating Power (VLM case).

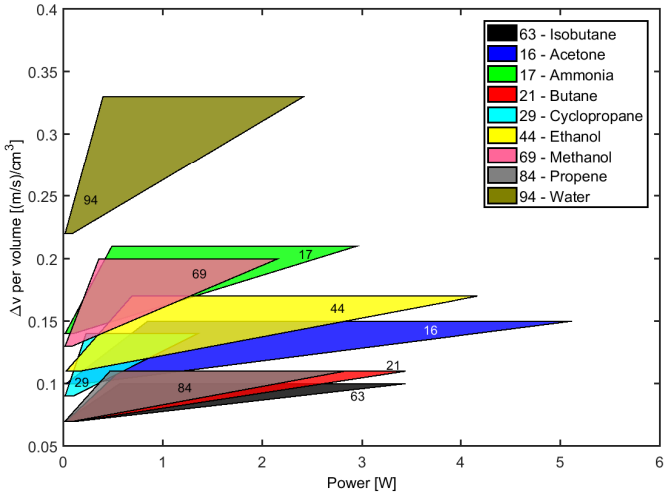

Figure 2.8: ΔV per volume of fluid vs. Heating Power (LPM case).

of Delta-V per unit volume to power ratio for the VLM. However, it presents the highest level of hazard that might be not appropriate for a large number of very small satellite missions.

2.5. CONCLUSIONS

A selection methodology was proposed to compare fluids that could be promising choices as propellant for micro-resistojets. This methodology helped in narrowing down the number of choices from 95 fluids to nine that were analysed in depth and discussed in terms of performance and safety. The methodology can also be extended to other applications with different micro-propulsion systems or other types of propellant.

It is shown that Water is the most promising propellant for both micro-resistojet concepts considered. Even though it has a higher power consumption, it also has the best velocity increment per volume of propellant, almost twice higher than all the other analysed fluids. Another important aspect is that Water is the safest propellant, and the easiest one to handle and acquire. However, other propellants from the top nine list might be interesting for other applications or missions.

Finally, this chapter and the analysis presented here can be considered as a reference for future developments of micro-propulsion systems, and in particular micro-resistojets.

3

NUMERICAL ANALYSIS OF DIVERGING MICROCHANNELS

The beginning is the most important part of the work.

Plato, The Republic

Heat transfer and fluid flow through different microchannel geometries in the transitional regime are analysed by means of Direct Simulation Monte Carlo simulations. Four types of three-dimensional microchannels, intended to be used as expansion slots in micro-resistojet concepts, are investigated using Nitrogen as working fluid. The main purpose is to understand the impact of the channel geometry on the exit velocity and the transmission coefficient, parameters which are well known to affect directly the thruster performance. Although this analysis can be applied in principle to several possible microfluidics scenarios, particular focus is given to its application in the field of space propulsion for micro-, nano- and pico-satellites, for which the requirements ask for low thrust levels from some μN *to a few* mN *and moderate specific impulse, as well as a low power consumption in the order of a few Watts.*

The content of this chapter has been published in ASME Journal of Heat Transfer **138**, 11 (2016).

3.1. INTRODUCTION AND NUMERICAL MODELLING

So far, research has been focused on heater chip with wide and thin expansion slots (Ketsdever et al., 2005; Cervone et al., 2015b). In this chapter, a new approach with a grid of circular microchannels is investigated. Circular microchannels have a better surface area to volume ratio which improves the heat transfer, although they have a lower transmission coefficient value. A sensitivity analysis of different divergent circular microchannels is performed using Direct Simulation Monte Carlo simulations (DSMC) in order to identify the geometry that presents the best thrust performance.

The 3-D DSMC code from open source C++ CFD toolbox *OpenFOAM*, has been used to analyse the flow dynamics and thermal properties of the microchannels. As in all DSMC tools, the motion of particles in a small cell volume, where Δx_{cell} is the cell dimension, is analysed. In each cell, a set of representative collisions is processed at each time step Δt_{step}. The DSMC does not use the actual number of particles due to the high simulation cost required, even though the sample of particles used in the simulations represent well the solution. Δx_{cell}, Δt_{step} and the number of particles used play an important role in the accuracy of the simulation and they are estimated according to Bird (1994) as

$$\Delta x_{cell} \leq \frac{\lambda}{3} \tag{3.1}$$

$$\Delta t_{step} = \frac{\xi \lambda}{\bar{c}} \tag{3.2}$$

where (λ) is the mean-free path, ξ is the fraction of mean free time (the mean time between collisions) at the mean stream conditions, and $\bar{c}$ is the mean thermal speed which is calculated as

$$\bar{c} = \sqrt{\frac{2kT}{m}} \tag{3.3}$$

where k is the Boltzmann's constant, T is the thermodynamic temperature, and m is the mass of the particle. According to the equations above the mesh size has to be less than 12 μm and the time step has to be close to 2×10^{-7} s. Additionally, the typical value of the actual- to simulated-particle ratio S per cell is taken in the range from 10^{14} to 10^{18} for a three-dimensional computation Oran et al. (1998). On the other hand, values of S close to 1 are typically used to simulate completely free molecular flows. However, in the cases studied in this Chapter, both the transitional and the free molecular regimes are present, and for this reason an intermediate value has been chosen for S. This means that the flow regions under the free molecular regime, which are less interesting for the scopes of this study, have been simulated less accurately due to the relatively low number of particles considered. Taking these constraints into account, a suitable value of S (in terms of computational cost) was defined. Table 3.1 shows a summary of the main simulation parameters, set in agreement with the indications provided by literature and common practice Oran et al. (1998); Bird (1994); Scanlon et al. (2010). Gaseous Nitrogen was used as propellant in order to make comparison to existing literature results easier.

A sketch of the baseline modelling (case 1) can be seen in Figure 3.1. The sketch is divided in three sections: a portion of the plenum, the microchannel and a portion of

Table 3.1: Simulation setting according to Bird (1994) and Scanlon et al. (2010)

Element	Model/Value
Gas interaction	Variable Hard Sphere
Energy exchange	Larsen-Borgnakke
Gas-Surface interaction	Diffuse
Molecular species	N_2 (nitrogen)
Rotational degree of freedom	2
Mass of the particle m	46.5×10^{-27} kg
Diameter of the particle d_{ref}	4.17×10^{-10} m
Fraction of mean free time ξ	0.1
Temperature coefficient of viscosity ω	0.74
Cell dimension Δx_{cell}	≤ 5 μm
Time step Δt_{step}	2×10^{-7} s
Actual- to simulated-particle ratio S	10^4

the outer space. The main purpose of these simulations is to understand and characterize the gas behaviour in the microchannel, with portions of the plenum and the outer space simulated in order to better understand how the external and boundary conditions influence the fluid dynamics into the channel. The reference frame is placed with its origin at the microchannel entrance (x=0), with the channel exit at x=L where L is the microchannel length which, in this study, is equal to 500 μm. The microchannel is designed with a circular cross-sectional area of 10,000 μm^2. The inlet boundary condition is represented by a blue line and corresponds to a plenum or reservoir under stagnation conditions at a temperature of 300 K and a pressure of 50, 150 or 300 Pa depending on the simulated case. Vacuum conditions are imposed at the outlet boundary that is represented by a black line and corresponds to the outer space. The channel wall boundary condition (red line) was considered at a fixed constant temperature, namely 300, 573, 700 or 900 K depending on the simulated case. Additionally, the green dashed line represents a symmetric plane boundary condition, applied to simplify the modelling and reduce the simulation time.

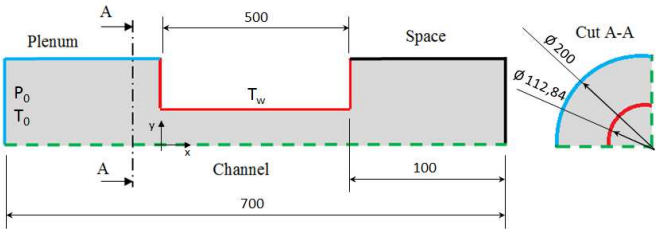

Figure 3.1: Scheme of the baseline microchannel modelling (case 1, dimensions in μm). The plenum boundary condition is represented by a blue line, the channel wall by a red line, the space by a black line and the green dashed line represents the symmetric plane boundary conditions.

Moreover, three additional configurations with a (partially or totally) divergent microchannel were simulated. Figure 3.2 shows the four cases which were analysed, namely:

case 1 (Baseline microchannel), case 2 (Entirely divergent microchannel), case 3 (Second-half divergent microchannel), and case 4 (First-half divergent microchannel). The same inlet cross-sectional area has been used for all the cases. The angle of the divergent part β has been varied from 0 to 40° for each case. The same boundary conditions and parameters as in the baseline have been used, but only one value of the plenum pressure (150 Pa) and wall temperature (573 K) has been considered for cases 2, 3 and 4. This choice is motivated and discussed in the next section together with the results achieved. The variable input parameters used in the simulations for different cases are summarized in Table 3.2.

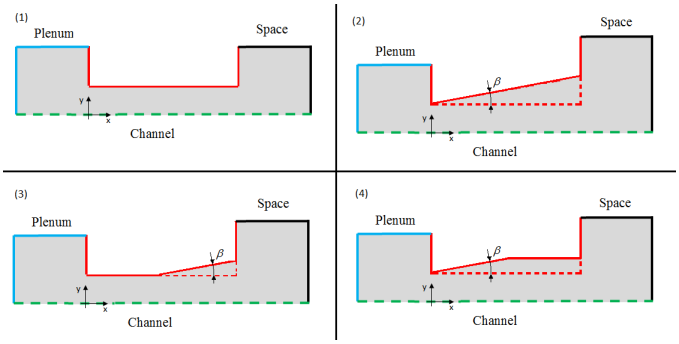

Figure 3.2: Scheme of the four configurations analysed. (1) Baseline microchannel, (2) Entirely divergent microchannel, (3) Second-half divergent microchannel, and (4) First-half divergent microchannel.

Table 3.2: Variable input parameters for the different cases analysed. $\prod$ is the ratio of microchannel's inlet pressure to outlet pressure.

Cases	P_0 [Pa]	T_w [K]	β [°]	Kn_{in}	$\prod$
1	50	300 - 900	0	1.3	13 - 17
	150	300 - 900	0	0.4	14 - 17
	300	300 - 900	0	0.3	14 - 17
2	150	573	0 - 40	0.5	15 - 262
3	150	573	0 - 40	0.5	15 - 480
4	150	573	0 - 40	0.5	15 - 35

3.2. RESULTS AND DISCUSSION

3.2.1. DSMC VALIDATION

A plenum pressure of 50 Pa and a wall temperature of 300 K have been used to validate the numerical parameters used in the simulations. The Knudsen number Kn in the microchannel varies between 1.1 at the microchannel entrance and 14.2 at the microchannel exit. Besides the baseline cell size of 5 μm, two other values were used: 2.5 and 10 μm. Table 3.3 shows the mean velocity u_e and the mean pressure P_e at the microchannel exit for different cell size values. The exit pressure does not show significant variations, but for the exit velocity a difference of 1.3% (in the worst case) in relation to the baseline

parameter is present. For the time step, besides the baseline of 2×10^{-7} s, two other values were tested: 1×10^{-7} and 5×10^{-7} s. Table 3.3 shows the results in terms of the mean exit velocity and the mean exit pressure. The exit pressure also in this case does not show significant changes, but the exit velocity shows a maximum difference of 1.9%. Another numerical parameter that has been analysed is the particles-per-cell value. Besides the actual- to simulated-particle ratio S of 10^4, two other values were tested: 10^3 and 10^5, see Table 3.3. The exit pressure also does not show significant changes and the exit velocity differs by a maximum difference of 1.3%. In conclusion, the uncertainty due to the numerical modelling is expected to be not bigger than 2.6%.

Table 3.3: Sensitivity analysis of numerical results obtained with different parameters.

Parameters		u_e [m s^{-1}]	P_e [Pa]	Difference [%]
Δx_{cell}	2.5 μm	297	2.8	1.3
	5 μm	301	2.8	—
	10 μm	299	2.8	0.7
Δt_{step}	1×10^{-7} s	302	2.8	0.1
	2×10^{-7} s	302	2.8	—
	5×10^{-7} s	296	2.7	1.9
S	10^3	301	2.8	0.3
	10^4	302	2.8	—
	10^5	298	2.8	1.3

An additional validation of the baseline parameters has been carried out by comparing the pressure variation along the microchannel centerline from the current numerical code to an analytical expression given in Karniadakis et al. (2005):

$$\begin{aligned}\tilde{P}^2 - 1 + 2(6+\bar{\alpha})\frac{2-\sigma_v}{\sigma_v}Kn_o(\tilde{P}-1)+ \\ 2(6b+\bar{\alpha})\frac{2-\sigma_v}{\sigma_v}Kn_o^2 log_e(\frac{\tilde{P}-bKn_o}{1-bKn_o}) = B(1-\frac{x}{L}),\end{aligned} \tag{3.4}$$

where $\tilde{P}$ is the ratio of local pressure to outlet pressure, Kn_o is the outlet Knudsen number, σ_v is the thermal accommodation (set equal to 1), B is a constant such that $\tilde{P} = P(x=0)/P_o$, and b and $\bar{\alpha}$ are constants too. The comparison is presented in Figure 3.3, which shows very good matching with the findings of Karniadakis et al. (2005), where it is indicated that at higher Knudsen numbers and, thus, under free molecular flow conditions, the pressure distribution along the channel centerline is much closer to what would be obtained by assuming a linear pressure drop. Equation 3.4 gives, however, still sufficiently accurate results, with a maximum difference of 3.0% for a plenum pressure of 50 Pa, 2.7% for a plenum pressure of 150 Pa, and 2.9% for a plenum pressure of 300 Pa. A wall temperature of 300 K was used for this comparison.

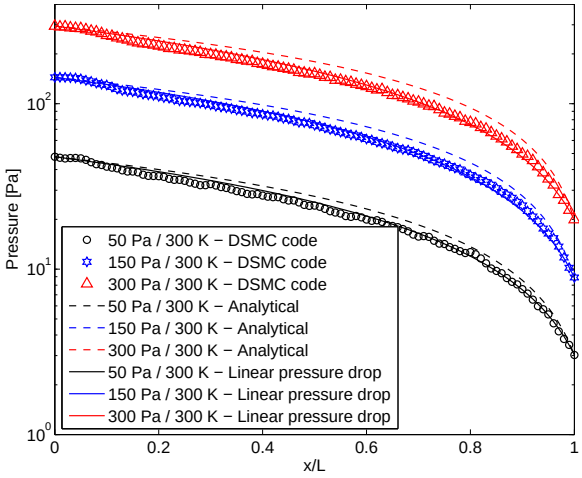

Figure 3.3: Pressure along the channel centerline: comparison of the current DSMC code with the analytical solution from Karniadakis et al. (2005)

3.2.2. CASE 1. BASELINE MICROCHANNEL ANALYSIS

In Figure 3.4, the pressure normalized with respect to the plenum pressure P_0 along the microchannel is shown for different plenum pressures and wall temperatures. The pressure slightly raises in the first part of the channel, followed by a gradual decrease very close to a linear function, where the slope depends mainly on the plenum pressure. Furthermore, when the wall temperature T_w is the same as the plenum temperature T_0, in this study 300 K, the entrance pressure is less than the plenum pressure. On the other hand, when the wall temperature exceeds the plenum temperature, the entrance pressure increases and becomes higher than the plenum pressure, but the pressure converges to the same value at the microchannel outlet.

Due to the random direction of particles and the high number of collisions in the channel entrance area, the heat transfer from wall to particles is more effective in the first 30% of the microchannel length, after which the mean gas temperature is almost constant and close to the wall temperature, see Figure 3.5. The mean gas temperature decreases slightly in the last 20% of the microchannel due to the low outer space temperature. The complete temperature field is shown in Figure 3.6-(a) for plenum pressure of 150 Pa and wall temperature of 573 K.

Since there is no change in the cross-sectional area along the baseline channel, the Mach number along the channel presents a similar value for the different cases studied independently on the Knudsen number, plenum pressure and channel wall temperature. The Mach number converges to sonic velocity at the channel outlet, see Figure 3.6-(b). The Knudsen number depends mainly on the plenum pressure and microchannel wall temperature. When the plenum pressure increases the Knudsen number tends to decrease, and when the wall temperature increases the Knudsen number tends to increase, see Table 3.4. For, plenum pressure of 50 Pa, the flow regime turns into a free molecular flow in the last part of the channel.

The molecules are accelerated in the microchannel mainly due to collisions with the

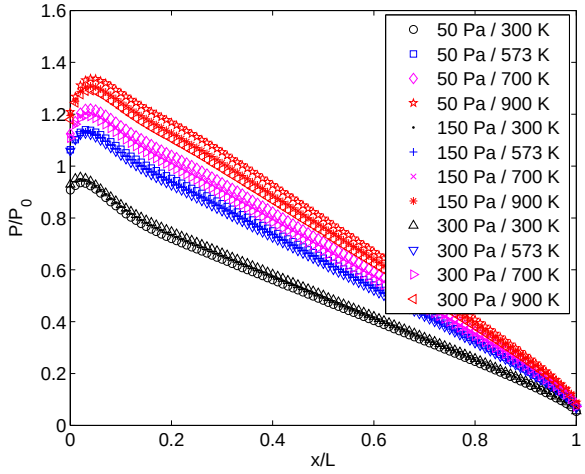

Figure 3.4: Mean pressure along the channel (normalized) for the baseline microchannel (case 1), for different plenum pressures and wall channel temperatures.

Table 3.4: Knudsen number at the channel inlet and outlet, baseline microchannel (case 1).

P_0 [Pa]	T_w [K]	300	573	700	900
50	Kn_{in}	1.1	1.3	1.4	1.5
150		0.4	0.4	0.5	0.5
300		0.2	0.2	0.2	0.3
50	Kn_{out}	14.2	20.1	22.3	25.4
150		4.6	6.9	7.7	8.9
300		2.3	3.6	4.0	4.7
50	$\prod$	17.0	14.9	14.4	13.7
150		16.7	15.2	14.6	14.1
300		16.8	15.6	15.2	14.6

hot channel walls, and the exit velocity increases from 293 to 503 m/s when the channel wall temperature increases from 300 to 900 K, respectively. Table 3.5 shows the transmission coefficient and exit velocity for different channel wall temperatures and plenum pressures. Varying from 17 to 19 %, the transmission coefficient changes are not significant, although the increase in exit velocity is significant. Therefore, one initial step to improve the transmission coefficient was expected to be by a divergent channel, helping the particles to be expelled more effectively. The results obtained by using different types of divergent geometries are presented in the next subsections.

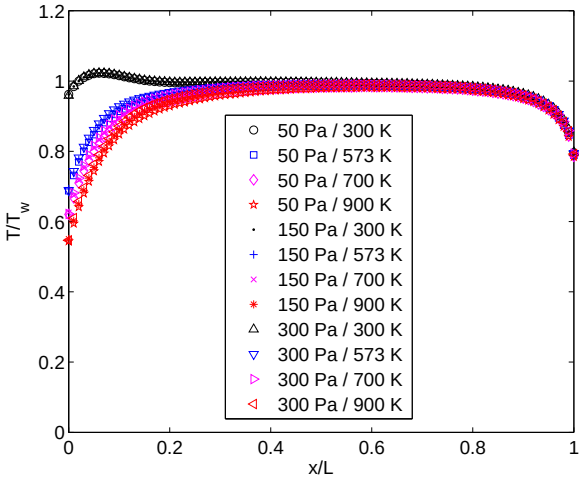

Figure 3.5: Mean temperature along the channel (normalized) for the baseline microchannel (case 1), for different plenum pressures and wall channel temperatures.

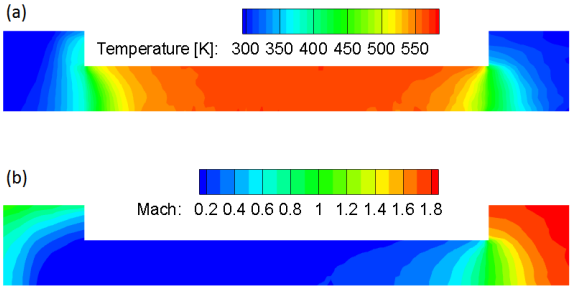

Figure 3.6: Temperature (a) and Mach number (b) maps for a plenum pressure of 150 Pa and channel wall temperature of 573 K, for the baseline microchannel (case 1).

Table 3.5: Transmission coefficient and Exit Velocity, baseline microchannel (case 1).

P_0 [Pa]	50	150	300	50	150	300
T_w [K]	Transmission Coefficient			Exit Velocity [metre/s]		
300	0.189	0.189	0.190	292	283	299
573	0.187	0.183	0.179	401	403	411
700	0.186	0.181	0.176	442	444	453
900	0.186	0.180	0.174	499	503	514

3.2.3. CASE 2. ENTIRELY DIVERGENT MICROCHANNEL ANALYSIS

The main effect of the divergent channel is to alleviate the problems caused by the high entrance pressure, so that the passage of molecules throughout the channel is facilitated, as seen in Figure 3.7. The entrance pressure decreases significantly with increasing angle

of the divergent part. This reduction is up to about 75% with respect to the baseline (i.e., no divergence angle), for a divergence angle of 40 degrees. In addition, the pressure drops dramatically through the microchannel, with most of this drop moved towards the channel inlet when the divergence angle increases. The channel exit pressure also decreases with increasing divergence angle.

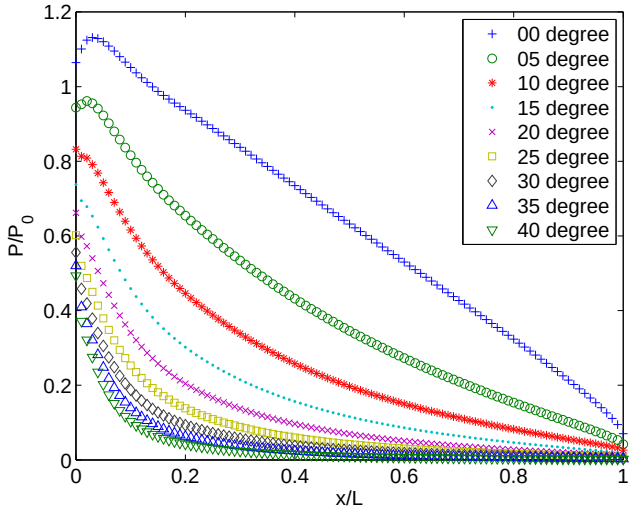

Figure 3.7: Mean pressure along the channel, entirely divergent microchannel (case 2), for different divergent angles at a plenum pressure of 150 Pa and wall temperature of 573 K.

Although on one hand the desired reduced entrance pressure effect is achieved, on the other hand the heat transfer becomes less effective than the baseline and the maximum temperature is less close to the channel wall temperature, as seen in Figure 3.8. When the divergent angle increases, the number of collisions decreases (in particular the particle-surface ones) and the heat transfer becomes less efficient. The complete temperature field for the case of divergent angle of 25 degrees can be seen in Figure 3.9-(a).

The gas temperature decrease at higher divergent angles implies that the molecules are accelerated less efficiently by the hot channel walls through collisions. However, when the divergent angle increases, the acceleration due to thermal expansion, which characterizes the conventional propulsion concepts, increases. For this reason the Mach number increases, and the flow becomes supersonic in the channel for divergent angles higher than 10 degrees. Figure 3.9-(b) shows the increasing Mach number throughout the channel at a divergent angle of 25 degrees. Increasing divergent angles make the Knudsen number rise dramatically through the channel as it can be seen in Table 3.6.This is caused by a flow which reaches the free molecular regime before being expelled at the channel exit.

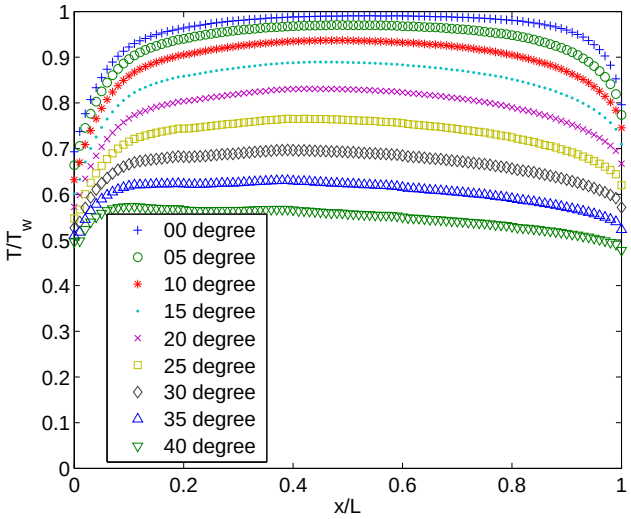

Figure 3.8: Mean temperature along the channel, entire divergent microchannel (case 2), for different divergent angles at a plenum pressure of 150 Pa and wall temperature of 573 K.

Table 3.6: Knudsen number at the channel inlet and outlet, entirely divergent microchannel (case 2), for different divergent angles at a plenum pressure of 150 Pa and wall temperature of 573 K.

$\beta[^\circ]$	05	10	15	20
Kn_{in}	0.5	0.5	0.6	0.6
Kn_{out}	10.9	16.2	23.3	32.6
$\prod$	22.5	31.7	43.9	61.2
$\beta[^\circ]$	25	30	35	40
Kn_{in}	0.6	0.6	0.6	0.7
Kn_{out}	44.7	60.1	79.9	105.2
$\prod$	86.1	122.75	177.8	261.6

The exit velocity increases gradually from 402.5 to 461.5 $\mathrm{m\,s^{-1}}$ when the divergent angle raises from 0 to 30 degrees, respectively. For values higher than 30 degrees the exit velocity slightly decreases, Figure 3.10. Although the exit velocity only shows a relatively moderate change with respect to the baseline, the transmission coefficient increases significantly when the divergent angle increases, going from 18 to 93% for a divergent angle values from 0 to 40 degrees. This represents an increase of about 80% in mass flow rate effectively expelled by the channel.

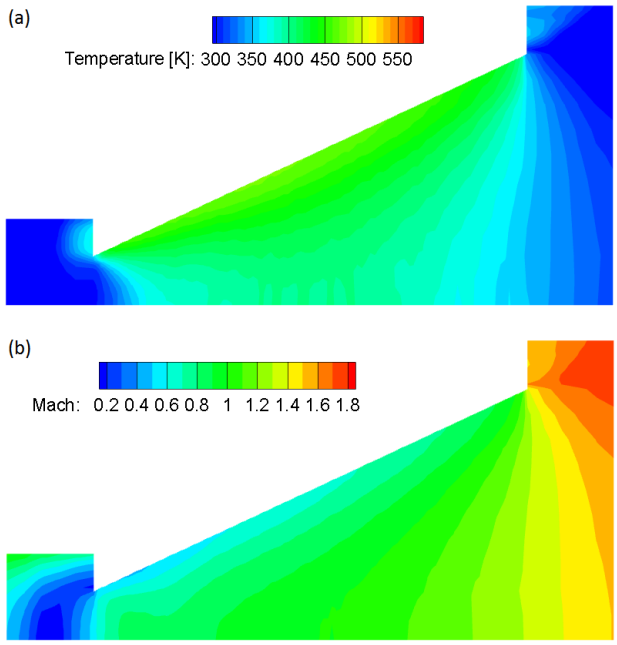

Figure 3.9: Temperature (a) and Mach number (b) maps for the entirely divergent microchannel (case 2), for a divergent angle of 25 degrees, plenum pressure of 150 Pa and wall temperature of 573 K.

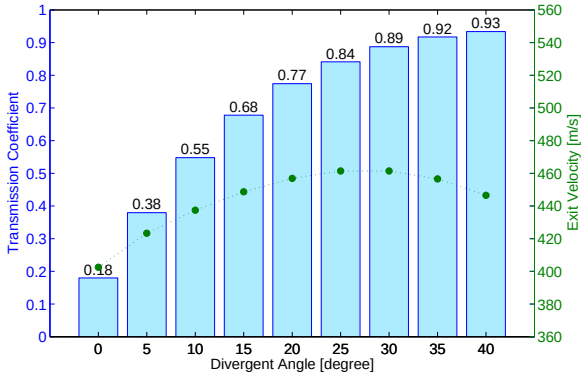

Figure 3.10: Transmission coefficient and exit velocity for different divergent angles at a plenum pressure of 150 Pa and wall temperature of 573 K, entirely divergent microchannel (case 2).

3.2.4. CASE 3. SECOND-HALF DIVERGENT MICROCHANNEL ANALYSIS

As it has been shown in the previous subsection, the entirely divergent angle geometry (case 2) shows an important increase in mass flow rate. However, a less effective heat transfer is obtained. In case 3, the idea is to increase the heat transfer effectiveness in the first half of the microchannel (constant area) as compared to case 2 and improve the

thermal expansion of the flow and, thus, the transmission coefficient in the second half (divergent). Figure 3.11 shows that the entrance pressure is slightly reduced when the divergent angle increases up to 25 degrees, while for angles higher than 25 degrees it does not change significantly. Generally speaking, the pressure through the microchannel decreases significantly with increasing divergent angle.

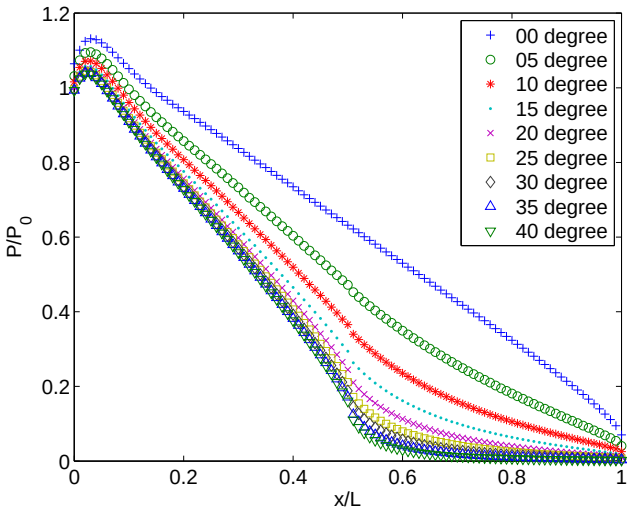

Figure 3.11: Mean pressure along the channel, second-half divergent microchannel (case 3), for different divergent angles at a plenum pressure of 150 Pa and wall temperature of 573 K.

The heat transfer does not show significant changes with increasing divergent angle, because the gas is mainly heated in the first half of the channel and when the molecules enter in the divergent part, they are already aligned and the number of collisions with the walls are insignificant. Due to this, the gas temperature in the second half of the channel decreases significantly when the divergent angle increases, see Figure 3.12. The complete temperature field for a divergent angle of 25 degrees can be seen in Figure 3.13-(a).

Differently to the previous geometry (case 2), the Mach number presents a significant increase only in the second half of the microchannel, but still converges to similar supersonic values at the channel exit, compare Figures 3.9-(b) and 3.13-(b). The Knudsen number at channel outlet for this configuration is as high as in case 2, and the flow also changes to free molecular regime before the microchannel exit, see Table 3.7.

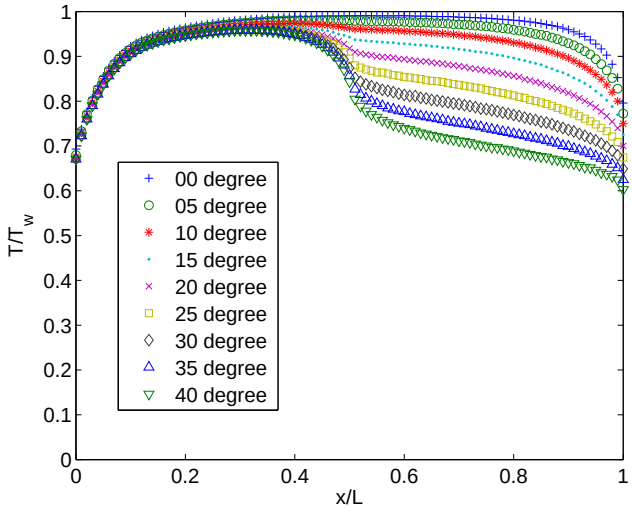

Figure 3.12: Mean temperature along the channel, second-half divergent microchannel (case 3), for different divergent angles at a plenum pressure of 150 Pa and wall temperature of 573 K.

Table 3.7: Knudsen number at the channel inlet and outlet, second-half divergent microchannel (case 3), for different divergent angles at a plenum pressure of 150 Pa and wall temperature of 573 K.

$\beta[^\circ]$	05	10	15	20
Kn_{in}	0.5	0.5	0.5	0.5
Kn_{out}	11.2	16.9	24.6	34.7
$\prod$	25.4	40.4	62.7	95.9
$\beta[^\circ]$	25	30	35	40
Kn_{in}	0.5	0.5	0.5	0.5
Kn_{out}	47.8	64.8	86.4	114.3
$\prod$	144.4	217.0	322.0	479.6

A significant difference between cases 2 and 3 can be noticed in the exit velocity and the transmission coefficient, by comparing Figures 3.10 and 3.14. The exit velocity increases with respect to case 2 (for instance 496.1 $m\,s^{-1}$ instead of 461.5 $m\,s^{-1}$, for the same divergent angle of 30 degrees). The highest exit velocity (500.1 m/s) is achieved for a divergent angle of 35 degrees and there is a slight decrease for divergent angles larger than 35 degrees. The transmission coefficient presents an increase with respect to the baseline (case 1) but is significantly lower with respect to the entirely divergent angle (case 2). This happens because the mass flow rate is limited by the presence of the first constant-area microchannel section, independently on the divergent angle in the second part. The transmission coefficient is never larger than 31% (value for a cylindrical tube with aspect ratio of 2.5), in accordance to the results obtained in Lafferty (1998), and the largest transmission coefficient is achieved for an angle of 25 degrees.

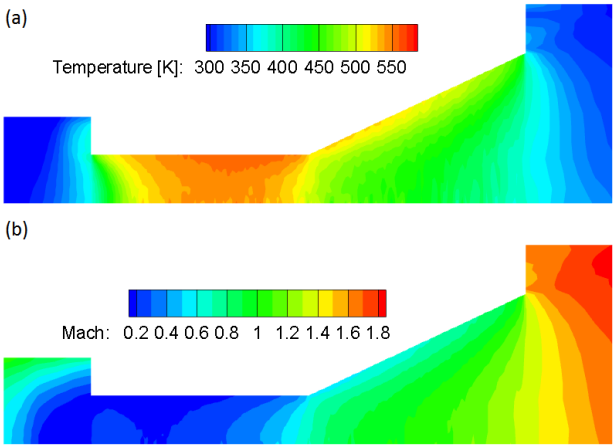

Figure 3.13: Temperature (a) and Mach number (b) maps for the second-half divergent microchannel (case 3), for a divergent angle of 25 degrees, plenum pressure of 150 Pa and wall temperature of 573 K.

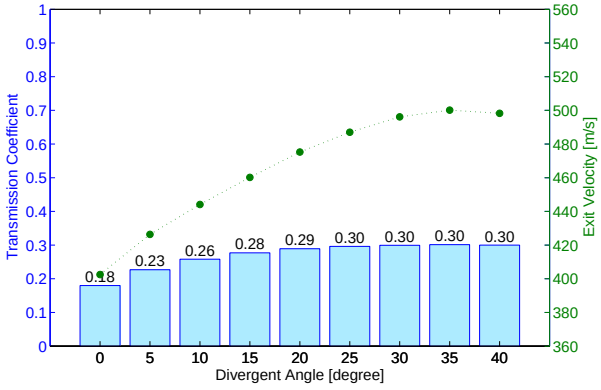

Figure 3.14: Transmission coefficient and exit velocity for different divergent angles at a plenum pressure of 150 Pa and wall temperature of 573 K, second- half divergent microchannel (case 3).

3.2.5. CASE 4. FIRST-HALF DIVERGENT MICROCHANNEL ANALYSIS

Following the analysis of case 3, a conclusion is that when the highest gas temperature is achieved due to a high number of collisions, the mass flow rate is lower and when the mass flow rate is increased due to the increased divergent angle, the number of collisions decreases and the gas temperature is lower. In order to combine these effects, in case 4 the first half of the microchannel (divergent) is used for the thermal expansion to increase the mass flow rate, and the second half (constant area) is used to increase the temperature. Figure 3.15 shows that the entrance pressure decreases significantly as it happened for the entirely divergent angle (case 2). Additionally, the gas temperature through the channel is larger than in case 2, comparing Figures 3.8 and 3.16.

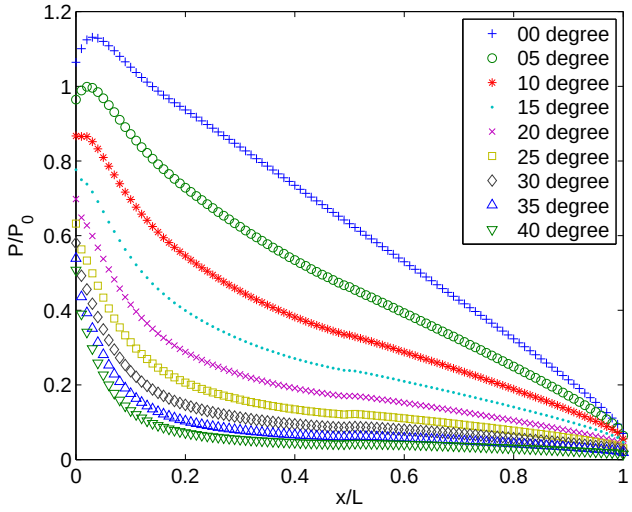

Figure 3.15: Mean pressure along the channel, first-half divergent microchannel (case 4), for different divergent angles at a plenum pressure of 150 Pa and wall temperature of 573 K.

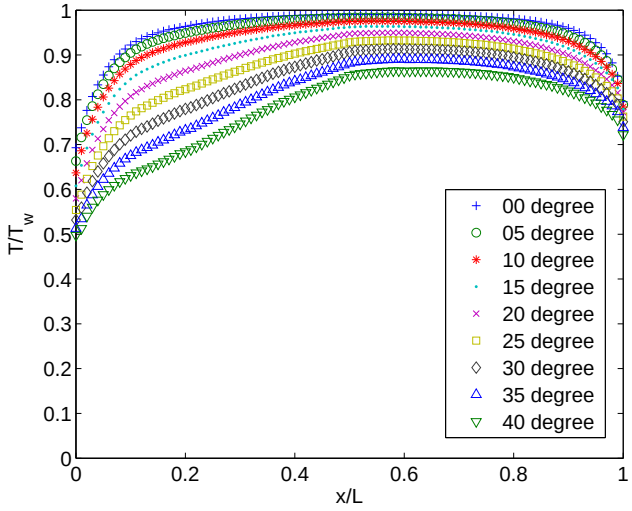

Figure 3.16: Mean temperature along the channel, first-half divergent microchannel (case 4), for different divergent angles at a plenum pressure of 150 Pa and wall temperature of 573 K.

The complete temperature field in the channel can be seen in Figure 3.17, in the case of 25 degrees divergence angle, as well as the Mach number map. In the first half of the microchannel, the Mach number presents a similarity to case 2, reaching a value of 0.6 in the beginning of the channel due to the thermal expansion, while the situation in the second half is similar to case 1 and the Mach number tends again to reach the sonic regime at the end of the microchannel, see the example in Figure 3.17-(b). In this

case the flow changes to the free molecular regime just at the microchannel exit, for a divergent angle higher than 15 degrees, see Table 3.8.

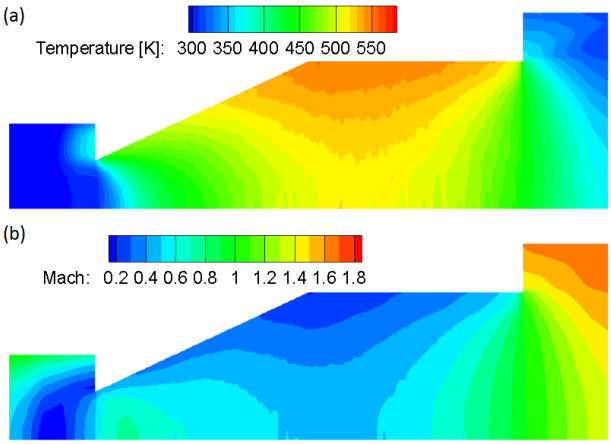

Figure 3.17: Temperature (a) and Mach number (b) maps for the first-half divergent microchannel (case 4), for a divergent angle of 25 degrees, plenum pressure of 150 Pa and wall temperature of 573 K.

Table 3.8: Knudsen number at the channel inlet and outlet, first-half divergent microchannel (case 4), for different divergent angles at a plenum pressure of 150 Pa and wall temperature of 573 K.

$\beta[^\circ]$	05	10	15	20
Kn_{in}	0.5	0.5	0.5	0.6
Kn_{out}	7.5	8.5	10.1	12.3
$\prod$	15.1	15.6	16.8	18.5
$\beta[^\circ]$	25	30	35	40
Kn_{in}	0.6	0.6	0.6	0.6
Kn_{out}	15.2	18.9	23.8	30.1
$\prod$	20.9	24.3	28.9	35.1

The exit velocity does not show a significant change with the divergent angle, and the highest exit velocity (413.3 m/s) is achieved for a divergent angle of 10 degrees, see Figure 3.18. On the other hand, the transmission coefficient increases significantly with increasing divergent angle. This result is comparable to the case of entirely divergent channel (case 2). Another interesting result is that a divergent angle of 40 degrees shows almost the same exit velocity as the baseline, but with a very high transmission coefficient of 91%.

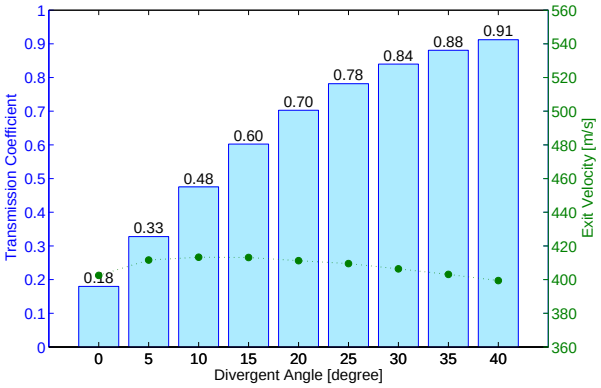

Figure 3.18: Transmission coefficient and exit velocity for different divergent angles at a plenum pressure of 150 Pa and wall temperature of 573 K, first-half divergent microchannel (case 4).

3.2.6. THRUSTER PERFORMANCE ANALYSIS

Each of the studied cases shows its own specific flow characteristics, as previously described. In case the microchannels are used as flow acceleration elements in a space thruster, these characteristics can be used to compute the expected propulsion performance (thrust, specific impulse and power consumption, in particular). This subsection will present the propulsion performance and the different parameters that influence it directly.

Figure 3.19 shows how the exit velocity profile along the y axis is influenced by the channel geometry. In particular, a divergent angle at the channel exit makes the flow significantly more bi-dimensional, with a less uniform axial component of the exit velocity and a non-negligible component along the y axis. This effect becomes even more prominent at higher divergent angles, as shown in Table 3.9, where the maximum V_y/V_x ratio at the microchannel exit (for $y/r = 1$) is shown for all cases and different values of the divergent angle.

Table 3.9: Maximum V_y/V_x ratio at the channel exit (for $y/r = 1$), for all cases and different values of the divergent angle.

$\left(\frac{V_y}{V_x}\right)_{max}$		Case 2	Case 3	Case 4
	0°	0.2035	0.2035	0.2035
	5°	0.2400	0.2399	0.2169
	10°	0.2808	0.2823	0.2148
	15°	0.3253	0.3227	0.2225
β	20°	0.3752	0.3810	0.2132
	25°	0.4364	0.4371	0.2160
	30°	0.5089	0.5166	0.2178
	35°	0.5936	0.6029	0.2174
	40°	0.6943	0.6943	0.2222

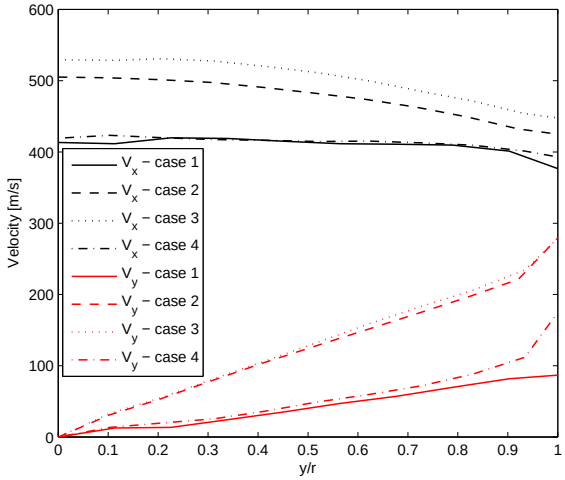

Figure 3.19: Velocity profile along the y axis at the channel exit (x = 500 μm), for all cases, with a divergent angle of 25°.

For the baseline (case 1), Figure 3.20 shows the relationship between thrust and specific impulse under different plenum pressure and channel wall temperature. In Figure 3.20 it can be seen that the specific impulse increases when the channel wall temperature increases and the thrust increases significantly with the plenum pressure and also, slightly, with the channel wall temperature.

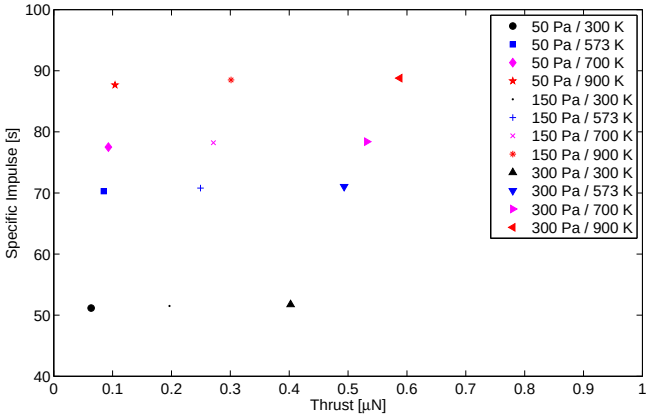

Figure 3.20: Thrust versus specific impulse for different values of the plenum pressure and wall temperature, baseline microchannel (case1).

Another important result is obtained in relation to the specific energy, that is the ratio of power (thermal energy) consumption per mass flow rate. Figure 3.21 shows that the

specific energy rises with the wall temperature and, consequently, the specific impulse. An increase in plenum pressure tends to slightly decrease the specific energy.

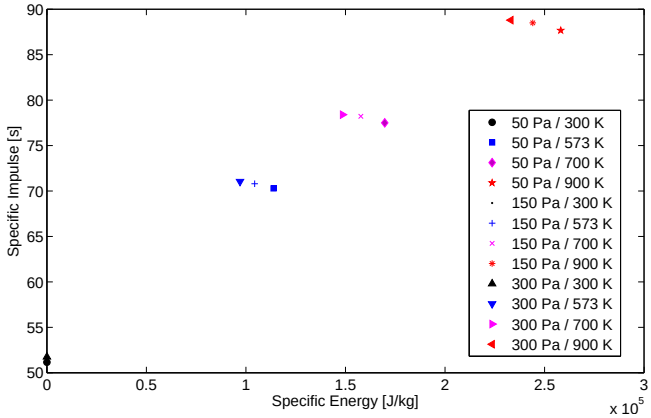

Figure 3.21: Specific energy versus specific impulse for different values of the plenum pressure and wall temperature, baseline microchannel (case 1).

The specific impulse increases when the gas temperature increases as a consequence of the higher wall temperature, or when the molecular mass decreases by changing the molecular species, as it is already shown by Ketsdever et al. (2005). On the other hand, the thrust can be increased by increasing the plenum pressure, the channel wall temperature, the exit area or the transmission coefficient, as also shown by Ketsdever et al. (2005). However, the channel wall temperature does not affect significantly the thrust and is obviously also limited by the material properties. For what concerns the plenum pressure, when it is increased, the flow tends to move from the rarefied gas regime to the continuum flow one, for which completely different equations and considerations should be applied. It is obviously also possible to increase the flow exit area by increasing the number of slots/microchannels, at least up to a certain level after which a too large heater chip and plenum volume would be obtained. The transmission coefficient depends basically on the geometry and, in particular, the aspect ratio. However, when the aspect ratio decreases, the heat transfer becomes less effective and thus the gas temperature and specific impulse decrease. The power consumption is crucial, since it is one of the most important design drivers of satellites, especially very small satellites, with limited power available. In summary, it is desirable to achieve the maximum possible thrust and specific impulse with the minimum power consumption.

Figure 3.22 shows a comparison among different geometries, at plenum pressure of 150 Pa and channel wall temperature of 573 K. For the entirely divergent channel, case 2, when the angle increases the thrust increases dramatically due to the increased transmission coefficient, and the specific impulse decreases significantly due to the lower gas temperature. For the second-half divergent angle, case 3, the aspect ratio of the first part of the microchannel represents a sort of "barrier" to the mass flow rate, so the thrust does not change much and the specific impulse decreases significantly with the angle. For the first-half divergent angle, case 4, the thrust increases significantly with the angle

in the same way as case 2, and the specific impulse slightly decreases.

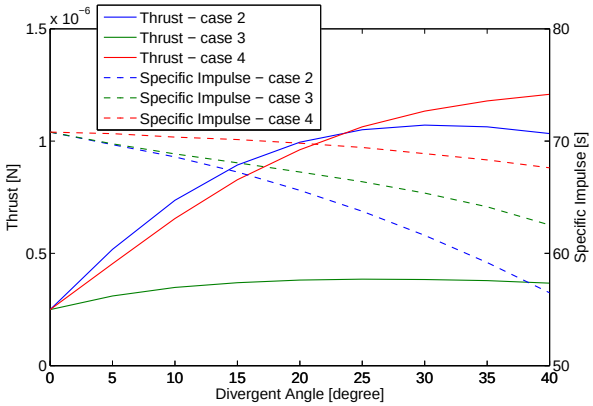

Figure 3.22: Thrust and specific impulse as functions of the divergent angle, for plenum pressure of 150 Pa and wall temperature of 573 K (cases 2, 3 and 4).

As it can be seen in Figure 3.23, the specific energy presents an interesting behaviour. In case 3 there is a slight decrease of specific energy with a divergent angle up to 10 degrees, followed by a significant increase for higher divergent angles. In cases 2 and 4 there is a significant decrease in the specific energy with the divergent angle.

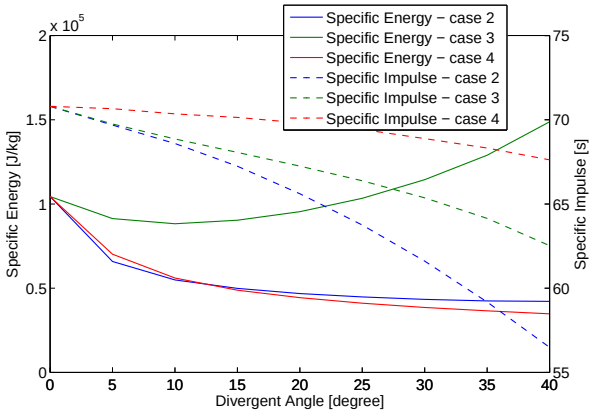

Figure 3.23: Specific energy and specific impulse as functions of the divergent angle, for plenum pressure of 150 Pa and wall temperature of 573 K (cases 2, 3 and 4).

As explained before, in space propulsion, the total thrust produced by a system is generated by two different contributions: the momentum thrust (caused by change of momentum in the fluid) and the pressure thrust (caused by pressure difference between channel exit and ambient), see Equation 1.1. Each contribution plays a different role for the studied cases 1-4. In the baseline case (case 1) the pressure thrust represents about

42% of the total thrust. In cases 2 and 3, where the exit pressure decreases due to the divergent angle, the pressure thrust becomes a smaller portion of the total thrust, about 19% for a divergent angle of 40 degrees. In case 4, with the same divergent angle, the pressure thrust represents again a larger portion of the total thrust (about 40%), due to the heat transfer in the second half of the microchannel. In any case, it is clear that the pressure thrust contribution is not negligible in this concept, differently to what happens in traditional propulsion systems especially when used under vacuum conditions.

3.3. CONCLUSION

The DSMC method was applied to simulate the flow and thermal behaviour in four different microchannel geometries for the LPM. The baseline case with constant channel area was analysed to study the influence of different plenum pressures and channel wall temperatures on the mass flow rate, thrust and specific impulse. The other cases, in which a divergent section is present in the channel, a plenum pressure of 150 Pa and microchannel wall temperature of 573 K have been considered with divergent angles ranging from 0 to 40 degrees in different configurations. In addition, the heat transfer and fluid flow in the microchannels have been discussed.

It is shown that the transmission coefficient increases significantly with increasing divergent angle, which improves the mass flow rate through the channel and, consequently, the thrust. On the other hand, when the divergent angle increases, the heat transfer effectiveness tends to decrease significantly, which influences in a negative way the exit velocity. The case of first-half divergent channel is the best combination of these two contrasting effects. In terms of thrust performance, therefore, this is the most promising case. It combines a relatively small reduction of specific impulse with a significant increase of thrust. As a comparison, the thrust of one microchannel with divergent angle of 40 degrees is equivalent to 4.8 microchannels of the baseline case, with a specific impulse decrease of just 5% and a reduction in power consumption of 67%, for a plenum pressure of 150 Pa and a channel wall temperature of 573 K.

4

ANALYTICAL MODELLING

Pure mathematics is, in its way,
the poetry of logical ideas.

Albert Einstein

To simplify the engineering design of the Low-Pressure Micro-Resistojet (LPM) an analytical model has been developed using fundamental physical relations. This analytical model is based on the kinetic theory of gases and the Maxwell-Boltzmann distribution of molecular velocities to describe the macroscopic flow parameters such as mass flow rate, velocity and pressure. This model is then used to estimate the thruster performance. Although conventional equations have been used, they are applied here specifically to describe the physics of this micro-propulsion system. Comparisons between the results of numerical simulations using the DSMC method and the results of the analytical model, as well as experimental results, have been carried out.

The content of this chapter has been submitted to Acta Astronautica (Under review).

4.1. INTRODUCTION AND OPERATION PRINCIPLE

In this chapter, an analytical model to estimate the thruster performance is presented. This model facilitates the engineering design and parametric study of the Low-Pressure Micro-Resistojet (LPM). In this model the pressure and momentum thrust are considered based on Equation 1.1, improving the model presented in Ketsdever et al. (2005) which considers the momentum thrust only. The efficiency of the system is estimated taking into account the necessary power to sublime/evaporate the propellant in the tank and heat up the expelled propellant gas. The analytical model is validated by comparing its results to results of numerical simulations. Additionally, some available experimental results are compared to the analytical model's results. The objective of the developed analytical model is to improve the model presented in Ketsdever et al. (2005) when compared to the numerical and experimental results.

A simplified architecture of the LPM concept is presented in Figure 1.5. The propellant is stored in the tank in solid or liquid state. Due to the working principle of the LPM, it is important to keep the tank pressure as low as possible, otherwise a pressure reducer or a proportional valve would be necessary to reduce the vapour pressure downstream the tank making the system more complex. An open/close valve is placed between the tank and the plenum in order to control the mass flow rate. An important part of the system is the heater chip that is a flat plate with a grid of microchannels in which the propellant particles are accelerated and expelled into space. The gas flow regime changes from the continuum flow regime inside the tank to the free molecular regime in outer space.

Basically, the propellant is evaporated or sublimed inside the tank. The propellant vapour goes from the tank to the plenum through the feed system. In the plenum, the Knudsen number Kn is kept between 0.1 and 10 which is defined as transitional flow regime. As an example, the nominal pressure has to be kept below 300 Pa for a microchannel with a diameter of 100 μm. The propellant molecules go towards the microchannels where they collide with the high temperature wall increasing their energy. This allows to increase the thrust and specific impulse. The wall is heated by an electric resistance attached to the heater chip, similar to any conventional micro-resistojet.

4.2. ANALYTICAL MODEL

The thruster part of the propulsion system is composed by plenum and microchannel. It is designed to work in a transitional flow regime defined by a Knudsen number Kn between 0.1 and 10. The flow behaviour inside the microchannel plays a key role in the thruster performance. In order to estimate its behaviour the kinetic theory of Maxwell is used. According to Equation 1.1 the unknown parameters to define the thrust are mass flow rate, exhaust velocity and exhaust pressure. Based on that, this section presents the analytical equations to estimate them. Additionally, analytical equations are defined to estimate the required electric power and the efficiency of the propulsion system.

Assuming thermodynamic equilibrium inside the plenum and given the degree of rarefaction, the Maxwellian or equilibrium distribution function f (Equation 1.9) can be used. Additionally, the flux ψ of a quantity ψ (mass, momentum or energy) through a surface per unit area in the axis x direction, which is the flow direction towards the

microchannels, is defined Bird (1994)

$$\dot{\psi} = n \int_{-\infty}^{\infty} \int_{-\infty}^{\infty} \int_{0}^{\infty} u \psi f(u,v,w) \mathrm{d}u \mathrm{d}v \mathrm{d}w \tag{4.1}$$

where n is the molecular number density, and u, v and w are the velocity components of the molecules for a Cartesian axis x, y and z, respectively.

Mass flow rate The actual mass flow rate $\dot{m}$ through the microchannel depends on the geometry of the microchannel which is discussed below. It also depends on the mass flow rate in the free-molecular limit ($\dot{m}_{fm}$) which is defined by setting $\psi = m_a$ in the Equation 4.1 and multiplying by the microchannel exit area A_e. Then we have

$$\dot{m}_{fm} = n \sqrt{\frac{k m_a T}{2\pi}} A_e. \tag{4.2}$$

The dependency of the actual mass flow rate on the mass flow rate in the free-molecular limit is described by the transmission coefficient α which, as previously defined, is expressed as

$$\alpha = \frac{\dot{m}}{\dot{m}_{fm}}. \tag{4.3}$$

Combining Equations 4.2 and 4.3 with the ideal gas equation ($n = P/kT$), and replacing P with plenum pressure P_0 and T with plenum temperature T_0 the actual mass flow rate can be described as Ketsdever et al. (2005):

$$\dot{m} = \alpha P_0 \sqrt{\frac{m_a}{2\pi k T_0}} A_e \tag{4.4}$$

Several empirical equations have been proposed for the transmission coefficient depending on the geometry Lafferty (1998), for instance:

- **Short Uniform Circular Cross Section (circular microchannel)**:

$$\alpha = 1 + \delta^2 - \delta\sqrt{\delta^2+1} - \frac{\left[(2-\delta^2)\sqrt{\delta^2+1} + \delta^3 - 2\right]^2}{4.5\delta\sqrt{\delta^2+1} - 4.5\ln(\delta + \sqrt{\delta^2+1})} \tag{4.5}$$

  where δ is the channel length to diameter ratio L/d. The relation is valid for $\delta < 50$. By way of example, a cylindrical channel with an aspect ratio of 5 has a transmission coefficient of 0.19.

- **Short Uniform Rectangular Cross Section (cuboid microchannel)**:

$$\alpha = 0.5(1 + \sqrt{1+\phi^2} - \phi) - \frac{1.5\left[\phi - \ln(\phi + \sqrt{1+\phi^2})\right]^2}{\phi^3 + 3\phi^2 + 4 - (\phi^2+4)\sqrt{1+\phi^2}} \tag{4.6}$$

  where if a and b are the cross-sectional dimensions with $b \geq a$, and l is the length in the direction of the gas flow, ϕ is the slot length to small cross-sectional dimension ratio l/a. This expression is valid for $b \gg a$ and $b \gg l$. As an example, in a slot with an aspect ratio of 5, the transmission coefficient is 0.36.

Exhaust velocity The exhaust velocity u_e is the average gas velocity at the microchannel exit which depends on the translational kinetic temperature. It can be modeled using $\psi = u$ in Equation 4.1 and dividing by the total number flux through the surface as

$$u_e = \frac{n\int_{-\infty}^{\infty}\int_{-\infty}^{\infty}\int_{0}^{\infty} u^2 f(u)\mathrm{d}u\mathrm{d}v\mathrm{d}w}{n\int_{-\infty}^{\infty}\int_{-\infty}^{\infty}\int_{0}^{\infty} u f(u)\mathrm{d}u\mathrm{d}v\mathrm{d}w}. \tag{4.7}$$

Solving Equation 4.7 and replacing T with translational kinetic temperature T_{tr} we obtain

$$u_e = \sqrt{\frac{\pi k T_{tr}}{2m_a}}. \tag{4.8}$$

4

Exhaust pressure The exhaust pressure P_e at the expansion microchannel exit is another important parameter to define the thruster performance. In order to model P_e, the mass flow rate is rewritten according to the microchannel exit parameters as

$$\dot{m} = m_a n_e u_e A_e \tag{4.9}$$

where n_e is the molecular number density at microchannel exit. According to Bird (1994), the scalar pressure is related to the translational kinetic temperature in the perfect gas relation $P = nkT_{tr}$. Replacing P with the pressure at the microchannel exit P_e and n with the molecular number density at the microchannel exit n_e, then n_e can be replaced in Equation 4.9 as

$$\dot{m} = m_a \frac{P_e}{kT_{tr}} u_e A_e. \tag{4.10}$$

Substituting equations 4.4 and 4.8 in the equation 4.10, it is obtained

$$P_e = \frac{\alpha P_0}{\pi}\sqrt{\frac{T_{tr}}{T_0}}. \tag{4.11}$$

Translational kinetic temperature The translational kinetic temperature is an unknown parameter which is needed to estimate the thruster performance. During gas expansion into a very low pressure environment, there is a gas temperature drop (Gavasane et al.; Wang and Li, 2004; Roohi et al., 2009). Using the conservation of energy and the equipartition principle, the energy throughout the microchannel can be analysed. According to the first law of thermodynamics for an open system considering the microchannel as the control volume (Figure 4.1), the equation in the steady state can be written as

$$\dot{Q} = E_e - E_0 = \dot{m}\left(h_e + \frac{u_e^2}{2}\right) - \dot{m}h_0 \tag{4.12}$$

where $\dot{Q}$ is the heat transferred to the gas, E_e is the total energy at the microchannel exit, E_0 the total energy at the microchannel entrance, h_e is the enthalpy at the microchannel exit, h_0 the enthalpy at the microchannel entrance. The propellant gas is assumed to be under stagnation conditions in the plenum, meaning that the entrance velocity is

negligible. For an ideal gas, the variation of enthalpy between microchannel entrance and the exit can be replaced by

$$h_e - h_0 = C_p\,(T_e - T_0) \tag{4.13}$$

where C_p is the specific heat of the propellant at constant pressure and T_e is the overall temperature at the microchannel exit. The quantity $\dot{Q}$ can be computed as

$$\dot{Q} = \dot{m} C_p\,(T_w - T_0)\,. \tag{4.14}$$

Substituting Equations 4.13 and 4.14 into Equation 4.12, the following one is obtained

$$C_p\,(T_w - T_e) = \frac{u_e^2}{2}. \tag{4.15}$$

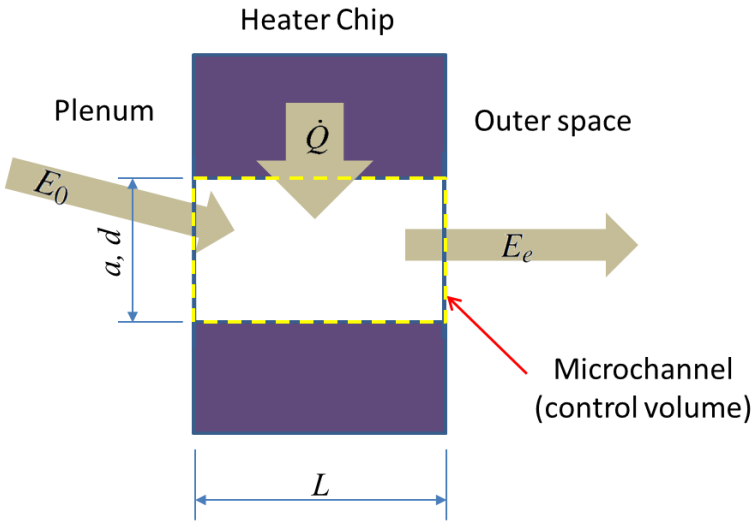

Figure 4.1: Balance of energy inside the microchannel where E_0 is the energy which gets in the control volume, E_e is the energy which gets out the control volume and $\dot{Q}$ is the heat transferred to the gas inside the control volume.

The specific heat of the propellant at constant pressure C_p for an ideal gas depends on the total number of degrees of freedom ζ

$$C_p = \frac{(\zeta + 2)}{2}\frac{k}{m_a}. \tag{4.16}$$

For monatomic molecules, the translational kinetic temperature T_{tr} is equal to the overall temperature T. However, for diatomic and poly-atomic molecules the overall temperature T is divided into translational kinetic temperature T_{tr} and internal temperature T_{int} (Bird, 1994). Assuming the internal gas temperature T_{int} at the microchannel exit equal to the wall temperature T_w, the overall temperature at the microchannel exit T_e can be written as

$$T_e = \frac{(3T_{tr} + (\zeta - 3)T_{int})}{\zeta} = \frac{(3T_{tr} + (\zeta - 3)T_w)}{\zeta}. \tag{4.17}$$

Additionally, the total number of degrees of freedom ζ also defines the well known specific heat ratio γ as (Bird, 1994)

$$\gamma = \frac{\zeta + 2}{\zeta}. \tag{4.18}$$

Substituting Equations 4.8, 4.16, 4.17 and 4.18 into Equation 4.15, it is possible to write the translational kinetic temperature T_{tr} in terms of the wall temperature T_w and specific heat ratio γ as

$$T_{tr} = \left(\frac{6\gamma}{\pi + 6\gamma}\right) T_w. \tag{4.19}$$

Thruster Performance Substituting Equations 4.4, 4.8, 4.11 and 4.19 into Equation 1.1 and assuming P_a equal to zero in space, the obtained thrust is

$$\Im = \alpha P_0 A_e \frac{(\pi + 2)}{2\pi} \sqrt{\frac{T_w}{T_0}\left(\frac{6\gamma}{\pi + 6\gamma}\right)}. \tag{4.20}$$

Now, substituting Equations 4.4 and 4.20 into Equation 1.2, the specific impulse is derived as

$$I_{sp} = \frac{(\pi + 2)}{g_0} \sqrt{\frac{kT_w}{2\pi m_a}\left(\frac{6\gamma}{\pi + 6\gamma}\right)}. \tag{4.21}$$

Thruster Power The thruster power $\wp_w$ is the power necessary to heat up the propellant inside the microchannel. Neglecting the heat transfer loses, the thruster power can be computed as

$$\wp_w \approx \dot{Q} \tag{4.22}$$

where $\dot{Q}$ is the heat transferred to the propellant, Equation 4.14.

Tank Power As previously described, the tank has to be designed such that the propellant is predominantly in a liquid or solid state. Basically, the phase change occurs inside the tank and only gas is expected to pass through the feeding system. Assuming that the fluid in thermodynamic equilibrium inside the tank is most of the time in a saturation region during standby. However, when the thruster is operating, the tank is no longer in equilibrium. In this case, the phase change is an endothermic process, meaning that to keep a certain sublimation/evaporation rate (or mass flow rate) it is necessary to increase the enthalpy by providing power to the system. Therefore, a heater device shall be used in the tank in order to offset the power lost due to the mass flow rate exiting the tank. The required power in the tank $\wp_t$ is calculated as

$$\wp_t = \dot{m}\Delta h_{pc} \tag{4.23}$$

where Δh_{pc} is the enthalpy required by the phase change.

Efficiency Finally, the propulsion system efficiency η is given by the following relationship between thrust, specific impulse and consumed power

$$\eta = \frac{\Im I_{sp} g_o}{2\left(\wp_t + \wp_w\right)}. \tag{4.24}$$

4.3. RESULTS AND DISCUSSIONS

Table 4.1 compares the numerical results presented in Chapter 3, which presents maximum thrust differences of 2.6%, to the results obtained with the analytical method presented in the previous section. The results shown in Table 4.1 are related to Nitrogen propellant flowing in a single circular microchannel with an aspect ratio of 5. The plenum temperature is 300 K, and the plenum pressure varies in the range from 50 to 300 Pa. The wall temperature varies in the range of 300 to 900 K. The main source of uncertainty of the analytical model is the empirical Equation 4.5 to calculate the transmission coefficient, since it does not take into account the thermal effect and it is based only on the geometry of the channel. This difference in the transmission coefficient increases at higher wall temperatures and higher plenum pressures. As a consequence, it affects the thrust as calculated by the analytical model. Comparing the semi-analytical model results, taking the transmission coefficient results from the numerical simulation, to the fully numerical results, the thrust difference does not exceed 3%.

Table 4.1: Comparison between the numerical results presented in Chapter 3 and the results of the analytical model for Nitrogen flowing in a single microchannel with aspect ratio of 5 and plenum temperature of K.

P_0 [Pa] / T_w [K]	α_{num}	α_{ana}	$\Delta\alpha$ [%]	$\Im_{\text{num}}$ [nN]	$\Im_{\text{ana}}$ [nN]	$\Delta\Im$ [%]
50 / 300	0.190	0.190	0.0	63.6	63.0	-0.9
50 / 573	0.185	0.190	2.7	85.0	87.1	2.5
50 / 700	0.183	0.190	3.7	92.8	96.3	3.7
50 / 900	0.182	0.190	4.4	104.2	109.2	4.8
150 / 300	0.195	0.190	-2.4	196.7	189.1	-3.9
150 / 573	0.180	0.190	5.6	249.3	261.3	4.8
150 / 700	0.177	0.190	7.0	271.3	288.8	6.5
150 / 900	0.174	0.190	8.7	301.3	327.5	8.7
300 / 300	0.198	0.190	-4.2	402.3	378.2	-6.0
300 / 573	0.177	0.190	6.9	493.4	522.6	5.9
300 / 700	0.173	0.190	9.1	531.9	577.7	8.6
300 / 900	0.169	0.190	11.2	587.9	659.1	12.1

Figure 4.2 shows the comparison among the numerical results presented in Chapter 3, the analytical model proposed in Ketsdever et al. (2005) and the current analytical model for a single circular microchannel using Nitrogen with aspect ratio of 5 and

plenum temperature of 300 K. The analytical model proposed in Ketsdever et al. (2005) presents a difference of about 30% when compared to the numerical results. Similarly, Figure 4.3 shows a comparison between the numerical results presented in Guerrieri et al. (2015), the analytical model proposed in Ketsdever et al. (2005) and the current analytical model for a single microchannel using Water with aspect ratio of 5 and plenum temperature of 300 K. The analytical model proposed in Ketsdever et al. (2005) presents a thrust difference between 20 and 30% when compared to the numerical results while the current analytical model presents a thrust difference up to 10%.

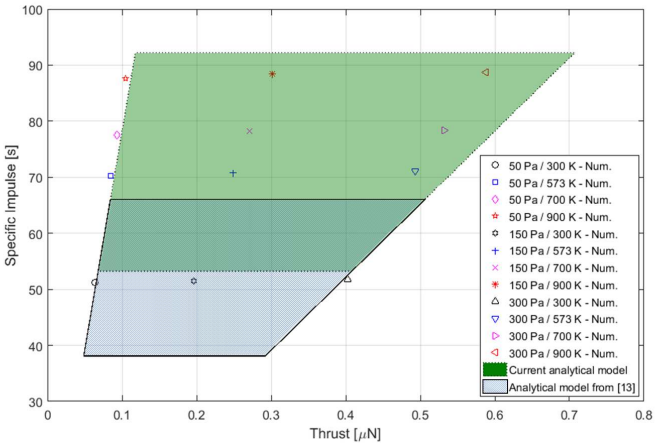

Figure 4.2: Thrust versus Specific Impulse for different values of the plenum pressure ranging from 50 to 300 Pa and wall temperature ranging from 300 to 900 K. Comparison between the numerical results presented in Chapter 3, the analytical model proposed in Ketsdever et al. (2005) and the current analytical model for a single circular microchannel using Nitrogen with aspect ratio of 5 and plenum temperature of 300 K.

Numerical results presented by Mancas (2013), which studies the behaviour of the flow inside a cuboid microchannel, are used to compare to the current analytical results, see Table 4.2. A single cuboid microchannel with aspect ratio of 5 (length of 500 μm, short slot dimension of 100 μm and large slot dimension of 5.375 mm) under plenum temperature of 300 K using Nitrogen as propellant is the analysed case. Here, a plenum pressure varying from 50 to 200 Pa and a wall temperature varying from 300 to 900 K is considered. In this case, the thrust differences are considered acceptable since the uncertainty in the simulations is reported to be around 4.4%. Additionally, there is also the uncertainty from empirical Equation 4.6 that does not consider the thermal effect. Comparing the results provided by Mancas (2013) and the results from analytical model proposed in Ketsdever et al. (2005), there is a difference between 35 and 45 %.

The analytical model is also compared to the experiment performed in Ketsdever et al. (2005). The heater chip was made out of silicon wafer with thickness of 500 μm presenting 44 slots with dimensions of 100 μm wide and 5.375 mm long, meaning aspect ratio of 5. The experiment was performed using a nano-Newton thrust stand in a large vacuum chamber that was capable to keep the background pressure below 10^{-2} Pa.

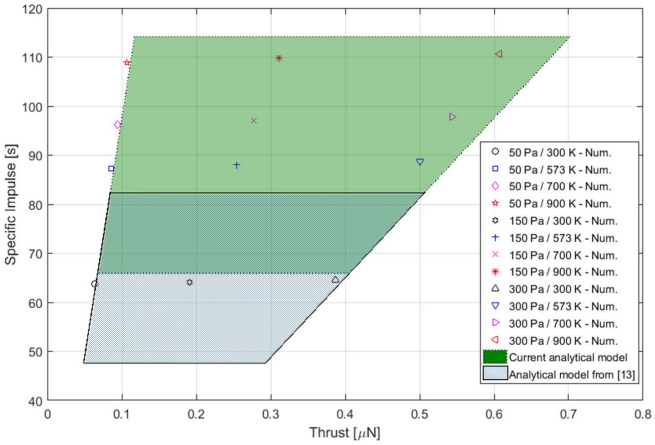

Figure 4.3: Thrust versus Specific Impulse for different values of the plenum pressure ranging from 50 to 300 Pa and wall temperature ranging from 300 to 900 K. Comparison between the numerical results presented in Guerrieri et al. (2015), the analytical model proposed in Ketsdever et al. (2005) and the current analytical model for a single circular microchannel using Water with aspect ratio of 5 and plenum temperature of 300 K.

Table 4.2: Comparison between the numerical results presented by Mancas (2013) and the analytical model for a single slot using Nitrogen with aspect ratio of 5 and plenum temperature of 300 K.

P_0 [Pa] / T_w [K]	$\Im_{num}$ [μN]	$\Im_{ana}$ [μN]	$\Delta\Im$ [%]
50 / 300	6.8	6.3	-7.9
50 / 600	9.2	8.9	-3.4
50 / 900	10.9	10.9	-0.2
100 / 300	13.6	12.6	-7.9
100 / 600	18.1	17.8	-1.7
100 / 900	21.4	21.7	1.4
150 / 300	20.4	18.9	-7.9
150 / 600	26.8	26.6	-0.8
150 / 900	31.9	32.6	2.1
200 / 300	27.3	25.2	-8.3
200 / 600	36.0	35.5	-1.4
200 / 900	42.6	43.5	2.1

They provide fit equations for the thrust as well as the specific impulse both as functions of T_w, and using a constant mass flow rate of 50 sccm. Different propellants were used such as Nitrogen (N_2), Argon (Ar) and Carbon dioxide (CO_2). Figure 4.4 shows the comparison of thrust between experiment and analytical results presented in Ketsdever et al. (2005) and the current analytical model. Similarly, Figure 4.5 shows the specific impulse comparison. The differences between experimental and the current analytical results can be considered acceptable, taking into account the uncertainties in the applied measurements of the experimental setup and the description of the experiment setup and procedures.

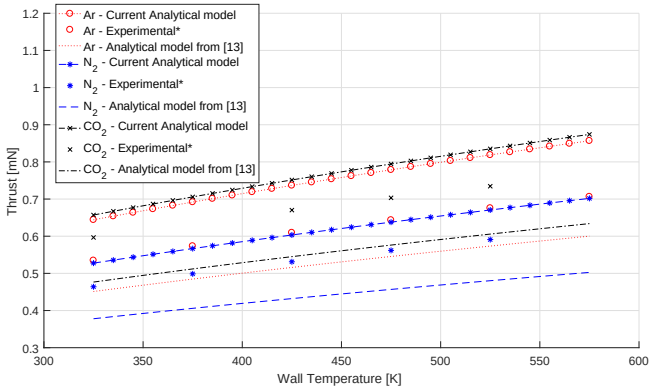

Figure 4.4: Thrust as a function of T_w for different propellants and constant mass flow rate. *The experimental results were plotted from the fit equations presented in Ketsdever et al. (2005).

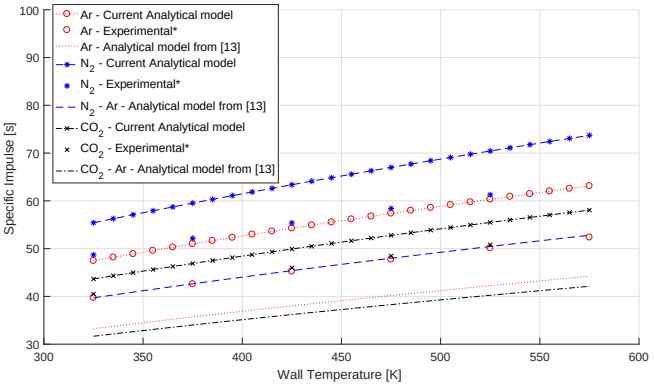

Figure 4.5: Specific impulse as a function of T_w for different propellants and constant mass flow rate. *The experimental results were plotted from the fit equations presented in Ketsdever et al. (2005).

The analytical model, developed in this chapter, is recommended to be used in order to estimate the LPM performance during the initial engineering design phase. It is

particularly useful to perform parametric analysis to define how different design parameters influence the thruster performance. However, it presents a limitation when the microchannel is not straight as in this case the flow characteristics can not be accurately reproduced by this simplified analytical model.

4.4. CONCLUSION

An analytical model to estimate the performance of Low-Pressure Micro-Resistojets was developed. This analytical model simplifies the engineering design of the propulsion system, allowing faster decision-making and detailed parametric analysis. The proposed analytical model presents a much better accuracy when compared to the analytical model proposed in Ketsdever et al. (2005). The main uncertainty in the proposed model is the empirical equation to calculate the transmission coefficient which does not take into account the heat effect. Using a more accurate estimation of the transmission coefficient obtained from numerical analysis, the difference between the performance predictions obtained by numerical DSMC results and the results of the analytical model are lower than 3%.

5

Fabrication and Characterization of the Heater Chip

Tell me and I forget, teach me and I may remember, involve me and I learn.

Benjamin Franklin

Three different LPM heater chips with integrated heater and temperature measurement functionality were designed, manufactured and characterized in this chapter. The devices were manufactured using Silicon-based Micro Electro Mechanical Systems (MEMS) technology including a heater made of Molybdenum (Mo) for better operations at high temperature. The resistance of the heaters is used to estimate the chip temperature giving them a double function as heater and sensor simultaneously. The manufacturing steps are described in detail. A special interface was manufactured to hold the MEMS device considering the mechanical and electrical aspects. The MEMS devices are characterized for three different aspects: mechanical, electrical and propulsive. The three designed devices were tested mechanically and electrically, and one design was tested in terms of propulsion performance in a near-operational condition.

The content of this chapter has been published in Journal of Micromechanics and Microengineering **27**, 12 (2017).

5.1. INTRODUCTION AND DESIGN DESCRIPTION

As a first step towards the development of a flight demonstration model of the LPM. This chapter presents the first LPM prototype developed by TU Delft in order to meet the strict requirements of nano- and pico-satellites. A cooperation between the Department of Space Engineering (SpE) and the Else Kooi Laboratory (EKL) was established to develop one of the LPM parts, the heater chip, that is manufactured using MEMS processing techniques.

The EKL provides micro fabrication capabilities aiming to develop the micro-electro-mechanical systems (MEMS) technology and to link Academia and Industry. They have laboratories including for instance, the Integrated Circuit (IC) Processing Lab is a Class 100 (ISO5) cleanroom which provides a fully equipped processing environment: from mask making to silicon manipulation to metallisation for a wide assortment of structures, devices and complete ICs EKL (2018). This is where the heater chip is manufactured. The SpE provides a class 100,000 cleanroom (ISO 8) and a workshop with the intention to facilitate high-level research on space systems and to provide students with education and training in a professional environment SpE (2018). It is where the LPM prototype is integrated and tested.

Three different microchannel geometries based on results presented in the previous Chapters are considered for the heater chip design: a grid of 40×40 holes with a diameter of 100 μm, a grid of 1×10 large slots with a width of 200 μm and length of 6.28 mm, and a grid of 1×20 small slots with a width of 100 μm and length of 6.28 mm. Those devices are characterized by the same exit area of 16 mm^2, a value designed to provide a measurable thrust level, and the same nominal resistance. Figure 5.1 shows the mask for the grid of holes (GH), the grid of large slots (GLS), the grid of small slots (GSS), and the heater (resistance).

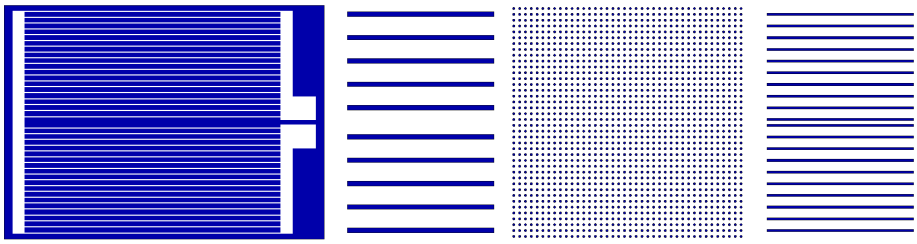

Figure 5.1: Masks used in the manufacturing process of the devices. The same heater mask was used in all devices, namely GLS, GH and GSS chips.

As shown in Figure 5.1-a, the heater is composed of 38 resistances arranged into two sets of 19 resistances in parallel, with these two sets arranged in series. Each resistance was designed to have length of 100 mm, width of 20 μm, and thickness of 200 nm. The thickness is a standard dimension deposited by the machine. The length and the width are defined accordantly to the desired resistance that in this case was defined to be 105 Ω to produce 1.4 W of power given a voltage of 12 V. The resistance material used was

Molybdenum (Mo) which has a resistivity of 400 $n\Omega\,m^{-1}$. The Mo presents a linear resistivity response to the temperature up to 700°C (Mele et al., 2012).

The propellant used to perform the experiment in order to characterize the thruster was Nitrogen because it is cheap, easy to handle, and a well-known propellant used for this purpose (Ketsdever et al., 2005; Palmer et al., 2013). In addition this allows to validate the previous results since Nitrogen was also used as propellant in chapter 3. Based on that, for a range of plenum pressures from 50 to 300 Pa and a heater chip temperature from 300 to 600 K, each designed device works at different range of mass flow rate and thrust. For the GH the range of mass flow rate is from 0.2 to 1.0 $mg\,s^{-1}$ and the range of thrust is from 0.1 to 0.5 mN, for the GLS they are from 0.4 to 2.5 $mg\,s^{-1}$ and from 0.2 to 1.3 mN, and for the GSS they from 0.3 to 2.0 $mg\,s^{-1}$ and from 0.1 to 1.0 mN. The expected specific impulse has the same range in all devices from 51 to 72 s.

5.2. DESCRIPTION OF MANUFACTURING PROCESS

The used silicon wafer was a double side polished wafer with thickness of 500 μm. First, lithographic alignment marks are etched on the wafer surface to enable high accuracy alignment of subsequent layers. A layer of 500 nm of LPCVD (Low Pressure Chemical Vapour Deposition) silicon nitride was deposited to isolate the wafer and the resistance, see Figure 5.2-a. A layer of 200 nm of Mo was deposited over the layer of silicon nitride by sputtering. A layer of 300 nm of PECVD TEOS (Plasma-Enhanced Chemical Vapour Deposition Tetraethoxysilane) was deposited to make the hard mask for Mo, see Figure 5.2-b. The heater mask, Figure 5.1-a, was made by photoresist, see Figure 5.2-c. The TEOS (hard-mask) was etched with buffered hydrofluoric acid (BHF), and then the Mo was also etched with aluminum etch at 35°C. Both processes were a wet etching, see Figure 5.2-d. To complete this step of the process, the photoresist was stripped off with plasma, and the TEOS was removed with BHF, see Figure 5.2-e.

To etch through the wafer, it is necessary to have the hard-mask layer on one side, and a stopping layer on another side. On both sides a layer of 5 μm of silicon dioxide was deposed, see Figure 5.2-f. On the hard-mask the photoresist to make the soft-mask was also deposed, see Figure 5.2-g. Figure 5.1 shows the three masks used for the GH, GLS, and GSS. Each of these masks was used on one wafer, producing three different wafers. The soft-mask was used to etch the hard-mask (silicon dioxide) and the silicon nitride with plasma etching, see Figure 5.2-h. Finally, the soft- and hard-mask were used to etch the silicon by anisotropic Deep Reactive Ion Etching (DRIE), see Figure 5.2-i. Then, the cleaning and removal of the soft-mask, hard-mask and stopping layers were done. Figure 5.2-j shows the schematic cross-section of the device after the manufacturing process. Finally, the wafers were diced as shown in Figure 5.3. As it is possible to see in Figure 5.3, 16 heater chip devices of same design were made using one single wafer.

5.3. EXPERIMENTAL PROCEDURE

In total, three wafers were processed, each one with a specific design (GLS, GH, GSS). The heater chips were characterized in terms of mechanical, electrical and propulsion aspects. For this reason, a special interface was designed and built to provide the mechanical and electrical interface, see Figure 5.4. It is made of teflon and aluminium, with

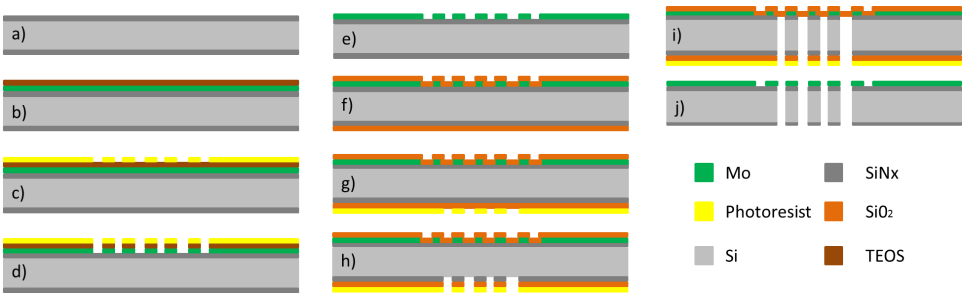

Figure 5.2: Schematic cross section of heater chip during the steps of the manufacturing process.

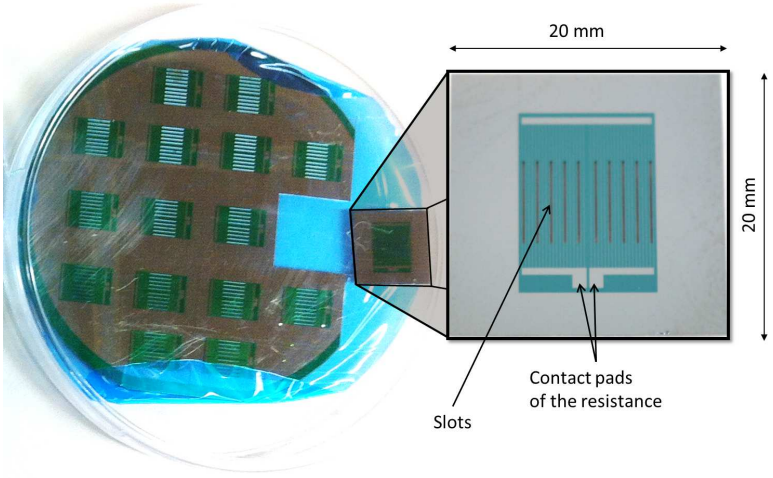

Figure 5.3: Wafer with large slots chips (GLS) after manufacturing and dicing process.

teflon providing good isolation that supports a moderately high temperature and aluminum sufficient structure strength.

5.3.1. MECHANICAL CHARACTERISTICS

A sample of the manufactured device was measured in order to compare the actual dimensions to the design ones. An optical microscope was used for the main dimensions, and an electron microscope for small details. According to the nominal design, the GH has a hole diameter of 100 μm and a pitch of 200 μm, the GLS has width of 200 μm and length of 6.28 mm, the GSS has width of 100 μm and length of 6.28 mm, and the resistance width of 20 μm and length of 11 mm.

5.3.2. ELETRICAL CHARACTERISTICS

The material and the geometry play a major role in the performance of the resistors. This can be mathematically expressed by the following equation:

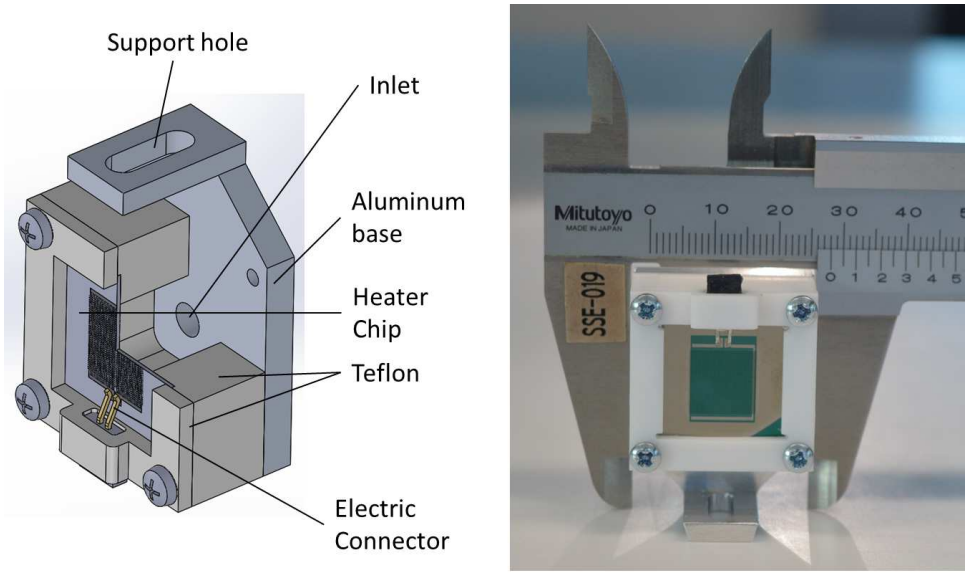

Figure 5.4: Left: Sketch of the interface prototype of the thruster. Right: Picture of the actual assembled prototype.

$$R_0 = \frac{\rho L}{A_R} \tag{5.1}$$

where R_0 is the resistance measured at room temperature T_0, ρ is the material resistivity, L is the length and A_R the cross-sectional area of the specimen. Another important relation is the equation relating the resistance and temperature, expressed as

$$\beta = \frac{R - R_0}{R_0 (T - T_0)} \tag{5.2}$$

where β is the temperature coefficient of the resistance, and R is the resistance measured at temperature T. Even though the value of β is basically related to the material, it is good practice to characterize its value for each device as any impurities induced by the manufacturing process can affect this value. A complete characterization of a similar device has been performed by (Mele et al., 2012).

The devices' resistances were measured at room temperature in order to compare them to the design ones. In addition, a test bench using a thermal camera with 5% accuracy and a power supply was set up to characterize the temperature coefficient of the resistance β. The experimental setup and a sequence of images taken with the infrared camera from the backside of the GLS heater chip is shown in Figure 5.5. These measurements are used to estimate the average temperature of the heater chip over time. It is performed by applying a constant voltage to the heaters in order to measure the resistance. Then, β can be determined using Equation 5.2.

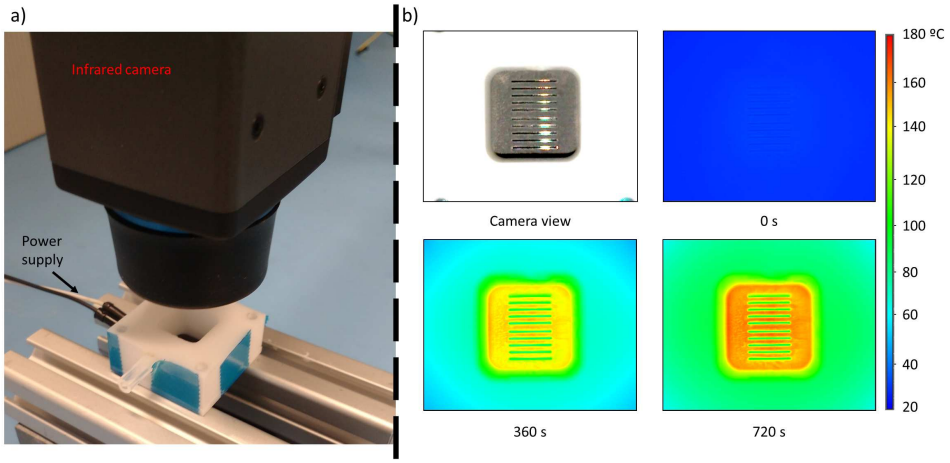

Figure 5.5: a) Setup used to define the temperature coefficient of the resistance (β) in Equation 5.2. b) The temperature measurement of the chip surface using an infrared camera. The left top side shows the camera view; the chip is painted with graphite ink that provides an uniform emissivity of 0.97. The other images are from the infrared camera at different moments after applying a constant voltage of 39 V.

5.3.3. PROPULSION CHARACTERISTICS

A test bench using a pendulum was used to measure the thrust. Figure 5.6 shows a simplified piping and instrumentation diagram of the test bench, and Table 5.1 presents the features of the sensors. The propellent is stored in a tank outside the vacuum chamber and is fed through a flexible tube attached to the rotation point of the pendulum in order to reduce disturbances produced by the flow of gas inside the tube. A valve is used to regulate the plenum pressure and to operate the thruster during the tests. A capacitive sensor is placed behind the pendulum to measure its displacement.

The pendulum presents an error due to the calibration process of about 13 μN, as described in detail in (Bijster, 2014; Jansen, 2016). The experiment was performed in a vacuum oven under different background pressures ranging from 15 to 35 Pa and different heater chip temperature: room temperature 24°C; and high temperature 149°C.

Using the results obtained from the electrical characterization, the resistor on the chip was used as a double function heater and temperature sensor. Based on the voltage and current measurements, a PID controller was used to control the heater chip temperature during the high temperature experiment. This temperature sensor was characterized for a temperature range from 20 to 160°C with an accuracy of 8°C due to the noise given mainly by the power supply.

In order to have a low pressure inside the plenum, the valve (FC-01) is controlled by Pulse-Width Modulation (PWM). Thus, the mass flow rate depends on the tank pressure (PT-01), tank temperature (TT-01) and the PWM signal. When the valve is opened the propellant is expelled into the vacuum chamber increasing the background pressure quickly. Due to this, the only considered measurement for this chapter are the data just after the valve opening.

To assure that the background pressure is the same in all measurements, an auto-

matic control of the experiment was implemented. When the pressure sensor (PT-02) measures the desired background pressure, a command is sent to the valve (FC-01) starting the propellant flow to the thruster. When the vacuum chamber reaches a pressure 5 Pa higher than the desired background pressure, a new command is sent, closing the valve. Then, the cycle starts again.

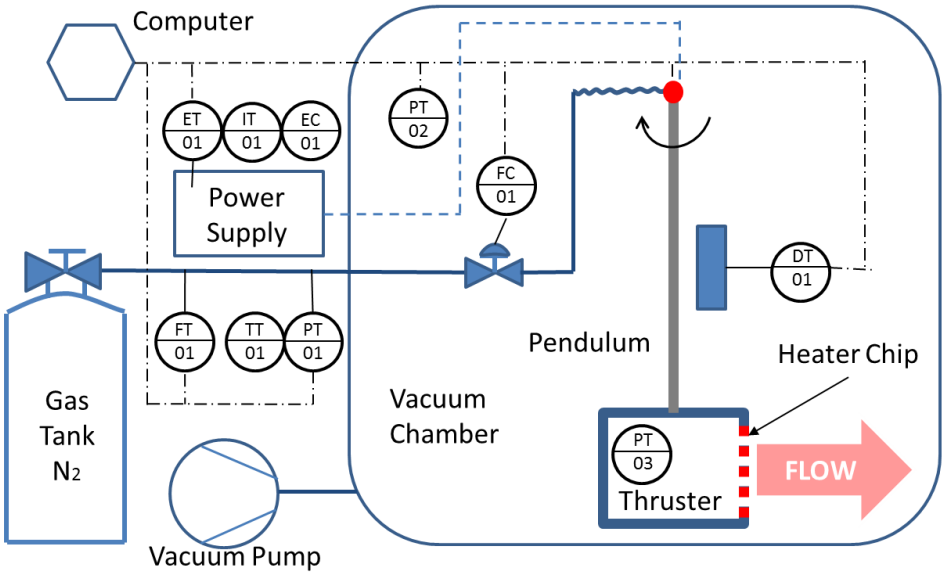

DT – Displacement Transmitter; EC – Voltage Controller; ET – Voltage Transmitter; FC – Flow Controller; FT – Flow Transmitter; IT – Current Transmitter; PT – Pressure Transmitter; TT – Temperature Transmitter.

Figure 5.6: A simplified piping and instrumentation diagram of the test bench.

The pendulum provides an indirect measurement of the thrust and needs to be calibrated before each test. The pendulum is calibrated using a known force generated by a coil and the displacement, measured from DT-01, is recorded. This calibration defines the linear relationship between displacement and force. More details can be found in (Bijster, 2014; Jansen, 2016). This relation is used to calculate the thrust based on the measured displacement. During the experiment, the measurements from all sensors shown in Figure 5.6 were recorded. The propellant used to perform the test was Nitrogen.

5.4. RESULTS AND DISCUSSION

The results of the three characterizations (mechanical, electrical, and propulsive) are presented and discussed in this section.

Table 5.1: Datasheet characteristics of the sensors and actuators used in the test bench.

#	Sensors/Actuators	Manuf. number	Operation range	Accuracy
DT-01	Displacement	DT6220 - CS05 (Micro-Epsilon)	0 - 0.5 mm	± 40 nm
ET-01	Voltage	SM7020	0 - 70 V	± 70 mV
IT-01	Current	(Delta Elekt. BV)	0 - 20 A	± 20 mA
FT-01	Flow	5850S (Brooks)	0 - 2 ln/min N2	± 2 mln/min
PT-01	Pressure	MS5803-05BA	0 - 5 bar	± 1.5 mbar
TT-01	Temperature	(TE connectivity)	-40 - 80 °C	± 2.5 °C
PT-02	Pressure	VSP 3000 (Vacuubrand)	0.001 - 1000 mbar	± 15% of displayed value
PT-03	Pressure	HCLA12X5DU (First sensor)	0 - 12.5 mbar	± 0.016 mbar

5

5.4.1. MECHANICAL CHARACTERIZATION

The design dimensions given in Subsection 5.3.1 were compared to the measured values shown in Figure 5.7. It is possible to see a slight difference between the design and manufactured values. The most relevant difference is that there is a layer of silicon nitride in the stop layer side that was not etched equally compared to the silicon wafer, giving a small protuberance of about 3 μm as seen in Figure 5.8. The same difference can be seen in Figure 5.7 through the measurements made in the GH chip: the measured hole in the silicon wafer is 106.3 μm while in the silicon nitride layer is 100.7 μm. Figure 5.8 also shows the roughness in the wall which might affect the thruster performance. Another relevant difference is related to the thickness of the Mo layer, where less Mo than expected was deposed, resulting in a higher resistivity as it is showed in Subsection 5.4.2. This affects the amount of voltage necessary to be applied to achieve the expected power.

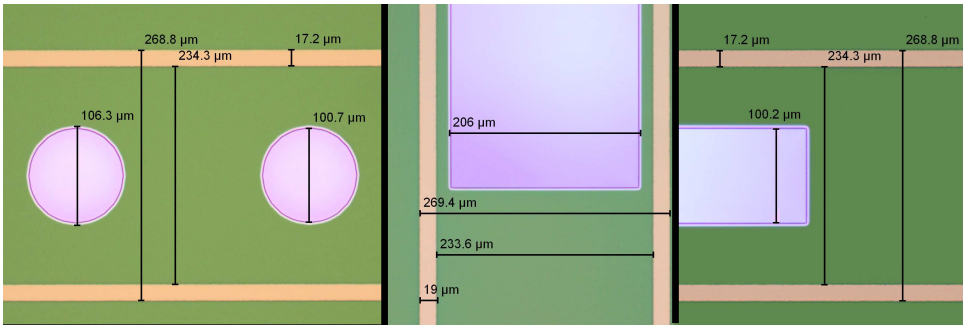

Figure 5.7: Dimensions of the chip geometries measured using an optical microscope with 10× magnification. On the left side the GH, in the center the GLS and on the right side the GSS.

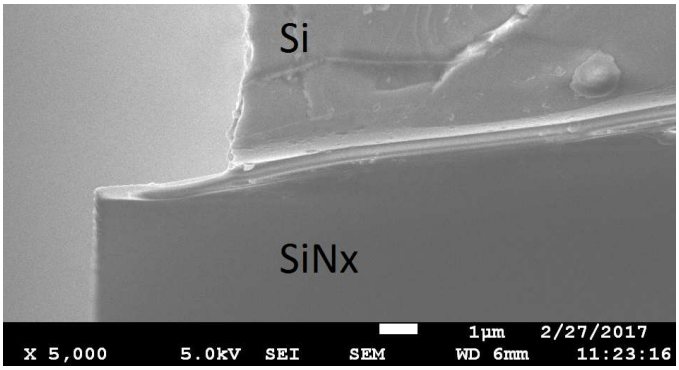

Figure 5.8: Cross-sectional view of the GLS chip using a scanning electron microscope.

5.4.2. ELECTRICAL CHARACTERIZATION

The measured resistances of the devices are higher than designed due to inaccuracies in the manufacturing process. There are two main reasons for that during the manufacturing process: the deposition of Mo was less than expected, or the exposition time to etch the TEOS (hard-mask) was longer than expected resulting in etching the Mo layer reducing its thickness. The GLS and GSS present, respectively, an average resistance of $272.76 \pm 8.18\,\Omega$ and $263.40 \pm 7.85\,\Omega$, around 2.5 times larger than expected. The GH, that was processed at a different moment, presents an average resistance of $435.13 \pm 31.96\,\Omega$, around 4 times larger than expected. This increased resistance results in a higher voltage to achieve the required power, however this is not an issue for the tests presented here.

The temperature, as measured using the thermal camera, is plotted against the resistance measured for each device and shown in Figure 5.9. Those measured values were used to determine β in order to measure the temperature according to the heater chip resistivity. The average value of β for the three tested heater chips is $0.0015°C^{-1}$ and the standard deviation is $8.63\times10^{-5}°C^{-1}$. Figure 5.10 presents the comparison between the measurements with the thermal camera and the estimation done with Equation 5.2 for the GSS, GH and GLS. It is possible to see that they match quite well, proving that using the resistivity method gives an acceptable temperature estimation. This approach is useful to control the temperature of the thruster with no addition of electronic component such as thermocouple or similar, making this propulsion system even more suitable for use in very small satellites.

5.4.3. PROPULSION CHARACTERIZATION

The thrust was characterized performing tests using the pendulum as described in section 5.3. The tests were performed using the GLS chip which provides higher thrust with the same plenum pressure due to its geometry. Due to the background pressure, it was decided to perform the tests with the plenum pressure between 200 and 280 Pa. The minimum pressure 200 Pa is chosen because, with this pressure the background pressure represents less than 10% of the plenum pressure. The maximum pressure 280 Pa has been selected because it represents the boundary between the transitional regime

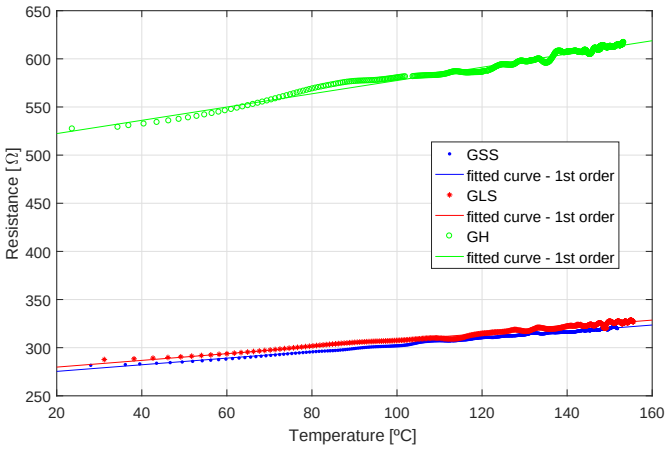

Figure 5.9: Relationship between the heater resistivity and the average chip temperature for the three heater chips. The sample heater chip used here presents a resistivity at room temperature of 520 Ω for GH, 276 Ω for GLS and 269 Ω for GSS.

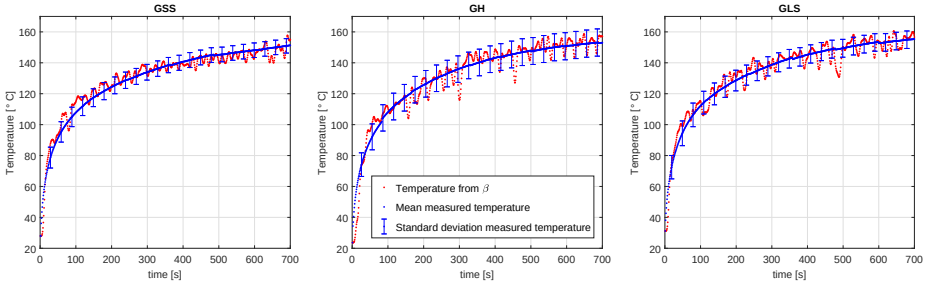

Figure 5.10: Comparison between the temperature measurement from the infrared camera and the calculated temperature based on Equation 5.2.

and the slip flow regime i.e. a Knudsen number of 0.1. Thus, the tests using high temperatures were performed in the slip flow regime. This happens because the plenum temperature increases due to the high heater chip temperature with a consequent increase in plenum pressure. The range of mass flow rates was kept between 2.2 and 3.6 mg s^{-1}. A careful comparison between both pressure scenarios has to be done in order to assess the differences between the two regimes. However, such comparison is out of the scope of this chapter that is dedicated to the characterization of the devices/thrusters.

Figure 5.11 shows the relationship between the mass flow rate and the plenum pressure for different background pressure and different plenum temperature (room temperature or higher heater chip temperature). An estimation of the plenum temperature can be done using the ideal gas equation. Assuming an isochoric process considering the same mass flow rate with different pressures, the gas temperature changes from room temperature (24°C) to 134.5°C. This temperature is close to the controlled chip tempera-

ture which is 149 ± 8°C. This difference is expected due to the heat transfer mechanism.

Figure 5.12 presents the thrust measurement as a function of the plenum pressures for different chip temperatures and background pressures. It shows the influence of the background pressure on the thrust level. As expected, the thrust tends to increase with decreasing background pressure, meaning that in the space environment a higher thrust is expected. As a comparison, the Table 5.2 presents the expected thrust performance based on the analytical model presented in Chapter 4 assuming the space environment.

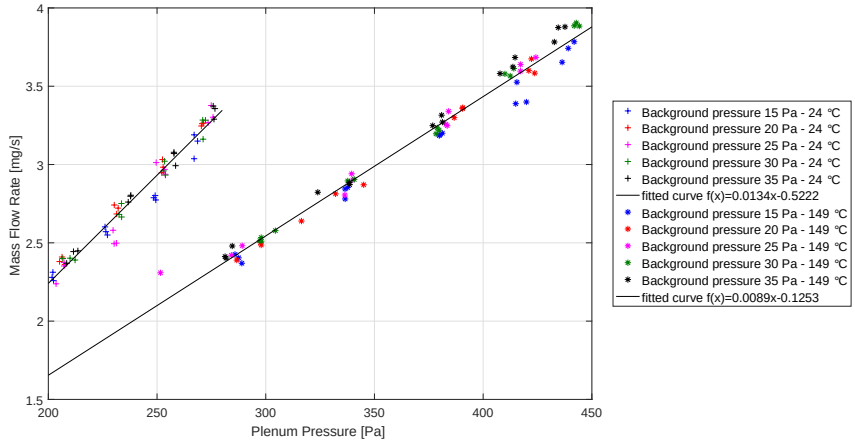

Figure 5.11: Relationship between the plenum pressure and the mass flow rate for different background pressures and different heater chip temperatures. The 1st order fitted curve present a R-square of 0.9663 for the room temperature 24°C and 0.9844 for the high temperature 149°C.

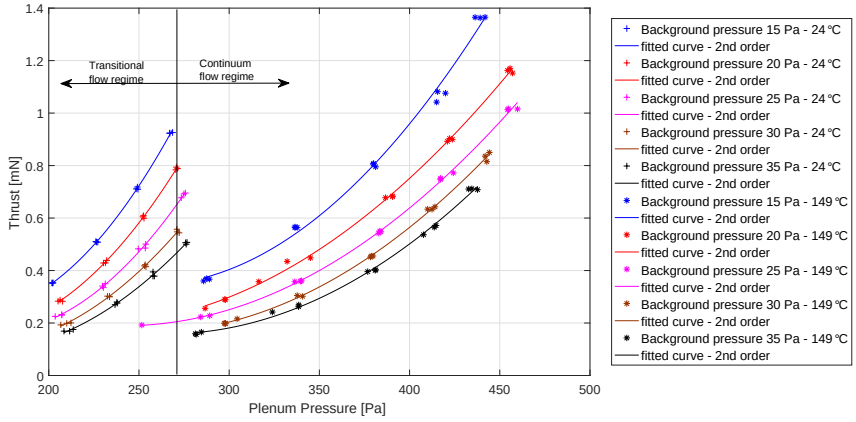

Figure 5.12: Relationship between the plenum pressure and the thrust for different background pressure and different heater chip temperature for GLS chip.

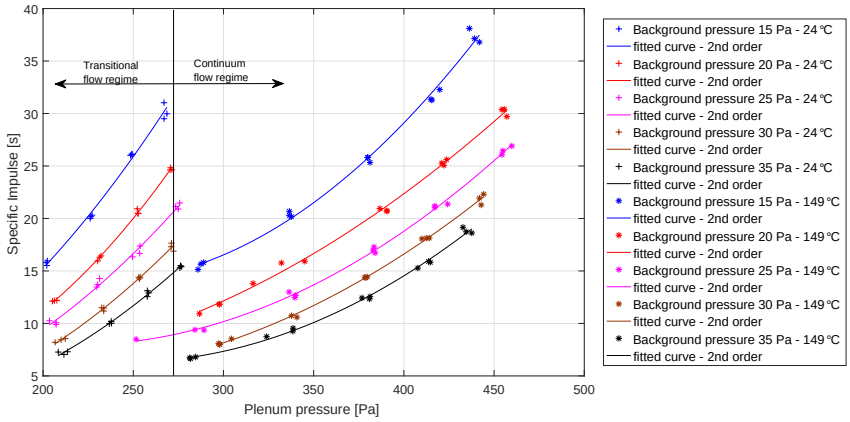

Figure 5.13: Relationship between the plenum pressure and the specific impulse for different background pressure and different heater chip temperature for GLS chip.

5

Table 5.2: Thrust performance based on the analytical equations presented in Chapter 4.

P_0 [Pa]	T_w [°C]	$\Im$ [mN]	I_{sp} [s]
200	24	0.6	53
200	149	0.7	63
300	24	0.9	53
300	149	1.1	63

Although higher chip temperatures appear at first sight to result in higher thrust, this is not true since Figure 5.11 reveals that for the same mass flow rate the plenum pressure is different but the thrust is similar (see Figure 5.12). Similar conclusions can be drawn for the specific impulse in Figure 5.13. To analyse these results, two points have to be considered: 1) there is a transition between the transitional regime and the continuum flow regime; 2) the high temperature of the chip raises the temperature of the gas in the plenum, thus raising the plenum pressure.

Even though the tests were performed at non-ideal conditions, different than the actual space environment, they are very useful for the development and characterization of the LPM. The considered background pressure is one of the main issues in performing the tests, because it represents about 7.5% of the minimum plenum pressure, which was 200 Pa. Furthermore, the flow regime changes in the high temperature tests, and the corresponding increased plenum temperature is not a desired behaviour since it makes significantly more difficult to compare the results of tests conducted at different chip temperatures as the plenum pressure is also increased.

5.5. CONCLUSION

The design, manufacturing and characterization of a Low-Pressure Micro-resistojet with an integrated heating and temperature sensing was discussed. Three different heater chip designs (GH, GLS and GSS) were assessed in terms of their mechanical and electrical characterization. One design (GLS) was used to assess the propulsion performance in near-operational conditions using Nitrogen as propellant. It was successfully demonstrated that this propulsion system has the potential for usage in very small satellites. Apart from its performance, its inherent simplicity makes this design suitable for this class of satellites.

The manufacturing process was effective producing a total of 48 devices with only two damaged. The two damaged devices were related to the GH chips. In one, the holes were not etched properly and, in another one, the Mo was not deposited correctly showing a discontinuity. In fact the GH wafer presented the highest electric resistivity as showed in the electric characterization. Generally speaking the deposition of the Mo was found to be the main issue during the manufacturing process, depositing less Mo than expected.

The mechanical and electrical characterization shows some differences between the designed and manufactured MEMS devices, but they were acceptable for initial testing purposes. The Mo heater proved to be a good choice due to its stability at high temperatures up to 850°C allowing the measurement of the temperature as function of the resistance. Due to that, the temperature was measured and controlled through the PID controller in real-time during the propulsion test. The propulsion characterization shows the potential of the thruster under near-operational condition.

The special interface used to hold the heater chip was considered robust enough for the tests. However, for the next design and for the flight demonstration model, it is suggested to use a ceramic material instead of teflon. The use of ceramic material has benefits such as much better isolation and resistance to very high temperature. The electric wires and components have to support high temperatures since the heater chip is supposed to achieve temperatures up to 300°C, and in special cases even up to 600°C. This will require a careful re-design of the electrical path to the power supply.

6

Optimum LPM Design

...to optimize is natural. Every moving thing does it freely,
animate and inanimate.
Every river alters its course and bed cross section
to flow more easily.
Every animal group varies its migration routes to facilitate its movement,
i.e., its life...

(Bejan, 2015)

This Chapter discusses the optimization of the Low-Pressure Micro-Resistojet (LPM) design applied to two different missions, one for a two-satellite CubeSat mission which requires formation flight and an another one for a PocketQube mission which performs technology demonstration. Scalability of the LPM and performance are the two aspects which are analyzed and discussed in this Chapter.

The content of this chapter has been published in the proceedings of Space Propulsion Conference, Sevilla, Spain, 2018.

6.1. INTRODUCTION

The miniaturization of satellites implies constraints mainly in size, mass, and power, that have to be taken into account when designing spacecraft propulsion subsystems. Moreover, those satellites are usually put into orbit by piggy-back launches. Therefore, launch providers impose a number of constraints related to the safety of the main payload of the rocket. Other constraints stem from the standardization of these satellite classes as well as the specific mission. All these premises and the outcomes from previous chapters are used in this Chapter as baseline in order to optimize the LPM design to two different mission scenarios. Here, optimization is not meant in rigorous mathematical or modeling sense. Rather, it is understood as identifying key characteristics of parameters of the LPM in the presence of multiple complex requirements and constraints.

The first mission scenario is based on two identical CubeSats which are supposed to perform a formation flight. An along-track separation of 1000 km is expected by using a total velocity increment of 15 $\mathrm{m\,s^{-1}}$ considering the formation acquisition and the formation keeping (Gill et al., 2013; Cervone et al., 2015a).The second mission scenario is based on a PocketQube which are supposed just to perform a flight propulsion system demonstration. Velocity increment is not required (Pallichadath et al., 2017, 2018). The specific requirements of these mission scenarios can be seen in Tables 1.1 and 1.2.

In addition to the defined requirements by the mission scenarios, a few more requirements are set accordingly to the conclusions of the previous Chapters. Based on the numerical analysis presented in Cervone et al. (2017) and in Chapter 3 as well as the fabrication aspects presented in Chapter 5, it is decided to:

1. The straight microchannels with aspect ratio of 5 is chosen, because the idea is to have, for the next heater chip version, an improved geometry as proposed in Chapter 3.

2. The plenum pressure has to be less than 300 Pa to be within the transitional flow regime;

3. The heater chip temperature shall not exceed 700 [K] to preserve the system functionality in terms of handling high temperatures.

The propulsion system is optimized to increase the thrust, to reduce the heater chip area, to reduce the power consumption, and to reduce the tank size. Additionally, suitable tank designs for this propulsion system are discussed. One of the main precautions designing the tank to store the propellant is to avoid sloshing. Previous publications suggested to store water under a pressure below 611.66 Pa and temperature lower than 273.16 K in order to keep it in the frozen state (ice) (Cervone et al., 2017; Guerrieri et al., 2015). However, keeping water in a solid state is difficult in a space environment. Especially, it is difficult to keep it solid during the time from integration to launch; or in space, to make sure that the temperature is always below 273.16 K with a constrained power consumption.

6.2. DESIGN OPTIMIZATION

The optimization is performed analyzing the two key parameters, scalability and performance. Objective is to understand the performance of the propulsion system when scal-

ing it down in order to derive the best relation between performance and size. Basically, when miniaturizing a spacecraft, it is important to miniaturize the propulsion system in order to keep a similar performance level. From the scalability point of view, the amount of propellant, the expected thrust, and the fixed parts (e.g. valve, feeding lines, structure) are key for the final size of the propulsion system. Then, from the performance point of view, the performance depends in turn on the propellant, the delivered thrust, the Delta-V, and the available power. The propellant is not discussed in this Chapter since it is already covered in Chapter 2.

The LPM thruster is designed to work under low-pressure as discussed in the previous Chapters. The propellant can be stored as liquid or solid, i.e., at a higher density. This is a crucial aspect for miniaturization. The low-pressure environment inside the tank, combined with the liquid or solid propellant, allows to reduce the structural mass and complexity.

Based on that, the discussion is focused on the effect of the heater chip size and the tank size. The heater chip size depends on the amount of required thrust and the available power. For simplicity, as presented in Figure 6.1, the heater chip area, A_{hc} , is calculated as

$$A_{hc} = (a+2b)^2 \tag{6.1}$$

where a is the width and height of the useful heater chip area where the microchannels are placed, and b is the dimension between the useful area and the heater chip edge, see Figure 6.1. It is assumed that the useful area, a^2, is twice the exit cross-sectional area A_e, so a^2=2A_e and b = 1 cm. This ensures that the heat chip is strong enough to support any mechanical strength, and there is also enough room to deposit the electrical resistance material between the microchannels.

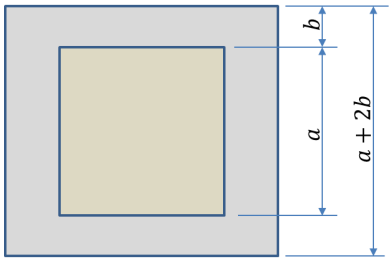

Figure 6.1: Heater chip scheme showing the assumptions made for the total area. It is assumed a^2=2A_e and b=1 [cm].

The tank size is related to the amount of required propellant and the needed mechanical strength against the internal pressure. The amount of propellant is determined based on the specific mission according to the requirements. Since water is assumed as propellant, the inner tank pressure can be as low as possible compatibly to the possibility of storing it in liquid or solid phase. The tank thickness can therefore be calculated based on the expected launch loads, allowing to reduce the dry tank mass. Different tank designs are discussed in the next sections in order to define the suitable solution

to store the propellant. These solutions presented are based on the lessons learned from the preliminary numerical analysis presented in Guerrieri et al. (2015), summarized in Appendix-B, and the preliminary experimental analysis presented in Maxence et al. (2017).

The equations used on the optimization are described in Chapter 4. The constraints are presented in the mission scenario requirements, Tables 1.1 and 1.2, plus the requirements based on the lessons learned of the previous Chapters such as microchannel aspect ratio equal to 5, plenum pressure less than 300 Pa, and heater chip temperature ranging 300 to 700 [K]. Objectives of the optimization are to increase the thrust, to reduce the heater chip area, to reduce the power consumption, and to reduce the tank size. The thrust is calculated based on Equation 4.20. The heater chip area is estimated accordantly to the Equation 6.1. The total power consumption is estimated summing the thruster power, Equation 4.22, and the tank power, 4.23. The power needed by the control system (electronics, valve, etc.) is neglected. Additionally, the velocity increment ΔV is calculated based on the linear approximation of the rocket equation, Equation 1.3, in order to estimate the tank size.

6.3. RESULTS AND DISCUSSIONS

6.3.1. OPTIMIZATION

The main limitations of a miniaturized propulsion system for nano- or pico-satellites are the volume, mass, and the available power. The requirements showed in Table 1.1 and Table 1.2 are suitable requirements of missions that use these class of satellites. Based on that, Figure 6.2 and Figure 6.3 present the design space according to the requirements. Figure 6.2 is referred to the heater chip with a grid of holes and Figure 6.3 is referred to the heater chip with a grid of slots. The thrust is strictly limited by the available power. The maximum thrust for a maximum power of 10 W (formation flying requirements) is 2.72 mN, and for a maximum power of 4 W (PocketQube requirements) is 1.09 mN. Additionally, to achieve the minimum thrust level according to the formation flying requirements, which is 0.5 mN, a minimum power of about 2 W is necessary.

The natural decision is to choose the smallest heat chip that achieves the highest thrust level. Then, the smallest heater chip area based on the CubeSat case is 722.4 mm^2 for the grid of slots and 870.6 mm^2 for the grid of holes. The smallest heater chip area based on the PocketQube case is 593.8 mm^2 for the grid of slots and 676.6 mm^2 for the grid of holes.

On one hand, if the circular microchannel with a diameter of 100 μm is chosen, at least a grid of 68×68 microchannels are necessary to accomplish the CubSat mission, and a grid of 43×43 microchannels to accomplish the PocketQube mission. On the other hand, if the cuboid microchannel with a cross-sectional dimension of 100 μm × 4.73 mm is chosen, at least a grid of 50×1 microchannels are needed to accomplish the CubSat mission. While, with a slightly different cross-sectional dimension of 100 μm × 3.08 mm is chosen, it is necessary to use a grid of 31×1 microchannels to accomplish the PocketQube mission.

Figure 6.4 shows the relation between the Delta-V per volume of fluid and the spacecraft mass. Using the target mass of the spacecraft which is 3.6 kg for the CubeSat case

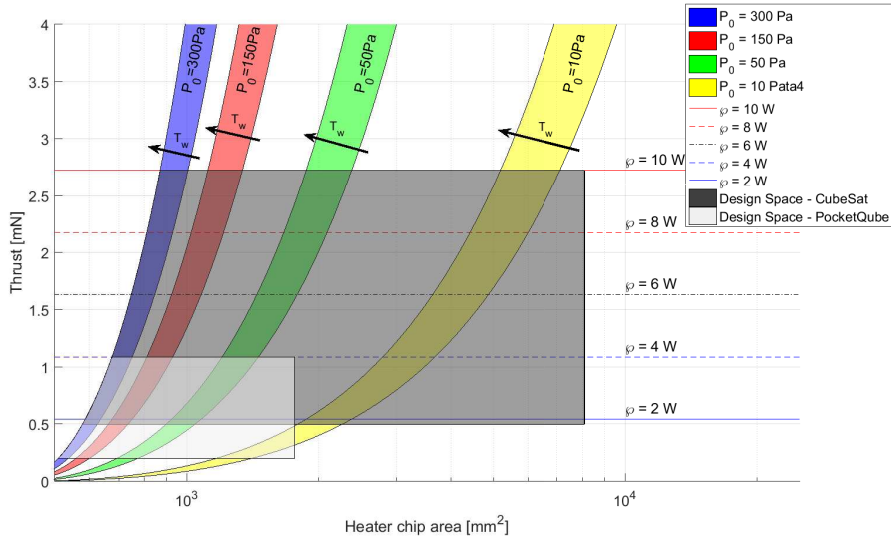

Figure 6.2: Design space for the CubeSat and PocketQube cases using the grid of holes.

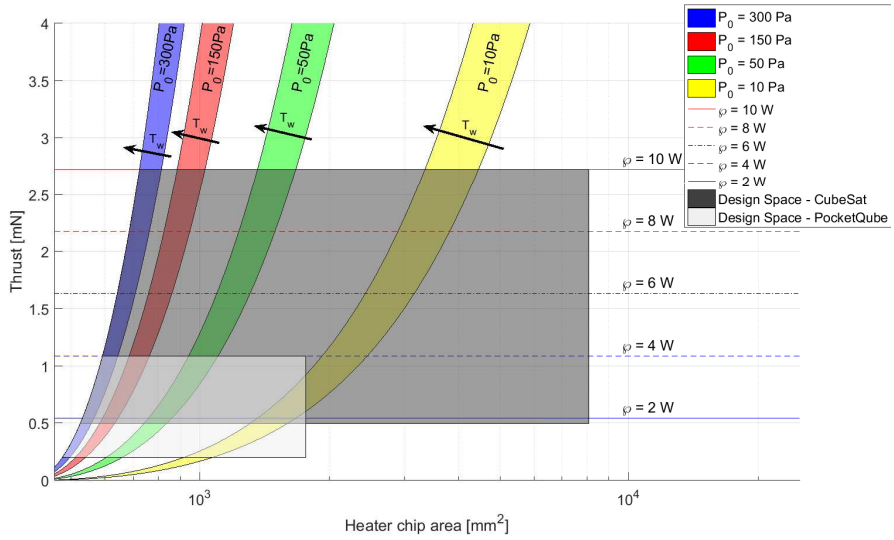

Figure 6.3: Design space for the CubeSat and PocketQube cases using the grid of slots.

and 0.7 kg for the PocketQube case, it is possible to estimate the amount of propellant needed according to the requirements. Therefore, the minimum propellant mass needed to accomplish the formation flying requirement is 59 g. Since the PocketQube case is based on performing a flight demonstration, it does not have a requirement on

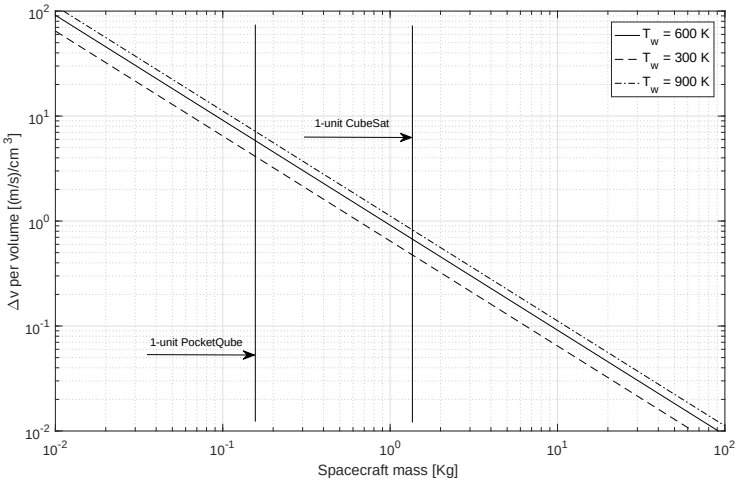

Figure 6.4: Relation between the Delta-V per volume of fluid and the spacecraft mass.

velocity increment. However, assuming the same required velocity increment from the formation flying case, the minimum propellant mass in the PocketQube case would be 11.5 g.

6.3.2. TANK DESIGN SOLUTION

Another important aspect when designing the propulsion system is how to store the propellant in order to avoid sloshing. Previous analysis has shown the difficulty of managing water in the tank. Guerrieri et al. (2015), summarized in Appendix-B, present a preliminary analysis of the tank design, and Maxence et al. (2017) present the preliminary experimental analysis of the tank using a small container (plastic vial) which showed that the heat flux plays a major role in the dynamics of the system. If the heat flux is relatively high the ice surrounding the heater starts to melt decreasing the heat transfer which affects directly the sublimation rate (delivered mass flow rate). The main conclusion that can be drawn is that, in order to increase the efficiency of the system, the surface area to volume ratio has to be increased. Moreover, it is advised to adapt a tank solution where water can be stored in any phase state (Liquid, Solid and Vapor) avoiding to waste electrical power to keep the desired phase state.

Figure 6.5 presents a generic Design Option Tree of tank design solutions. The classic rigid tanks are the natural choices to support high pressure level. Besides the typical shapes such as spherical, cylindrical and cubic, it is possible to select a different shape in order to optimize the volume. However, they are more problematic for this type of propulsion systems due to sloshing issues. Flexible tank options include bladder and pipe. The bladder tank is an interesting option considering an elastic material which reduces its size according to the propellant usage. However, it may not prevent sloshing, which may cause the bladder to deform in a random direction. On the contrary, the pipe tank is an interesting solution since the diameter of the pipe is small enough to al-

low capillary forces avoiding unacceptable mixing between the liquid and gaseous state of propellant. Another advantage of this suggested tank is that it can be placed in any available place within the spacecraft. It can be bent and inserted into places that are not been used, therefore optimizing the usage of space and the amount of propellant that can be carried on board. However, the disadvantage is that depending on the needed amount of propellant the length of the tubing might not be viable, causing an excessive friction force against the propellant movement within the pipe. As a consequence, this solution is interesting for pico-satellites, but it may not be viable for nano-satellites. It will be used for the first flight demonstration onboard of the Delfi-PQ satellite (Pallichadath et al., 2018).

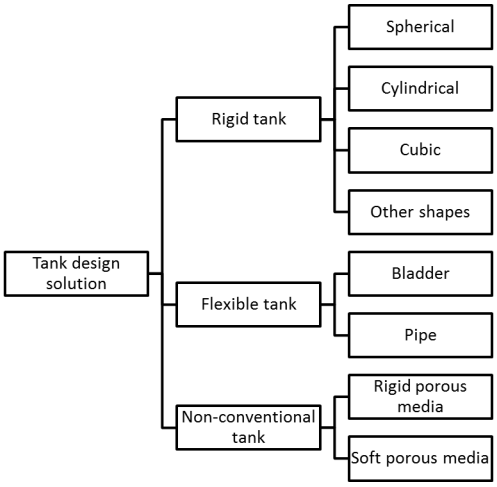

Figure 6.5: Tank design solutions Design Option Tree.

Table 6.1 presents the estimation of Delta-V and the expected lifetime depending on the pipe length assuming a inner diameter of 0.8 mm. Consuming the whole amount of propellant the propulsion system can be demonstrated accordingly to the minimum and maximum expected lifetime which are related to the plenum pressure of 300 and 50 Pa, respectively. The minimum Delta-V is based on the heater chip temperature of 300 K, while the maximum Delta-V is based on the heater chip temperature of 700 K.

Other non-conventional tanks could also be used such as the rigid and soft porous media. The soft porous media (sponge) tank is a combination of a rigid tank with a sponge inside. The sponge minimizes the sloshing effect, but it does not avoid it completely. Another interesting solution is to use a rigid porous media with controlled cavities or microchannels as tank, again taking advantage of capillary force in the cavities. Another advantage of this suggested tank is that there is a large contact area between the porous media structure and the propellant. It improves the efficiency of the heat transfer during the phase change (evaporation or sublimation) in order to increase the mass flow rate to supply the thruster. This solution is interesting when a large amount of propellant is needed. For instance, it might be a viable solution to be applied for the two CubeSat formation flying scenario mission.

Table 6.1: Estimation of Delta-V and the expected lifetime based on the pipe length for the PocketQube propulsion demonstration mission.

Pipe length [m]	Prop. mass [g]	Min. Delta-V [m s^{-1}]	Max. Delta-V [m s^{-1}]	Min. exp. lifetime	Max. exp. lifetime
1	0.503	0.49	0.84	7 min 48 s	46 min 46 s
2	1.005	0.99	1.69	15 min 35 s	1 h 33 min 32 s
3	1.508	1.48	2.54	23 min 23 s	2 h 20 min 17 s
4	2.011	1.97	3.38	31 min 11 s	3 h 7 min 3 s
5	2.513	2.47	4.23	38 min 58 s	3 h 53 min 49 s
6	3.016	2.96	5.07	46 min 46 s	4 h 40 min 35 s
7	3.519	3.45	5.92	54 min 33 s	5 h 27 min 21 s
8	4.021	3.94	6.76	1 h 2 min 21 s	6 h 14 min 7 s
9	4.524	4.44	7.61	1 h 10 min 9 s	7 h 0 min 52 s
10	5.027	4.93	8.45	1 h 17 min 56 s	7 h 47 min 38 s
11	5.529	5.42	9.30	1 h 25 min 44 s	8 h 34 min 24 s
12	6.032	5.92	10.14	1 h 33 min 32 s	9 h 21 min 10 s
13	6.535	6.41	10.99	1 h 41 min 19 s	10 h 7 min 56 s
14	7.037	6.90	11.83	1 h 49 min 7 s	10 h 54 min 42 s
15	7.540	7.40	12.68	1 h 56 min 55 s	11 h 41 min 27 s

6.4. CONCLUSION

Two different reference mission scenarios were used to optimize the LPM propulsion concept in terms of performance and scalability. One mission scenario was based on two CubeSats expected to perform formation flight. Another mission scenario was based on a PocketQube satellite expected to perform a technology demonstration. For each case an optimum heater chip size was determined and suitable tanks were discussed. This propulsion system is expected to be on board of one of the first launches of a Delfi-PQ satellite for an initial flight demonstration of its optimized design.

This Chapter was focussed on the optimization considering straight microchannels, because the analytical model described in Chapter 4 is specific to be applied to straight microchannels. However, as shown in Chapter 3 through a sensitivity analysis, different geometry of the microchannel can improve the efficiency and performance of this propulsion system.

7

CONCLUSION AND OUTLOOK

Every beginning has an end
and every end is a new beginning.

Santosh Kalwar

This conclusion Chapter provides a summary and conclusions of the Chapters 2-6 in order to synthesize the answers of the four research questions (RQ1-RQ4). This is followed by highlighting the main innovations of this research. Finally, it is presented the outlook to possible further research and engineering development.

7.1. SUMMARY AND CONCLUSIONS

This thesis is focussed on the development of a micro-resistojet called Low-Pressure Micro-Resistojet (LPM) to be applied in very small spacecraft. The development of this propulsion system concept has the goal to enable very small satellites to perform maneuvers. This improvement allows, for instance, to increase the spacecraft lifetime by active orbit keeping. Furthermore, it can enable orbit change manoeuvres and formation flight. In order to increase the technology readiness level of this concept, scientific and engineering challenges were defined and formulated as four research questions (RQ1-4).

Chapter 2 provides the answer to **RQ1. Which is the most promising "green" propellant for the proposed propulsion concept?** The methodology used to answer this question was divided into four steps: Data Collection; Feasibility Assessment; Qualitative Selection; and Conclusive Analysis. The first step was to collect data on a large number of fluids that could be used as propellants in micro-resistojet systems, resulting in 95 fluids. The second step was to select, among the identified fluids, only the ones which meet the criteria of being solid or liquid phase under a specific thermodynamic condition, resulting in 63 fluids. The third step was to use the Analytical Hierarchy Process (AHP) combined with a Pugh Matrix tool to compare the remaining fluids with respect to the three main criteria: performance, system density, and safety. Based on that, the nine best-scored fluids are selected, namely Acetone, Ammonia, Butane, Cyclopropane, Ethanol, Isobutane, Methanol, Propene, and Water. Finally, the fourth step was to analyze, in a more detailed manner, the substances that score the highest in the previous step.

After applying this methodology, 9 of 95 fluids, including conventional and unconventional propellants, were selected to be analysed in depth with respect to their thermal characteristics, performance parameters and safety issues. It was shown that Water is the most promising propellant for both micro-resistojet concepts considered, Low-Pressure Micro-Resistojet (LPM) and Vaporizing Liquid Micro-Resistojet(VLM). Even though Water has a high specific and latent heat, it provides excellent storability meaning it has the best ratio of velocity increment to propellant volume, almost twice as high as all the others. all the other analysed fluids. Another important aspect is that Water is the safest propellant, and the easiest one to handle and acquire. However, other propellants from the top nine list might be interesting for other applications or missions.

Chapter 3 handles **RQ2. How can we describe the fluid dynamic and the thermal properties of the fluid used in propulsive applications at high values of Knudsen number?** The methodology used to answer this question can be divided in literature review, implementation of a Direct Simulation Monte Carlo simulation (DSMC) numerical solver, and analysis of the fluid and thermal behaviour throughout the microchannels. Additionally, a sensitivity analysis among four different microchannel geometries was performed aiming to define the best microchannel geometry to be applied as thruster.

Two main aspects can be highlighted: the exit gas velocity is increased by efficient heat transfer, and the mass flow rate increases by increasing the transmission coefficient. These aspects are conflicting because increasing the transmission coefficient decreases the heat transfer efficiency. However, it was shown that a designed microchannel divided into two parts with a first-part divergent and a second-part straight results

in an increased transmission coefficient in the first-part and acceptable heat transfer efficiency in the second-part. This design implies a small reduction in specific impulse with a significant increase in thrust and, additionally, a considerable reduction in power consumption as compared to other analyzed designs. As a comparison, the thrust of one microchannel with divergent angle in the first-half of 40 degrees is equivalent to 4.8 straight microchannels, with a specific impulse decrease of just 5% but a reduction in power consumption of 67%, for a plenum pressure of 150 Pa and a heater chip temperature of 573 K.

Chapter 4 addresses **RQ3. How accurately can an analytical model characterize the performance of the proposed propulsion concept?** Starting with the most simple analytical model neglecting the pressure thrust, it was shown that the results of such model do not fit well the results from numerical models. Chapter 3 shows that the pressure thrust cannot be neglected, being found to represent about 40% of the total thrust in a straight microchannel. Additionally, the former analytical model overestimates the exit velocity for diatomic and polyatomic molecules, and therefore poorly represents the performance of this propulsion system. A new analytical propulsion system based on the Kinetic Theory of gases and the Maxwell-Boltzmann distribution was proposed in Chapter 4. It allows to describe the macroscopic flow parameters such as mass flow rate, velocity and pressure and, then, based on these parameters the thruster performance can then be described.

The former analytical model presented a thrust difference ranging from 20 to 30% when comparing to the numerical simulation, while the new analytical model presented a maximum thrust difference of 12%. Additionally, it was found that the main uncertainty in the proposed model is identified to be related to the equation for the transmission coefficient, an empirical equation that does not take into account the temperature effect. For instance, by using an improved estimation of transmission coefficient as the one provided from a numeric simulation, thrust differences could be reduced to less than 3%.

To answer **RQ4. Which optimization technique ca be used for the proposed propulsion concept, and what is the result of this optimization?**, it was necessary to consider both research and engineering aspects. Chapter 5 was exclusively dedicated to miniaturization and integration of the propulsion system. The focus was to fabricate and characterize the heater chip of the proposed propulsion system. Three main tests were performed in terms of mechanical, electrical and propulsion performance aspects. Based on the knowledge acquired from the performed experiments and the results from the previous **RQs**, Chapter 6 addresses the optimization of the LPM for very small satellites using two different mission scenarios. One is a CubeSat mission intended to perform a formation flight, and the other is Delfi-PQ, a PocketQube mission which will be used as a flight technology demonstration platform.

The optimization was performed in terms of scalability and performance, with a focus on the heater chip sizing and innovative tank concepts. It is shown that increasing the heater chip size by increasing the number of microchannels does not result in increasing the thruster performance, but, instead, being limited mainly by the available power. For each mission scenario an optimized heater chip size was defined and a suitable tank was suggested and discussed. A pipe tank with small diameter is an interesting

solution for pico-satellites, but it may not be viable for nano-satellites depending on the tube length. In this case, a porous media tank with controlled cavities or microchannels would be an interesting solution.

7.2. INNOVATIONS

The innovations of this research are addressed in the following.

1. **Selection methodology for propellants**

   Selecting appropriate fluids for any propulsion application is a challenge because of the large number of requirements. Existing selection methodologies have limitations, such as limited number of criteria and options, difficulty to obtain quantitative results, and being too subjective. In addition, existing methods typically do not allow to combine non-technical and technical choices. The selection methodology proposed in Chapter 2 combines well-known tools in such way that experts knowledge and technical requirements can easily be integrated. The methodology is divided in four steps, namely Data Collection, Feasibility Assessment, Qualitative Selection, and Conclusive Analysis. In this research, this proposed methodology was used in a specific case which was to select the promising "green" propellants to be applied to micro-resistojets (VLM and LPM). However, this methodology can be extended to any other application.

2. **Water as propellant**

   Water is the most common substance on the Earth, actually, it is critical for the proliferation of life, and it was one of the main feedstock during the industrial revolution where steam was used to generate power. It is not a coincidence that water is presented in this thesis as the most promising propellant for two types of microresistojets, namely VLM and LPM. Water has not for the first time been suggested as propellant, however in this thesis, its superiority to other propellants for the application considered, has been shown. Moreover, it might also be the first time it is feasible with competitive performance. Water has the disadvantage of having one of the highest heat coefficients, but comparing all the strict requirements for very small satellites it becomes the best choice. It is the safest substance, the easiest to handle and acquire, and presents the best ratio of velocity increment to propellant volume among the propellants analyzed in this thesis.

3. **Analysis of different expansion slot geometries**

   Conventional propulsion systems work under high pressure. They usually follow the same systematic way to design the nozzle based on the classical ideal rocket theory. However, the design of a nozzle to be used under very low pressure requires to think out of the box since the conventional equations such as Navier–Stokes equations are not applicable in this regime. Differently to the conventional propulsion systems, the Low-Pressure Micro-Resistojets work in the transitional flow regime and not in the continuum flow regime. Therefore, traditional convergent-divergent nozzles do not improve the thruster performance as already shown in previous works. Novel and promising nozzle geometry is presented in

this thesis, where the nozzle is divided into two parts, the first divergent and the second straight. It results in an increased transmission coefficient in the first part and acceptable heat transfer efficiency in the second part improving the thruster performance.

4. **Improved analytical model of the thruster performance**

   Having an analytical model to estimate the thruster performance is the ideal scenario to facilitate engineering design. A former analytical model proposed as an approximated model by Ketsdever et al. (2005) neglects the pressure thrust, which represents about 40% of the total thrust as presented in Chapter 3, and overestimates the exit velocity when considering diatomic or polyatomic molecules. In this research, these issues where overcome by extending the exit velocity considering either monatomic and polyatomic molecules, and an exit pressure equation is derived allowing to estimate the pressure thrust. This improvement allows an accurate estimation of thruster performance. Besides, this model simplifies the engineering design of the propulsion system, allowing faster decision-making and more detailed parametric analysis.

5. **Heater chip integration**

   This propulsion system is proposed to be applied in very small satellites with mass, volume and power budget as important constraints. The heater chip part might be manufactured using MEMS technology as it was already proposed by Ketsdever et al. (2005) where they presented the first prototype of the heater chip. A second design, with the same microchannel geometry, but with some isolation layers in order to reduce the thermal losses, was proposed by Palmer et al. (2013) where they focussed in improving the efficiency of the thruster. In this thesis, three different straight microchannel geometries are implemented on the heater chip. The electrical resistance of Molybdenum is used as a heater proving to be a good choice due to its stability at high temperatures up to 850°C, allowing the measurement of temperature as function of the resistivity. This is an innovation towards the integration of the microchannels, the heater resistor, and sensors on the same chip. Further innovative options are to implement the microchannel geometry suggested above, to implement an isolation layer on the chip side faced to the plenum, to integrate a pressure sensor, to integrate electronic circuit for both sensors (temperature and pressure), and improve the packaging using a combination of glop-top and ceramic packages.

6. **Tank solutions**

   Conventional tank solutions are not recommended to store water onboard the satellite. Two tank solutions to avoid sloshing are suggested. One is a flexible pipe with a diameter small enough that capillarity forces do not allow the mix between the liquid and gaseous state of the propellant. The flexible pipe is preferably recommended for pico-satellites due to the length of the pipe. It is most likely that for some nano-satellite missions the amount of propellant is considerably large resulting in a long pipe length which is not desirable. Another solution, to overcome this limitation, uses the same capillarity principle but the tank is in the form

of porous media. In addition, the large contact area between the porous media structure and the propellant improves the efficiency of the heat transfer.

7.3. OUTLOOK

This thesis focuses on the development of a micro-resistojet type called Low-Pressure Micro-Resistojet which is in a maturation technology phase. The LPM technology has been upgraded from a basic technology research to a technology development. In terms of Technology Readiness Level (TRL), the thruster part can be stated as TRL-5 (component and/or breadboard validation in relevant environment), but the storage part of the LPM can be stated as TRL-3 (analytical and experimental critical function and/or characteristic proof-of-concept). However, there is a plan to continue this research in order to have a flight demonstration on board of the Delfi-PQ pico-satellite.

It is expected that this propulsion system will share the tank with the Vaporizing Liquid Micro-Thuster (VLM). The tank will be a narrow pipe where the capillary forces are strong enough to avoid unacceptable mixing between the liquid and gaseous state of propellant. The thrusters will be attached to each end of the pipe. The VLM will use the liquid phase of the propellant (water), and the LPM will use the pressurant gas Nitrogen in the beginning and then will use water when the pressure drops in the tank. In this way, it is possible to use a large range of pressure inside the tank since the VLM needs a high pressure in the order of 2 bar when compared to the LPM which works under a pressure in the order of 2 mbar. More details about the demonstrator are expected to be presented in 2018 at the Space Propulsion Conference and at the International Astronautical Congress (IAC).

An analytical model of the LPM was developed in this thesis. However, it was found that the main source of uncertainty was related to the empirical equation of the transmission coefficient. The transmission coefficient has been studied by several researchers in the past, but mostly related to vacuum technology where the heat effect is usually neglected. Based on that, a next research step would require to map the transmission coefficient to a number of geometries of particular interest. Also, an adjustment to the empirical equation of the transmission coefficient considering the temperature and pressure influences may provide more accurate results.

Even though it is considered a great achievement to manufacture and to test the first LPM heater chip device at TU Delft, in the following several suggestions are made to improve the future design. From the heater chip manufacturing point of view an update on the manufacture flowchart needs to be done in order to avoid undesirable convergent or divergent microchannel geometries, and over- and under-material deposition. These improvements can be done by discussing them with experts of the specific machines needed during the MEMS manufacturing process. From the improvement point of view of the heater chip, a new version of the manufacture flowchart considering new steps is needed in order to be able to etch the microchannels geometries as suggested in Chapter 3, to improve the temperature sensor by adding a wheatstone bridge on the heater chip, and to integrate a pressure sensor on the heater chip. However, the high range of temperatures of the heater chip may be a challenge integrating a circuit on the heater chip. From the packaging point of view, improvements are also needed in order to avoid undesirable thermal conduction through the wires connected to the power supply, and the

heat lost through the interface used to hold the heater chip. These improvements may be done using a combination of a glop-top and ceramic packages. The glop-top may be used to protect the electric connection and the ceramic material as a holder of the heater chip. The ceramic material will also reduce the effect of the heater chip temperature in the gas inside the plenum.

Two tank suggestions to store the propellant are given in this thesis in Chapter 6. However, further analysis is needed because the storage is expected to have a multiphasic state and be controllable for phase change in order to deliver the desired mass flow rate. Currently, a master thesis is performed aiming to provide solutions for the controllability of the phase change in the tank.

REFERENCES

Ahmed, Z., Gimelshein, S. F., and Ketsdever, A. (2005). Numerical analysis of free molecule micro-resistojet performance. Tucson, Arizona. AIAA/ASME/SAE/ASEE, 41st AIAA/ASME/SAE/ASEE Joint Propulsion Conference and Exhibit.

Amri, R. and Gibbon, D. (2012). In orbit performance of butane propulsion system. *Advances in Space Research*, 49(4):648 – 654.

Bejan, A. (2015). Constructal law: Optimization as design evolution. *Journal of Heat Transfer*, 137:061003.

Bijster, R. J. F. (2014). Design, verification and validation of a micropropulsion thrust stand. Master thesis, Delft University of Technology.

Bird, G. A. (1994). *Molecular Gas Dynamics and the Direct Simulation of Gas Flow*. Oxford Engineering Science Series (Book 42). Clarendon Press.

Boshuizen, C. R., Mason, J., Klupar, P., and Spanhake, S. (2014). Results from the planet labs flock constellation. Logan, Utah. American Institute of Aeronautics and Astronautics (AIAA) and Utah State University (USU), 28th Annual AIAA/USU Conference on Small Satellites.

Cen, J. and Xu, J. (2010). Performance evaluation and flow visualization of a {MEMS} based vaporizing liquid micro-thruster. *Acta Astronautica*, 67(3–4):468 – 482.

Cervone, A., Deeb, A., van Wees, T., Jansen, E., Sundaramoorthy, P., Chu, J., and Zandbergen, B. (2015a). A micro-propulsion subsystem to enable formation flying ont he delffi mission. Delft, The Netherlands. TU Delft, and IAF, IWSCFF-2015-12.

Cervone, A., Mancas, A., and Zandbergen, B. (2015b). Conceptual design of a low-pressure micro-resistojet based on a sublimating solid propellant. *Acta Astronautica*, 108:30–39.

Cervone, A., Zandbergen, B., Guerrieri, D. C., Silva, M. A. C., Krusharev, I., and van Zeijl, H. (2017). Green micro-resistojet research at delft university of technology: new options for cubesat propulsion. *CEAS Space Journal*, 9(1):111–125.

Cheah, K. H. and Low, K.-S. (2015). Fabrication and performance evaluation of a high temperature co-fired ceramic vaporizing liquid microthruster. *Journal of Micromechanics and Microengineering*, 25(1):015013.

Chen, C.-C., Liu, C.-W., Kan, H.-C., Hu, L.-H., Chang, G.-S., Cheng, M.-C., and Dai, B.-T. (2010). Simulation and experiment research on vaporizing liquid micro-thruster. *Sensors and Actuators A: Physical*, 157(1):140 – 149.

Diaz, M. E., Guetachew, T., Landy, P., Jose, J., and Voilley, A. (1999). Experimental and estimated saturated vapour pressures of aroma compounds. *Fluid Phase Equilibria*, 157(2):257–270.

EKL (2018). Else kooi laboratory website. https://www.tudelft.nl/ewi/onderzoek/faciliteiten/else-kooi-lab/. Accessed on March 6, 2018.

Encyclopedia, G. (2016). Gas encyclopedia, air liquide. http://encyclopedia.airliquide.com/. Accessed from April 15, 2016 to August 15, 2016.

ESA (2015). European space technology master plan, issue 12th. Technical report, ESA.

Ferreira, A. and Lobo, L. (2009). Nitrous oxide: Saturation properties and the phase diagram. *The Journal of Chemical Thermodynamics*, 41(12):1394 – 1399.

Gavasane, A., Agrawal, A., Pradeep, A. M., and Bhandarkar, U.

Gill, E., Sundaramoorthy, P., Bouwmeester, J., Zandbergen, B., and Reinhard, R. (2013). Formation flying within a constellation of nano-satellites: The qb50 mission. *Acta Astronautica*, 82:110–117.

Gohardani, A. S., Stanojev, J., Demaire, A., Anflo, K., Persson, M., Wingborg, N., and Nilsson, C. (2014). Green space: Opportunities and propects. *Progress in Aerospace Sciences*, 71:128–149.

GRASP (2016). Green advanced space propulsion, european communities. https://www.grasp-fp7.eu/grasp/. Accessed from April 15, 2016 to August 15, 2016.

Guerrieri, D. C., Cervone, A., and Gill, E. (2016). Analysis of nonisothermal rarefied gas flow in diverging microchannels for low-pressure microresistojets. *Journal of Heat Transfer*, 138(11).

Guerrieri, D. C., Silva, M. A. C., Zandbergen, B. T. C., and Cervone, A. (2015). Development of a low pressure free molecular micro-resistojet for cubesat applications. Jerusalem, Israel. International Astronautical Federation, 66th International Astronautical Congress.

Guildner, L. A., Johnson, D. P., , and Jones, F. E. (1976). Vapor pressure of water at its triple point. *JOURNAL OF RESEARCH of the National Bureau of Standards -A. Physics and Chemistry*, 80A(3).

Guo, J., Bouwmeester, J., and Gill, E. (2016). In-orbit results of delfi-n3xt: Lessons learned and move forward. *Acta Astronautica*, 121:39 – 50.

Jansen, E. H. W. (2016). Improvement and validation of test stand performance for novel micropropulsion systems. Master thesis, Delft University of Technology.

Karniadakis, G., Beskok, A., and Aluru, N. (2005). *Microflows and Nanoflows Fundamentals and Simulation*, volume 29 of *0939-6047*. Springer-Verlag New York.

Karthikeyan, K., Chou, S., Khoong, L., Tan, Y., Lu, C., and Yang, W. (2012). Low temperature co-fired ceramic vaporizing liquid microthruster for microspacecraft applications. *Applied Energy*, 97:577 – 583. Energy Solutions for a Sustainable World - Proceedings of the Third International Conference on Applied Energy, May 16-18, 2011 - Perugia, Italy.

Ketsdever, A., Lee, R., and Lilly, T. (2005). Performance testing of a microfabricated propulsion system for nanosatellite applications. *Journal of Micromechanics and Microengineering*, 15:2254.

Ketsdever, A., Wadsworth, D., Vargo, S., and Muntz, E. (1998). A free molecule micro-resistojet: An interesting alternative to nozzle expansion. AIAA/ASME/SAE/ASEE, 34th AIAA/ASME/SAE/ASEE Joint Propulsion Conference and Exhibit.

Krejci, D. and Lozano, P. (2018). Space propulsion technology for small spacecraft. *Proceedings of the IEEE*, PP(99):1–17.

Kulu, E. (2018). Nanosatellite database by erik. http://www.nanosats.eu/index.html#database. Accessed on February 23, 2018.

Kundu, P., Bhattacharyya, T. K., and Das, S. (2012). Design, fabrication and performance evaluation of a vaporizing liquid microthruster. *Journal of Micromechanics and Microengineering*, 22(2):025016.

Lafferty, J. M. (1998). *Foundations of Vaccum Science and Technology*. John Wiley and Sons.

Lee, R., Bauer, A., Killingsworth, M., Lilly, T., Duncan, J., and Ketsdever, A. (2007). Performance characterization of the free molecule micro-resistojet utilizing water propellant. Tucson, Arizona. AIAA/ASME/SAE/ASEE, 43rd AIAA/ASME/SAE/ASEE Joint Propulsion Conference and Exhibit.

Mancas, A. (2013). Ice-propelled micro-resistojet. Master thesis, Delft University of Technology.

Maxence, D., Guerrieri, D. C., and Cervone, A. (2017). Preliminary results of a sublimating propellant tank for dedicated micropropulsion system. Adelaide, Australia. International Astronautical Federation, 68th International Astronautical Congress.

Mele, L., Santagata, F., Iervolino, E., Mihailovic, M., Rossi, T., Tran, A., Schellevis, H., Creemer, J., and Sarro, P. (2012). A molybdenum {MEMS} microhotplate for high-temperature operation. *Sensors and Actuators A: Physical*, 188:173 – 180. Selected papers from The 16th International Conference on Solid-State Sensors, Actuators and Microsystems.

Meyer, M. and Johnson, L. (2015). Nasa technology roadmaps, ta 2: In-space propulsion technologies. Technical report, NASA, Washington.

Muntz, E. P. (1989). Rarefied gas dynamics. *Annual Review of Fluid Mechanics*, 21:387–422.

Murphy, D. M. and Koop, T. (2005). Review of the vapour pressures of ice and supercooled water for atmospheric applications. *Q.J.R. Meteorol. Soc.*, 131(608).

NASA (2018). What are smallsats and cubesats? https://www.nasa.gov/content/what-are-smallsats-and-cubesats. Accessed on February 23, 2018.

Nervold, A. K., Berk, J., Straub, J., and Whalen, D. (2016). A pathway to small satellite market growth. *Advances in Aerospace Science and Technology*, 1(1):14 – 20.

NFPA (2010). *Fire Protection Guide to Hazardous Materials*. Natinal Fire Protection Association, 14th edition.

NIST. Nist chemistry webbook, nist standard reference database number 69. http://webbook.nist.gov. Accessed from April 15, 2016 to August 15, 2016.

Oran, E., Oh, C., and Cybyk, B. (1998). Direct simulation monte carlo: Recent advances and applications. *Annual Review of Fluid Mechanics*, 30(1):403–441.

Pallichadath, V., Radu, S., Silva, M. A. C., Guerrieri, D. C., Uludag, M. S., Maxence, D., Zandbergen, B., and Cervone, A. (2018). Integration and miniaturization challenges in the design of micro-propulsion system for picosatellite platforms. Sevilla, Spain. 3AF, ESA and CNES, Space Propulsion Conference 2018.

Pallichadath, V., Silvestrini, S., Silva, M. A. C., Maxence, D., Guerrieri, D. C., Mestry, S., Soriano, T. P., Bacaro, M., van Zeijl, H., Zandbergen, B., and Cervone, A. (2017). Mems based micro-propulsion system for cubesats and pocketqubes. Adelaide, Australia. International Astronautical Federation, 68th International Astronautical Congress.

Palmer, K., Nguyen, H., and Thornell, G. (2013). Fabrication and evaluation of a free molecule micro-resistojet with thick silicon dioxide insulation and suspension. *Journal of Micromechanics and Microengineering*, 23(6):065006.

Perry, R. H. and Green, D. W. (2008). *Perry's Chemical Engineers' Handbook, Eighth Edition*. McGraw-Hill.

Poghosyan, A. and Golkar, A. (2017). Cubesat evolution: Analyzing cubesat capabilities for conducting science missions. *Progress in Aerospace Sciences*, 88:59 – 83.

Pugh, S. (1991). *Total design: integrated methods for successful product engineering*. Addison-Wesley Pub. Co., 1st edition.

Rankin, D., Kekez, D. D., Zee, R. E., Pranajaya, F. M., Foisy, D. G., and Beattie, A. M. (2005). The canx-2 nanosatellite: Expanding the science abilities of nanosatellites. *Acta Astronautica*, 57(2–8):167 – 174. Infinite Possibilities Global Realities, Selected Proceedings of the 55th International Astronautical Federation Congress, Vancouver, Canada, 4-8 October 2004.

Roohi, E., Darbandi, M., and Mirjalili, V. (2009). Direct simulation monte carlo solution of subsonic flow through micro/nanoscale channels. *Journal of Heat Transfer*, 131:092402.

Sazhin, O. (2008). Dsmc-computation of the rarefied gas flow through a slit into a vacuum. *Journal Vacuum Science Technology*, 1084:1147–1152.

Scanlon, T. J., Roohi, E., White, C., Darbandi, M., and Reese, J. M. (2010). An open source, parallel dsmc code for rarefied gas flows in arbitrary geometries. *Computers and Fluids*, 39:2078–2089.

Selva, D. and Krejci, D. (2012). A survey and assessment of the capabilities of cubesats for earth observation. *Acta Astronautica*, 74:50 – 68.

Silva, M. A., Guerrieri, D. C., Cervone, A., and Gill, E. (2018). A review of mems micropropulsion technologies for cubesats and pocketqubes. *Acta Astronautica*, 143:234 – 243.

SpE (2018). Department of space engineering website. https://www.tudelft.nl/en/ae/organisation/departments/space-engineering/. Accessed on March 6, 2018.

Speretta, S., Soriano, T. P., Bouwmeester, J., Carvajal-Godinez, J., , Menicucci, A., Watts, T., Sundaramoorthy, P., Guo, J., and Gill, E. (2016). Cubesats to pocketqubes: Opportunities and challenges. Guadalajara, Mexico. International Astronautical Federation, 67th International Astronautical Congress.

Sutton, G. P. and Biblarz, O. (2010). *Rocket Propulsion Elements 8th edition*. Wiley, 8th edition.

Tummala, A. R. and Dutta, A. (2017). An overview of cube-satellite propulsion technologies and trends. *Aerospace*, 4(4).

Varoutis, S., Valougeorgis, D., Sazhin, O., and Sharipov, F. (2008). Rarefied gas flow through short tubes into vaccum. *Journal Vacuum Science Technology*, 26:228.

Wang, M. and Li, Z. (2004). Simulations for gas flows in microgeometries using the direct simulation monte carlo method. *International Journal of Heat and Fluid Flow*, 25(6):975 – 985.

Zahedi, F. (1986). The analytic hierarchy process: A survey of the method and its applications. *Interfaces*, 16(4):96–108.

A

PROPELLANT CANDIDATES

Table A.1: This table presents all propellant candidates that were analysed in Chapter 2. The information is from Ref. (NIST; Encyclopedia, 2016; Perry and Green, 2008; GRASP, 2016; Diaz et al., 1999; Ferreira and Lobo, 2009).

#	Fluid name	Formula	M_w [g/mol]	Selection step
1	1,1,1,2,3,3,3-Heptafluoropropane (R227ea)	C_3HF_7	170.03	3 - AHP and Pugh Matrix
2	1,1,1,2,3,3-Hexafluoropropane (R236ea)	$C_3H_2F_6$	152.04	3 - AHP and Pugh Matrix
3	1,1,1,3,3,3-Hexafluoropropane (R236fa)	$C_3H_2F_6$	152.04	3 - AHP and Pugh Matrix
4	1,1,1,3,3-Pentafluoropropane (R245fa)	$C_3H_3F_5$	134.05	3 - AHP and Pugh Matrix
5	1,1,2,2,3-Pentafluoropropane (R245ca)	$C_3H_3F_5$	134.05	3 - AHP and Pugh Matrix
6	1,1,2-Trichloro-1,2,2-trifluoroethane (R113)	$C_2Cl_3F_3$	187.38	3 - AHP and Pugh Matrix
7	1,1-Dichloro-1-fluoroethane (R141b)	$C_2H_3Cl_2F$	116.94	3 - AHP and Pugh Matrix
8	1,2-Dichloro-1,1,2,2-tetrafluoroethane (R114)	$C_2Cl_2F_4$	170.92	3 - AHP and Pugh Matrix
9	1-Chloro-1,1-difluoroethane (R142b)	$C_2H_3ClF_2$	100.49	3 - AHP and Pugh Matrix
10	2,2-Dimethylpropane	C_5H_{12}	72.15	3 - AHP and Pugh Matrix
11	2,4-xylidine	$C_8H_{11}N$	121.18	3 - AHP and Pugh Matrix
12	2-Methylbutane	C_5H_{12}	72.15	3 - AHP and Pugh Matrix
13	2-Methylpentane	C_6H_{14}	86.18	3 - AHP and Pugh Matrix
14	3-3'-diaminopropylamine	$C_5H_{14}N_2$	102.18	3 - AHP and Pugh Matrix
15	Acetic acid	$C_2H_4O_2$	60.05	3 - AHP and Pugh Matrix
16	Acetone	C_3H_6O	58.08	4 - Analysis
17	Ammonia	NH_3	17.03	4 - Analysis
18	Aniline	$C_6H_5NH_2$	93.13	3 - AHP and Pugh Matrix
19	Argon	Ar	39.95	2 - Feasibility Assessment
20	Benzene	C_6H_6	78.11	3 - AHP and Pugh Matrix
21	Butane	C_4H_10	58.12	4 - Analysis
22	Carbon dioxide	CO_2	44.01	2 - Feasibility Assessment
23	Carbon monoxide	CO	21.01	2 - Feasibility Assessment
24	Carbonyl sulfide	COS	60.07	2 - Feasibility Assessment
25	Chlorine	C_l2	70.1	2 - Feasibility Assessment
26	Chloropentafluoroethane (R115)	C_2ClF_5	154.47	3 - AHP and Pugh Matrix
27	Chlorotrifluoromethane (R13)	$CClF_3$	104.46	2 - Feasibility Assessment
28	Cyclohexane	C_6H_12	84.16	3 - AHP and Pugh Matrix
29	Cyclopropane	C_3H_6	42.08	4 - Analysis
30	Decafluorobutane	C_4F_{10}	238.03	3 - AHP and Pugh Matrix
31	Decane	$C_{10}H_{22}$	142.29	3 - AHP and Pugh Matrix
32	Dichlorodifluoromethane (R12)	CCl_2F_2	120.91	3 - AHP and Pugh Matrix
33	Dichlorofluoromethane (R21)	$CHCl_2F$	102.92	3 - AHP and Pugh Matrix
34	Dinitrogen monoxide	N_2O	44.01	2 - Feasibility Assessment
35	Dodecafluoropentane	C_5F_{12}	288.04	3 - AHP and Pugh Matrix
36	Dodecane	$C_{12}H_{26}$	170.34	3 - AHP and Pugh Matrix
37	Ethane	C_2H_6	30.07	2 - Feasibility Assessment
38	Ethane, 1,1,1,2-tetrafluoro- (R134a)	CH_2FCF_3	102.03	3 - AHP and Pugh Matrix
39	Ethane, 1,1,1-trifluoro- (R143a)	$C_2H_3F_3$	84.04	2 - Feasibility Assessment
40	Ethane, 1,1-difluoro- (R152a)	$C_2H_4F_2$	66.05	3 - AHP and Pugh Matrix
41	Ethane, 1-chloro-1,2,2,2-tetrafluoro- (R124)	C_2HClF_4	136.48	3 - AHP and Pugh Matrix
42	Ethane, 2,2-dichloro-1,1,1-trifluoro- (R123)	$C_2HCl_2F_3$	152.93	3 - AHP and Pugh Matrix
43	Ethane, pentafluoro- (R125)	C_2HF_5	120.02	2 - Feasibility Assessment
44	Ethanol	C_2H_6O	46.07	4 - Analysis
45	Ethene	C_2H_4	28.05	2 - Feasibility Assessment

#	Fluid name	Formula	M_w [g/mol]	Selection step
46	Ethyl formate	$C_3H_6O_2$	74.08	3 - AHP and Pugh Matrix
47	Ethyl nitrate	$C_2H_5NO_3$	91.07	3 - AHP and Pugh Matrix
48	Ethylammonium nitrate	$C_2NH_8NO_3$	108.1	3 - AHP and Pugh Matrix
49	Ethylenoxide	C_2H_4O	44.05	3 - AHP and Pugh Matrix
50	Fluorine	Fe_2	72	2 - Feasibility Assessment
51	Fluoromethane (R41)	CH_3F	34.03	2 - Feasibility Assessment
52	Furfuryl alcohol	$C_5H_6O_2$	98.1	3 - AHP and Pugh Matrix
53	Helium	He	4	2 - Feasibility Assessment
54	Heptane	C_7H_{16}	100.21	3 - AHP and Pugh Matrix
55	Hexafluoroethane (R116)	C_2F_6	138.01	2 - Feasibility Assessment
56	Hexane	C_6H_{14}	86.18	3 - AHP and Pugh Matrix
57	Hydrazine	N_2H_4	32.05	3 - AHP and Pugh Matrix
58	Hydrogen	H_2	2.02	2 - Feasibility Assessment
59	Hydrogen chloride	HCl	36.46	2 - Feasibility Assessment
60	Hydrogen cyanide	HCN	27.03	3 - AHP and Pugh Matrix
61	hydrogen peroxide	H_2O_2	34.01	3 - AHP and Pugh Matrix
62	Hydrogen sulfide	H_2S	34.08	2 - Feasibility Assessment
63	Isobutane	C_4H_{10}	58.12	4 - Analysis
64	Krypton	Kr	83.8	2 - Feasibility Assessment
65	Limonene	$C_{10}H_{16}$	136.24	3 - AHP and Pugh Matrix
66	Methane	CH_4	16.04	2 - Feasibility Assessment
67	Methane, chlorodifluoro- (R22)	$CHClF_2$	86.47	3 - AHP and Pugh Matrix
68	Methane, difluoro- (R32)	CH_2F_2	52.02	2 - Feasibility Assessment
69	Methanol	CH_4O	32.04	4 - Analysis
70	Monomethylamine	CH_5N	31.06	2 - Feasibility Assessment
71	Neon	Ne	20.18	2 - Feasibility Assessment
72	Nitric acid	HNO_3	63.01	3 - AHP and Pugh Matrix
73	Nitric oxide	NO	30.01	2 - Feasibility Assessment
74	Nitrogen	N_2	28.01	2 - Feasibility Assessment
75	Nitrogen trifluoride	NF_3	71	2 - Feasibility Assessment
76	Nonane	C_9H_{20}	128.2	3 - AHP and Pugh Matrix
77	Nitrous Oxide	NO_2	44.01	2 - Feasibility Assessment
78	Octafluorocyclobutane (RC318)	C_4F_8	200.03	3 - AHP and Pugh Matrix
79	Octafluoropropane (R218)	C_3F_8	188.02	3 - AHP and Pugh Matrix
80	Octane	C_8H_{18}	114.23	3 - AHP and Pugh Matrix
81	Oxygen	O_2	32	2 - Feasibility Assessment
82	Pentane	C_5H_{12}	72.15	3 - AHP and Pugh Matrix
83	Propane	C_3H_8	44.1	3 - AHP and Pugh Matrix
84	Propene	C_3H_6	42.08	4 - Analysis
85	Propyne	C_3H_4	40.06	3 - AHP and Pugh Matrix
86	Sulfur dioxide	SO_2	64.07	3 - AHP and Pugh Matrix
87	Sulfur hexafluoride	SF_6	146.06	2 - Feasibility Assessment
88	Tetrafluoromethane (R14)	CF_4	88	2 - Feasibility Assessment
89	Tetranitromethane	CN_4O_8	196.04	3 - AHP and Pugh Matrix
90	Toluene	C_7H_8	92.14	3 - AHP and Pugh Matrix
91	Trichlorofluoromethane (R11)	CCl_3F	137.37	3 - AHP and Pugh Matrix
92	Trifluoromethane (R23)	CHF_3	70.01	2 - Feasibility Assessment
93	Trimethylaluminium	$C_6H_{18}Al_2$	144.17	3 - AHP and Pugh Matrix
94	Water	H_20	18.02	4 - Analysis
95	Xenon	Xe	131.29	2 - Feasibility Assessment

B

PRELIMINARY TANK ANALYSIS

B.1. THEORETICAL AND NUMERICAL ANALYSIS

The analysed tank is designed to work with subliming ice as proposed by Cervone et al. (2015b), meaning that the temperature and pressure shall not be higher than 273.16 K and 611.657 Pa, respectively, which are the Triple Point conditions of water Guildner et al. (1976). The correlation between pressure and temperature that can be used for a range of temperatures from 110 K to the triple point is presented in the following equation by Murphy and Koop (2005)

$$P_{sub} = e^{9.550426 - \frac{5723.265}{T_{sub}} + 3.53068 \cdot T_{sub} - 0.00728332 \cdot T_{sub}} \tag{B.1}$$

where P_{sub} in Pa and T_{sub} in K are the sublimation pressure and temperature, respectively. Figure B.1 shows the sublimation pressure and temperature curve for a range of temperatures from 250 to 273.16 K. This range can be considered as the thruster nominal one, from the stand by to full operation.

A sublimation stationary model has been designed on COMSOL Multiphysics 4.4. The Conjugate Heat Transfer package that combines the heat equation with the equation for laminar flow was used. Also, equation B.1 was used as link to define the thermodynamic equilibrium on the ice-steam interface. The Deformed Geometry package has also been used to create a mesh deformation on the interface as the sublimation occurs.

For low pressure, the steam can be considered as an ideal gas,

$$\rho = \frac{P}{R_s T} \tag{B.2}$$

where P is the pressure, ρ the density, R_s the specific gas constant and T the temperature. This equation is used to predict the thermodynamic state from tank to plenum. The heat transfer equation was used to describe the heat transfer in both the ice and steam phases,

The content of this appendix has been published in the proceedings of 66th International Astronautical Congress, Jerusalem, Israel, 2015.

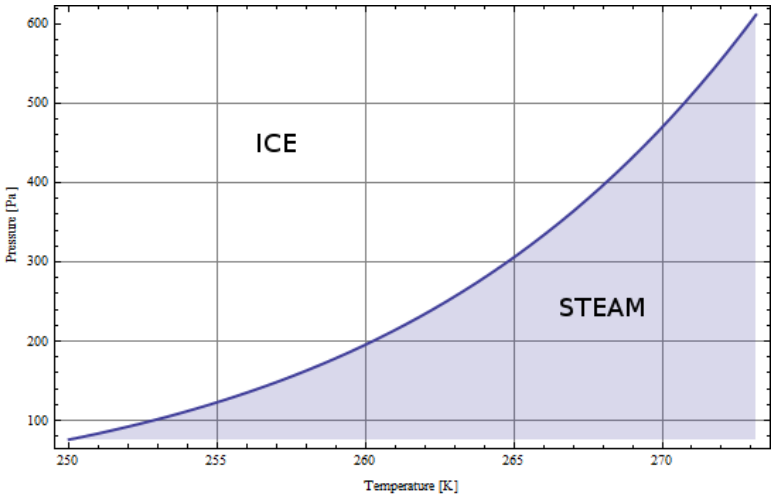

Figure B.1: Sublimation pressure and temperature curve for water.

$$\rho C_p \mathbf{u} \cdot \nabla T = \nabla \cdot (k_{th} \nabla T) + Q \tag{B.3}$$

where C_p is the specific heat capacity, $\mathbf{u}$ the velocity field (that is null for ice phase), k_{th} the thermal conductivity and Q the heat source per unit volume. Furthermore, the Navier-stokes and continuity equations were used as in the following, respectively

$$\rho (\mathbf{u} \cdot \nabla) \mathbf{u} = \nabla \cdot \left[-P\mathbf{I} + \mu \nabla \mathbf{u} + (\nabla \mathbf{u})^T - \frac{2}{3} \mu (\nabla \cdot \mathbf{u}) \mathbf{I} \right] \tag{B.4}$$

$$\nabla \cdot (\rho \mathbf{u}) = 0 \tag{B.5}$$

where $\mathbf{I}$ is the unit tensor and μ the viscosity.

Equation B.6 was implemented to describe the steam mass flow rate per unit area at the ice-steam interface, that depends of the sublimation.

$$\dot{m} = \rho_{ste} - \rho_{ice} \cdot V_s \tag{B.6}$$

where ρ_{ste} is the steam density, ρ_{ice} the ice density and V_s is the ice-steam interface normal velocity of the sublimation. It can be defined as

$$V_s = \frac{Q_s}{\rho_{ice} L_{ice}} \tag{B.7}$$

where Q_s is the normal heat flux at the ice-steam interface (negative due to the conventions on the direction of the normal to the surface) and L_{ice} the latent heat of sublimation of ice (it was assumed 2.84 MJ kg^{-1}). This velocity equation, V_s, was used on the Deformed Geometry package that allows us to see the deformation in time, that is an estimation of the deformation that occurs during the sublimation.

Figure B.2 presents the sublimation model design and the corresponding boundary conditions are presented in Table B.1, chosen in order to achieve the needed thermodynamic state into the plenum. The surfaces which are not indicated in the table are considered thermally insulated. Note that in this simulation it was assumed that the valve is completely open.

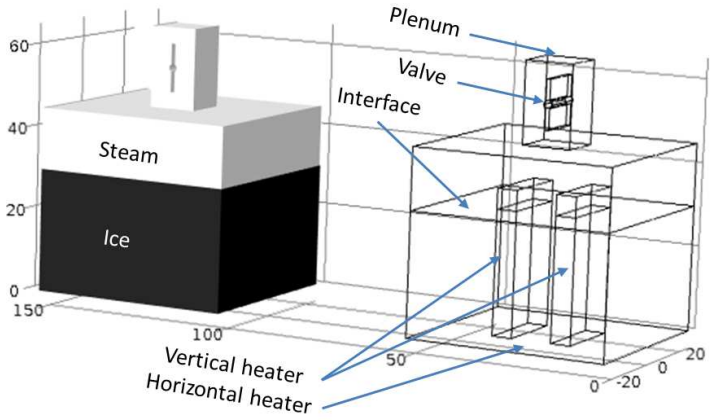

Figure B.2: Sublimation model (Dimensions in mm).

For this modelling it was assumed that sublimation occurs only at the "interface" (as it is presented in Figure B.2), therefore, the contact between the heater and the ice is always direct, i.e., the ice is always touching the heater. However, this is just a simplification because in reality this contact might be lost in the beginning of the operation. This aspect needs to be further investigated because it might influence performance, but this is not studied in this thesis.

Table B.1: Boundary conditions of the sublimation model.

Boundary Conditions	Description
Plenum	Pressure: 50 - 300 Pa Temperature: 273 K
Interface	Mass Flow: Equation B.6
Heat element	Heat flux: 0.5 - 4 W

B.2. RESULTS AND DISCUSSION

As presented before (Table B.1), the simulations are carried out for a plenum pressure of 50, 150 and 300 Pa and heat flux of the heater element range from 0.5 to 4 W with steps of 0.5 W. In order to present the dynamics inside the tank the condition of 150 Pa (pressure plenum) and 2 W (heat flux) were chosen, see Figure B.3 and B.4. In Figure B.3, the ar-

rows represent the heat conduction flux in the ice, the red streamlines the steam motion, the blue plane the ice-steam interface and the vertical slice the temperature gradient. As presented in the assumptions the ice-steam interface temperature is constant of 273 K nevertheless the vertical heater part, which is above the interface, increases the steam temperature helping to avoid any possibility of condensation and/or solidification during the passage from tank to plenum.

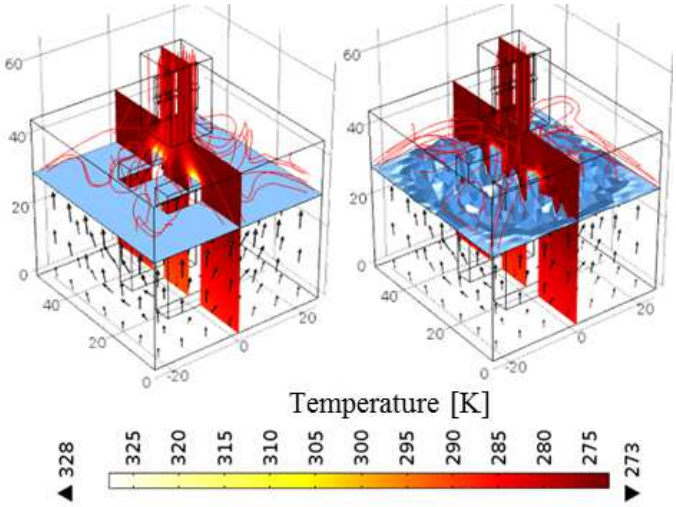

Figure B.3: Continuous Sublimation, mesh deformation. Left: time = 0 s, and Right: 1800 s.

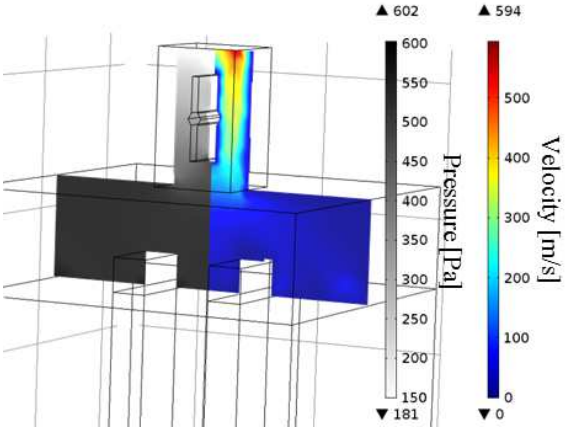

Figure B.4: Velocity and pressure field of the steam from the tank to plenum. Left hand side (Greyscale) pressure field, right hand side (Coloured) velocity field.

An estimated deformation of the ice-steam interface is presented in Figure B.3 (Right) after 30 min of operation, which represents a propellant consumption of 2.3 g. The de-

formation near to the vertical heater is larger due to the higher heat flux, meaning that the sublimation effect is larger near to the vertical heater. Not surprisingly, it is possible to see a tendency of the sublimation to happen on the contact between the ice and vertical heater.

As seen in Figure B.3, the temperature in the surface in contact with the horizontal heater is higher than the sublimation temperature which means that the assumption that the sublimation will occur only on the top surface might be incorrect and needs to be further investigated.

Inside the tank it is observed a low steam velocity until the passage entrance, where the valve is placed, and then there is a significantly increase in the velocity due to the pressure difference and the area reduction, as seen in Figure B.4.

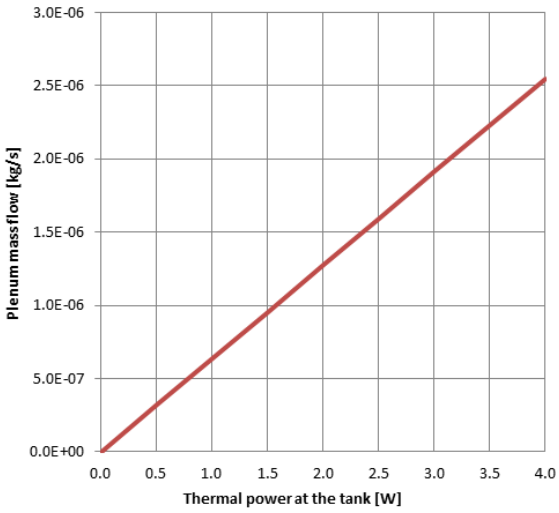

Figure B.5: Plenum mass flow versus thermal power consumption.

According to the present simplified analysis, the mass flow rate that goes into the plenum is a linear function of the thermal power applied to the tank's heater element as shown in Figure B.5. According to the maximum mass flow rate needed in this case which is 2.741×10^{-6} kg s^{-1}, the thermal power needed by the tank heater can be extrapolated from the curve shown in Figure B.5 to 4.3 W.

ACKNOWLEDGEMENTS

I would like to express my sincere gratefulness to my promoter Prof. Dr. Eberhard Gill and my co-promoter (daily supervisor) Dr. Angelo Cervone. Thank you for offering me such a great opportunity to work in the Space System Engineering group at TU Delft. It was an important step in my career where I could see research from a different perspective. I am very fulfilled with the way how this research was directed. When I look back I see that this research was done in a smooth and peaceful way. The invaluable guidance and critical feedback were fundamental to improve the quality of the research. It has been a great pleasure and a very nice experience to work with you both. Thank you very much. I would also like to take this opportunity to thank the examination committee members, for reading this thesis and providing valuable feedback.

This research would not be possible if my colleagues from CEFET-RJ did not give me the possibility to take a four year sabbatical so that I could dedicate my full time to this thesis. I am really grateful for it. Additionally, I acknowledge the CNPq which funded this research with generous support.

I appreciate the friendly atmosphere created by many of my colleagues in the Department of Space Engineering. Thank you all for the wonderful moments we had during the last four years, specially during the monthly space bar. A special acknowledgment to my fellow PhD colleagues, my friends, which were crucial during my whole journey. Thank you for every single moment we spent together whether during the after lunch walks, the PhD's monthly activity, the "saideiras" or simply the conversations. Marsil obrigado meu amigo. Johan and Adolfo gracias mi amigos "Pura vida mae". Minghe, Jing, Zixuan, and Linyu 谢谢好朋友们. Fiona Merci mon ami. Dennis Bedankt mijn Vriend. Prem Nandri nanbaa. Victor Gracias mi amigo. Mario Grazie amico mio. To my colleagues from the micro-propulsion system research, Angelo, Barry, Fiona, Marsil, Samiksha, Sevket, Silvana and Vidhya, I am proud of working with you all. A special thank you to my friends and Paranymphs Johan and Marsil, our technical discussions were fundamental to the development of this thesis. Additionally, I would like to acknowledge the staff members of the Else Kooi Laboratory (EKL) for all the teachings in MEMS. A special thank you to Henk van Zeijl, Silvana Milosavljevic, and Tom Scholtes.

My life in Delft would not have been so special without the amazing people I met here. To Saulo, Mini, lovely Yang and lovely Bel (this beautiful Brazil-China family), my warm thanks for you guys. Life is a surprise box, I used to be Saulo's neighbor in Rio, but we did not meet there, it was necessary to come to the small Delft being his neighbor again to have the opportunity to meet him. To Eduardo, Gabriela and lovely Leonardo, what to say to you guys? You guys have the power to read minds (at least my and Fernanda's). You guys were/are always there when we least expect(ed) it. I do not have words to acknowledge you guys. Thank you for everything. To Aline, Amaury, Ana Lucía, Carina, Carlos, Eshan, Fabricio, Fracesca, Hanna, Kirsty, Lucas, Mahboubeh, Marcelo, Martha, Marquinhos, Nicola, Sebastian, the lovely Silvia, Sruti, Tales, Tomás, Tiago, Víc-

tor, and Wesley thank you all for making this period lively, enjoyable, fun, etc. I also want to acknowledge some old friends who somehow were/are also part of this. Thank you Diego, Luci, Luiz Felipe and Renata. I know, I might have forgotten someone. So please, feel acknowledged. Glad to have met all of you guys. Thank you all for sharing wonderful moments with my family and me during this journey.

I am so glad to all the support I had from my lovely Fernanda. Thank you for every single moment. Becoming parents in the Netherlands was a challenge at the beginning mainly because we were out of our comfort zone and I was starting my PhD candidate life. Even though, we handled it in the best way, it was perfect in every single detail. Thank you, my sweet, beautiful daughter Zoé. You both made/make my life happier and enjoyable. You both helped me to keep my PhD journey smooth and peaceful. I love you both. Eu amo vocês demais!

A special thank you to my uncles, aunts and cousins which live in Germany. They were quite important during this journey as well. Omar, Paula, Geu, Renata, João Marcos, João Luiz, Luna, and Levi, thank you for every single moment we spent together. Muito obrigado, foi essencial ter vocês por perto durante esses anos.

To my dad and mom, I am not able to acknowledge you in the way you deserve, everything I write or say would never be enough. I am so much of what I learned from you. Without the inspiration, drive, and support that both have given me, I might not be the person I am today. I would also like to extend those words to my grandparents in memoriam. Obrigado por tudo!

To my brother Mardú, during the childhood we fought a lot for every single stupid thing, and during the youth we kept fighting for stupid thing. Then, you became taller and stronger than me, that was the perfect time to stop fighting. Anyway, thank you for supporting me in any situation. You will always be my little lovely brother. Muito obrigado por tudo!

CURRICULUM VITÆ

Daduí C. Guerrieri was born on November 5th 1985 in Rio de Janeiro, Brazil. He attended two different technical schools where he studied mechanical course at CEFET-RJ, and electrical course at FAETEC during 2000 and 2006. During 2005, he did the Brazilian military service. In 2011, he graduated from Universidade Estadual do Rio de Janeiro (UERJ) with a degree in Mechanical Engineering. During his studies, Daduí actively worked on the mini-baja (off-road vehicle) design for national college competition organized by Society of Automotive Engineers (SAE). The Master of Science in Mechanical Engineering was received from Universidade Federal do Rio de Janeiro (UFRJ) in 2014. In the same year, he received the best MSc thesis award from the "IV Prêmio CREA-RJ Oscar Niemeyer de Trabalhos Científicos e Tecnológicos". Currently, he is a lecturer from Centro Federal de Tecnologia do Rio de Janeiro (CEFET-RJ) since 2012, and a PhD candidate at the Space Engineering Department at TU Delft working on the topic of micro-propulsion systems since 2014. In addition, he is part of the microfluidics and microsystems committee at the Brazilian Association of Engineering and Mechanical Sciences (ABCM - Associação Brasileira de Engenharia e Ciências Mecânicas) since 2013. His research interests include MEMS, thermal science, and propulsion systems.

List of Publications

Journal Papers

9. **Daduí C. Guerrieri**, Marsil A. C. Silva, Angelo Cervone, and Eberhard Gill, *An Analytical Model for Characterizing the Thrust Performance of a Low-Pressure Micro-Resistojet*, Acta Astronautica **Under Review**.

8. Marsil A. C. Silva, Stefano Silvestrini, **Daduí C. Guerrieri**, Angelo Cervone, and Eberhard Gill, *A Comprehensive Model for Control of Vaporizing Liquid Microthrusters*, IEEE Transactions on Control Systems Technology **Manuscript Accepted**.

7. Ivana Fernandes de Sousa, Carolina Palma Naveira Cotta, **Daduí C. Guerrieri**, and Manish K. Tiwari, *On the Thermal Performance of a Micro Parallel Channels Heat Exchanger*, ASME Journal of Thermal Science and Engineering Applications **Manuscript Accepted**.

6. Marsil A. C. Silva, **Daduí C. Guerrieri**, Angelo Cervone, and Eberhard Gill, *A review of MEMS micropropulsion technologies for CubeSats and PocketQubes*, Acta Astronautica **143**, 234-243 (2018).

5. **Daduí C. Guerrieri**, Marsil A. C. Silva, Henk van Zeijl, Angelo Cervone, and Eberhard Gill, *Fabrication and Characterization of Low Pressure Micro-Resistojets with Integrated Heater and Temperature Measurement*, Journal of Micromechanics and Microengineering **12**, 27 (2017).

4. Marsil A. C. Silva, **Daduí C. Guerrieri**, Henk van Zeijl, Angelo Cervone, and Eberhard Gill, *Vaporizing Liquid Microthrusters with integrated heaters and temperature measurement*, Sensors and Actuators A: Physical , 265 (2017).

3. **Daduí C. Guerrieri**, Marsil A. C. Silva, Angelo Cervone, and Eberhard Gill, *Selection and Characterization of Green Propellants for Micro-Resistojets*, ASME Journal of Heat Transfer **10**, 139 (2017).

2. Angelo Cervone, Barry T.C. Zandbergen, **Daduí C. Guerrieri**, Marsil de Athayde Costa e Silva, I. Krusharev, Henk van Zeijl, *Green micro-resistojet research at Delft University of Technology: new options for Cubesat propulsion*, CEAS Space Journal **1**, 9 (2016).

1. **Daduí C. Guerrieri**, Angelo Cervone, and Eberhard Gill, *Analysis of Non-Isothermal Rarefied Gas Flow in Diverging Microchannels for Low Pressure Micro-Resistojets*, ASME Journal of Heat Transfer **11**, 138 (2016).

CONFERENCE PAPERS

15. **Daduí C. Guerrieri**, Marsil de Athayde Costa e Silva, Angelo Cervone, Eberhard Gill, *Optimum Design of Low-Pressure Micro-Resistojet Applied to Nano- and Pico-Satellites*, ESA Space Propulsion Conference, Seville, Spain, 2018.

14. Vidhya Pallichadath, Silvana Radu, Marsil de Athayde Costa e Silva, **Daduí C. Guerrieri**, Angelo Cervone, *Integration and Miniaturization Challenges in the Design of Micro-Propulsion Systems for Picosatellite Platforms*, ESA Space Propulsion Conference, Seville, Spain, 2018.

13. Marsil de Athayde Costa e Silva, **Daduí C. Guerrieri**, Angelo Cervone, Eberhard Gill, *Topology Optimization of Heating Chamber of Vaporizing Liquid Microthruster*, ESA Space Propulsion Conference, Seville, Spain, 2018.

12. Vidhya Pallichadath, Stefano Silvestrini, Marsil A. C. Silva, Didier Maxence, **Daduí C. Guerrieri**, Samiksha Mestry, Tatiana P. Soriano, Marco Bacaro, Henk van Zeijl, Barry Zandbergen, Angelo Cervone, *MEMS Based Micro-Propulsion System for Cubesats and Pocketqubes*, IAF 68th International Astronautical Conference, Adelaide, Australia, 2017.

11. Didier Maxence, **Daduí C. Guerrieri**, Angelo Cervone, *Preliminary Results of a Sublimating Propellant Tank for Dedicated Micropropulsion System*, IAF 68th International Astronautical Conference, Adelaide, Australia, 2017.

10. Serban Leveratto, Mathijs Van de Poel, Marsil A. C. Silva, **Daduí C. Guerrieri**, Angelo Cervone, *Characterisation of a Thrust Stand to Assess Micro-Thruster Performance*, IAF 68th International Astronautical Conference, Adelaide, Australia, 2017.

9. **Daduí C. Guerrieri**, Marsil de Athayde Costa e Silva, Barry T.C. Zandbergen, Angelo Cervone, *Heater Chip with Different Microchannels Geometries for a Low Pressure Free Molecular Micro-Resistojet*, ESA Space Propulsion Conference, Rome, Italy, 2016.

8. Marsil de Athayde Costa e Silva, **Daduí C. Guerrieri**, Angelo Cervone, *State space modeling of fluid flow for thrust control in mems-based micropropulsion*, ESA Space Propulsion Conference, Rome, Italy, 2016.

7. **Daduí C. Guerrieri**, Marsil de Athayde Costa e Silva, Barry T.C. Zandbergen, Angelo Cervone, *Development of a Low Pressure Free Molecular Micro-Resistojet for Cubesat Applications*, IAF 66th International Astronautical Conference, Jerusalem, Israel, 2015.

6. Marsil de Athayde Costa e Silva, **Daduí C. Guerrieri**, Angelo Cervone, *Investigation of Innovative Thrust-Vector Control Techniques for Micro Propulsion Systems*, IAF 66th International Astronautical Conference, Jerusalem, Israel, 2015.

5. Angelo Cervone, Barry T.C. Zandbergen, **Daduí C. Guerrieri**, Marsil de Athayde Costa e Silva, Henk W. van Zeijl, *Green Micro-Resistojet Research at Delft University of Technology: the New Frontiers of Cubesat Propulsion*, 5th CEAS Air and Space Conference, Delft, the Netherlands, 2015.

4. **Daduí C. Guerrieri**, Carolina Cotta, *Experimental And Theoretical Analysis Of A Microchannel Heat Exchanger For High Concentration Photovoltaic Cells*, CONV-14: International Symposium on Convective Heat and Mass Transfer, Kusadasi, Turkey, 2014.

3. **Daduí C. Guerrieri**, Carolina Cotta, *Numerical Analysis Of Micro Heat Exchangers For Cooling Of High Concentration Photovoltaic Panels*, Third International Conference on Computational Methods for Thermal Problems, Lake Bled, Slovenia, 2014.

2. Marcos Correa, **Daduí C. Guerrieri**, Carolina Cotta, *Design And Manufacture Of Microchannel Heat Sinks For High Concentration Photovoltaic Cells*, 22nd International Congress of Mechanical Engineering, Ribeirão Preto, São Paulo, Brazil, 2013.

1. **Daduí C. Guerrieri**, Fabio Viana, Saulo C. Fragoso, Mila R. Avelino, *Shell-And-Tube Heat Exchangers Using Nanofluids*, 14th Brazilian Congress of Thermal Sciences and Engineering, Rio de Janeiro, RJ, Brazil, 2012.